Dissertation zur Erlangung des Doktorgrades der Fakultät für Chemie und Pharmazie
der Ludwig-Maximilians-Universität München

Structural and functional insights into the mechanism of the Pex1/6 complex

Susanne Michaela Ciniawsky
aus Ebersberg, Deutschland

2015

Erklärung

Diese Dissertation wurde im Sinne von § 7 der Promotionsordnung vom 28. November 2011 von Frau Dr. Petra Wendler betreut.

Eidesstattliche Versicherung

Diese Dissertation wurde eigenständig und ohne unerlaubte Hilfe erarbeitet.

München, 13. April 2015

……

Susanne Ciniawsky

Dissertation eingereicht am	13. April 2015
1. Gutachterin:	Dr. Petra Wendler
2. Gutachter:	Prof. Dr. Roland Beckmann
Mündliche Prüfung am	08. Mai 2015

TABLE OF CONTENTS

Parts of this thesis have been published and summarized in:

Susanne Ciniawsky*, Immanuel Grimm*, Delia Saffian, Wolfgang Girzalsky, Ralf Erdman, Petra Wendler: Molecular snapshots of the Pex1/6 AAA+ complex in action.

Nat. Commun. 6:7331 doi: 10.1038/ncomms8331 (2015).

*These authors contributed equally

Acknowledgements

I owe my thanks to many people for their undivided support during my time as PhD student and thus, made this work possible.

First, I owe my thanks to Petra Wendler. I am truly grateful that you offered me the opportunity to do my PhD in your lab. I greatly benefited from your excellent scientific guidance and expertise, vast creativity and knowledge. I really appreciate your confidence in my work from the very early stage of this project, your patience and that you have always been ready to listen.

I would like to thank a very important group of people, who enthusiastically supported the Pex project and have been amazing help in the Wendler lab – Kai Hempel (yo mein Bro!), Maria Walker alias Walker B, Rieke Horst, Claudia Müller and Julia Wittmann. Particularly to Kai and Rieke: so many thanks for the wonderful time we've spent together!

My thanks extend equally to my PhD colleagues Sebastian Kube, Anindya Gosh Roy and Malte Kock. Many thanks for inspiring discussions and your support in many ways. I really appreciated our cosy lab atmosphere that made working in the lab truly enjoyable! Thanks guys!

Especially, I would like to thank Prof. Ralf Erdmann, Dr. Wolfgang Girzalsky, Dr. Delia Saffian and Immanuel Grimm for the close and successful collaboration. The Pex project greatly benefited from your inspiring ideas and joint discussions. Sincere thanks to Immanuel and Delia – it was great fun to work with you!

A very special thanks goes to Romy Böttcher. You've been always there for me and incessantly motivated me to keep on going. So many thanks for an amazing, unforgettable time and being such a good friend to me. Equally, a very special thanks goes to Juliane Horenk and Anja Kieser. I am really glad I've met you and supremely appreciated the time we've spent together.

I would like to thank Prof. Roland Beckmann for his scientific support and providing access to the microscopes. Equally, I am grateful to Otto Berninghausen and Charlotte Ungewickell, who introduced me to and provided technical advice and know-how for the microscopes and cryo-EM grid preparation.

I would like to thank the members of my thesis advisory committee, Prof. Roland Beckmann and Gregor Witte, for their encouraging scientific suggestions, which supported this thesis.

Foremost I truly thank my family, in particular my parents, who gave constant love and care, making everything possible throughout my way. Equally, I am very grateful to Andi's parents for being a continuous source of support!

I owe my thanks to my closest friends, particularly Vroni, who supported and encouraged me at all times and patiently listened when I was talking (or thinking) about strange structures of alien protein complexes.

Last but not least I am deeply grateful to Andi. Thank you so much for your continuous support ever since! You gave me the strength and the trust to carry on with this work and to deal with whatsoever came across.

All started with a recipe.

Abstract

Peroxisomes are highly dynamic organelles of eukaryotic cells, carrying out essential oxidative metabolic processes. These organelles scavenge reactive oxygen species such as hydrogen peroxide (H_2O_2) and catabolise fatty acids, which are particular hallmarks and highly conserved features of peroxisomes among different species. Peroxisomal proteins and enzymes are encoded by nuclear DNA and therefore, targeted post-translationally into the peroxisomal matrix. A special class of proteins, collectively called peroxins, perform certain cellular tasks, such as peroxisomal matrix protein import or membrane development in order to maintain peroxisome biogenesis as well as a constant flux of matrix proteins into peroxisomes. The type II AAA+ peroxins Pex1/Pex6 are a core component of the peroxisomal matrix protein import system. ATPases of the AAA+ family of proteins generally assemble into large, macromolecular machines, structurally remodelling their substrate protein, which is driven by the hydrolysis of ATP. The main function of Pex1/6 complexes is to release the receptor Pex5 from peroxisomal membranes after matrix protein import. This relocation of Pex5 into the cytosol ensures a constant pool of available receptor molecules for subsequent cycles of protein import into peroxisomes. Accordingly, certain mutations in mammalian Pex1/Pex6 proteins compromise peroxisome biogenesis and thus, lipid metabolism, causing severe genetic Zellweger diseases in humans.

In collaboration with Professor Ralf Erdmann and colleagues at the Ruhr-Universität Bochum, we characterize the structure and function of the AAA+ Pex1/6 complex from yeast *Saccharomyces cerevisiae*. Single particle electron microscopy (EM) in combination with biochemical assays allows us to analyze how ATP turnover is related to the biological function of the Pex1/6 complex. This study presents EM structures of Pex1/6 complexes assembled in the presence of ADP, ATP, ADP-AlFx and ATPγS, providing a comprehensive structural characterization of the heterohexameric type II AAA+ complex in different nucleotide states. Our EM reconstructions reveal an unexpected triangular overall shape, different than observed for the closely related and well-characterized homohexameric AAA+ protein p97. We show that the heterohexameric Pex1/6 complex is composed of a trimer of heterodimers with alternating subunit arrangement of Pex1 and Pex6 moieties. Furthermore, our results suggest that conserved aromatic residues, lining the central pore of the Pex1/6 D2 ring mediate substrate interactions. These residues correspond to substrate interaction regions in related AAA+ proteins. Comparing Pex1/6 EM reconstructions in different nucleotide states implicates that the mechanical function of Pex1/6 involves an N- to C-terminal protein translocation mechanism along the central pore. The Pex1/6 EM structures resolve symmetric and asymmetric large-scale domain motions, which likely create a power stroke during cycles

of ATP binding and hydrolysis. We conclude that Pex5 is probably partially or completely unfolded while it is threaded through the central pore of Pex1/6 complexes.

In addition, ATP hydrolysis assays of Pex1/Pex6 complexes containing single amino acid exchanges in individual Walker B motifs reveal that not all active sites are functionally equivalent. In isolated complexes, ATP turnover mainly occurs in Pex6 D2 domains, while Pex1 subunits sustain the structural integrity of the complex. We further resolve the structures of Pex1/6 Walker B variants and observe mutually exclusive protomer-protomer communication. In the Pex1/6 complex, a Walker B mutation induces ATP hydrolysis in the adjacent D2 domain, presenting a structural framework of protomer-protomer communication in the AAA+ heterohexamer.

Zusammenfassung

Peroxisomen stellen eine eigene Familie von Organellen dar, welche in nahezu allen eukaryotischer Zellen essentielle oxidative metabolische Prozesse ausführen. Ihre wesentlichen und konservierten Funktionen sind der Abbau von toxischen Stoffwechselprodukten wie Wasserstoffperoxid (H_2O_2) sowie von Fettsäuren, um die daraus resultierenden Produkte für weitere Stoffwechselprozesse zur Verfügung zu stellen. Peroxisomale Proteine und Enzyme werden von der genomischen DNA kodiert und müssen daher post-translational in die peroxisomale Matrix importiert werden. Eine spezielle Proteinklasse, sogenannte Peroxine, übernehmen bei diesem Prozess spezifische Aufgaben, wie den Import peroxisomaler Proteine oder die Synthese peroxisomaler Membranen, um die Biogenese von Peroxisomen und eine ständige Verfügbarkeit von peroxisomalen Proteinen zu gewährleisten. Die Typ II AAA+ Proteine Pex1/Pex6 spielen eine zentrale Rolle im Import peroxisomaler Matrixproteine. Generell bilden ATPasen der AAA+ Proteinfamilie multimere makromolekulare Maschinen, welche die Konformation ihrer Substratproteine unter ATP Verbrauch modifizieren. Die molekulare Funktion von Pex1/Pex6 in diesem Prozess ist die Freisetzung des Rezeptors Pex5 aus der peroxisomalen Membran nach dem erfolgten Import von Matrixproteinen. Diese Rückführung von Pex5 ins Zytosol erfolgt unter dem Verbrauch von ATP und stellt eine gleichbleibende Menge an freien Rezeptormolekülen für weitere Importzyklen zur Verfügung. Einzelne Mutationen in Pex1 oder Pex6 beeinträchtigen die Biogenese von Peroxisomen erheblich und stören dadurch den Lipidstoffwechsel. Daher führen diese Mutationen im Menschen zu folgenschweren genetische Krankheiten, die im Zellweger Spektrum zusammengefasst werden.

In Kollaboration mit der Arbeitsgruppe von Professor Ralf Erdmann von der Ruhr-Universität Bochum, charakterisieren wir deshalb die Struktur und Funktion des AAA+ Pex1/6 Komplexes der Hefe *Saccharomyces cerevisiae*. Zu diesem Zweck untersuchen wir den strukturellen Aufbau von Pex1/Pex6 Komplexen mittels Einzelpartikel-Elektronenmikroskopie (EM) und analysieren dessen biologische Funktion in biochemischen und genetischen Experimenten. In der vorliegenden Arbeit beschreiben wir die unterschiedlichen Strukturen des Pex1/6 Proteinkomplexes in Anwesenheit von ADP, ATP, ADP-AlFx und ATPγS. Unsere EM Rekonstruktionen des Pex1/6 Komplexes zeigen eine unerwartete dreieckige Form, welche sich von bekannten Strukturen des sehr ähnlichen, gut charakterisierten AAA+ Proteins p97 unterscheidet. Pex1/6 Hexamere bestehen aus alternierend angeordneter Pex1 und Pex6 Untereinheiten und bilden damit ein „Trimer von Heterodimeren“. Aus genetischen Experimenten schließen wir, dass stark konservierte, aromatische Aminosäurereste die Interaktion zwischen Pex1/6 Komplexen und ihrem

physiologischen Substrat vermitteln. Diese säumen die zentrale Pore der Pex1/6 D2 Domäne und ihre Position entpricht den Substratbindestellen in verwandten ATPasen der AAA+ Proteinfamilie. Der Vergleich der Pex1/6 Strukturen in unterschiedlichen Nukleotid-gebundenen Stadien legt eine prozessive N- zu C-terminale Substrattranslokation entlang der Pex1/6 Pore nahe. In Abhängigkeit des vorhandenen Nukleotids zeigen die Pex1/6 Komplexe umfangreiche symmetrische sowie asymmetrische Bewegungen in den D2 AAA+ Domänen. Diese Domänenbewegungen generieren möglicherweise die treibende Kraft für die Prozessierung von Pex5 durch die Pore und entfalten dabei das Zielprotein entweder komplett oder teilweise.

Darüberhinaus zeigen wir in ATPase Assays, dass sich die hydrolytische Aktivität der Pex1 oder Pex6 D2 Domänen erheblich voneinander unterscheidet. In aufgereinigten Pex1/6 Proteinkomplexen wird ATP scheinbar nur in den D2 Domänen von Pex6 hydrolysiert, während die Bindung von ATP in den Pex1 D2 Domänen die Komplexbildung unterstützt. Zusätzlich zeigt die strukturelle Untersuchung von Pex1/6 Komplexen mit mutiertem Walker B Motiv spezifische Interaktionen zwischen benachbarten Pex1/Pex6 Protomeren. Diese Interaktionen zeigen, dass die Mutation einer Walker B Untereinheit ATP Hydrolyse in der benachbarten Untereinheit induziert. Daher bilden diese Interaktion möglicherweise die molekulare Grundlage für die Kommunikation zwischen einzelnen Domänen im Pex1/6 Komplex.

1 Introduction

Peroxisomes are indispensible for a fully functional metabolism in humans. Malfunction of peroxisomes or defects during their biogenesis have grave consequences and manifest in clinical syndromes of the serious Zellweger spectrum. On-going peroxisome research already established robust mechanistic models for peroxisome biogenesis and function among species. Although the metabolic processes of human peroxisomes and the inherited disorders involved might be of particular clinical interest, a variety of yeast organism have proofed their rational as model system. Likewise, in this study, yeast homologs of human AAA+ Pex1/6 proteins are structurally characterized extending existing concepts of their role as key components of peroxisomal biogenesis on a molecular level. Notably, mutations in mammalian Pex1/Pex6 proteins are the predominant cause for severe Zellweger phenotypes (Geisbrecht *et al.*, 1998).
A wealth of genetic and biochemically data on peroxisomes accumulated over the last three decades. However, in subsequent chapters key features and redundant biochemical processes of peroxisomes are described, thus mainly referring to studies available for yeast *Saccharomyces cerevisiae (S. cerevisiae)*. Otherwise, species-specific results are stated correspondingly.

1.1 Peroxisomes - a new family of organelles

Peroxisomes were initially described by electron microscopical analysis of mouse kidneys and classified as so called microbodies (Rhodin, 1954). Upon the first isolation of mammalian microbodies, a peroxide-producing-oxidase and catalase were extracted as the primary enzymes (De Duve and Baudhuin, 1966). Both proteins are involved in ana- and catabolism of hydrogen peroxide (H_2O_2), changing the name of the newly discovered organelle to peroxisome over time. Besides scavenging reactive oxygen species such as H_2O_2, also oxidative breakdown of fatty acids was found to be compartmentalized in peroxisomes (Lazarow and De Duve, 1976). Hence, peroxisomes evolved as protective organellar compartments, shielding oxidation reactions, which would be otherwise harmful for the cell. Advances in cytochemical stains revealed during morphological studies of eukaryotic cells that peroxisomes are widespread among most cell types (Hruban *et al.*, 1972). It became evident that peroxisomes adopt their number and size dynamically in individual cell or tissue types according to environmental cues. Veenhuis et al. (1987) discovered in budding yeast *S. cerevisiae* that progression and protein content of peroxisomes is significantly up regulated upon consumption of oleic acid. Furthermore, studies in rodents discovered that peroxisome abundance and size is induced five to nine fold, particularly in liver cells, when the animals

are treated with synthetic peroxisome proliferators (Fahimi *et al.*, 1982; Reddy *et al.*, 1982). It appears that peroxisome function requires structural adaption of the entire compartment, resulting in organelles with a varying diameter of 0.1-1 µm (Lazarow and Fujiki, 1985). Peroxisomes consist of single lipid bilayers that round off a grainy matrix crowded with a multitude of soluble matrix proteins, able to form electron-dense crystalline core structures (Angermuller and Fahimi, 1986). Peroxisomes do not enclose DNA and distinct from other organelles, all matrix proteins are synthesized in the cytosol and traverse post-translationally into peroxisomes (Lazarow and Fujiki, 1985). Notably, peroxisomal membranes are impermeable to virtually all metabolites *in vivo* (Wanders and Waterham, 2006a). Hence, peroxisomal membrane transporters have to actively navigate metabolites, such as electron carriers (e.g. NAD/H^+, Bernhardt *et al.*, 2012) and nucleotides (ATP, Palmieri *et al.*, 2001) or even fully folded proteins across the peroxisomal membrane (Walton *et al.*, 1995).

The oxidative breakdown of H_2O_2 and fatty acids are evolutionary conserved processes in peroxisomes among species. Nevertheless, peroxisomes fulfil many key aspects of lipid metabolism and not surprisingly, specialized versions of the organelle exist. Plant peroxisomes house the glyoxylate cycle, which is the core enzymatic reaction for carbohydrate anabolism in plant seeds, thus the organelles are termed glyoxysomes (Breidenbach and Beevers, 1967). Peroxisomes of human pathogens *Trypanosoma*, namely glycosomes, orchestrate common peroxisomal proteins with glycolytic enzymes, thus partitioning the otherwise cytosolic glycolysis reaction to glycosomes (Opperdoes *et al.*, 1977). Peroxisomes of filamentous fungi, like *Neurospora crassa,* differentiate into Woronin bodies on a central hexagonal, crystalline core, serving as plug upon cell damage (Liu *et al.*, 2011).

1.2 Functions of peroxisomes

Besides the mitochondria and ER, peroxisomes are the major sites of oxygen consumption, which form H_2O_2 as metabolic precursor for oxidative downstream pathways. Compartmentalization of those reactions allows efficient and protective metabolic processing. Furthermore, catabolism of fatty acids provides a constant flux of high-energy intermediates, subsequently used for ATP synthesis in mitochondria. Hence, peroxisomes perform dedicated biological functions in order to maintain cell physiology and a vast repertoire of organism-specific metabolic processes has evolved (Islinger *et al.*, 2012).

1.2.1 Peroxisome metabolism from yeast to men

Amongst other biochemical pathways, processing of fatty acids is a particular hallmark and a highly conserved feature of peroxisomes among species (Poirier *et al.*, 2006) Notably, in

plants and fungi peroxisomes are the sole site of fatty acid β-oxidation (Tolbert, 1981). In contrast, metabolism of fatty acids in mammalian and human cells is targeted to both, peroxisomes and mitochondria (Wanders, 2000). While branched and very long chain fatty acids (VLCF) are degraded solely in peroxisomes, breakdown of long chain and medium chain fatty acids (LCFA, MCFA) occurs in mitochondria. During the process of β-oxidation, carbon-carbon bonds are ruptured thereby liberating chemical energy stored in the covalent bond. In this way fatty acids are converted into more polar molecules, facilitating further degradation, and their breakdown generates acetyl-CoA metabolites as vital energy source and reduced electron acceptors $FADH_2$/$NADH+H^+$ (Hiltunen *et al.*, 2003).

Furthermore, mammalian peroxisomes are crucial for ether lipid (plasmalogen) biosynthesis, which are fundamental components of heart and neuronal tissue (Nagan and Zoeller, 2001). Plasmalogens account for up to 80 % of ethanolamine phospholipids in myelin and are thought to be involved in oxidative stress protection (Brosche and Platt, 1998). Ether lipid anabolism is distributed between peroxisomes and ER, though. However, the first two steps of the metabolic process include strictly peroxisomal enzymes (Wanders, 2004). Moreover, the adult human liver processes roughly 500 mg cholesterol to bile acid daily, which in turn is essential for dietary fat adsorption upon micelle formation or emulsifying cholesterol and fat-soluble vitamins (Ferdinandusse and Houten, 2006). The conversion of intermediate to mature bile metabolites involves β-oxidation, which occurs entirely in peroxisomes of human liver cells (Russell, 2003). Additionally, peroxisomes exclusively accomplish α-oxidation of branched fatty acids, like phytanic acid (Jansen and Wanders, 2006). In phytanic acid, a methyl group occupies the carbon 3 position, thus oxidative removal of the alkyl group in form of CO_2 is mandatory to produce β-oxidation suitable metabolites, in this case pristanic acid (van den Brink and Wanders, 2006). Farther, peroxisomes are linked to cellular redox regulation and the generation of reactive oxygen species (ROS), thus suggesting a connection to pathological processes of age-related diseases and a considerable contribution to molecular reactions resulting in aging (Titorenko and Terlecky, 2011; Lizard *et al.*, 2012).

Additionally, molecular pathways in plant leaf peroxisomes involve macromolecular enzyme complexes, catalysing main reactions of photorespiration (Heupel and Heldt, 1994). In *Arabidopsis thaliana*, core enzymes of fatty acid oxidation together with an increasing number of newly identified ancillary enzymes control anabolism of hormonal signal molecules such as jasmonites and auxins (Baker *et al.*, 2006; Kienow *et al.*, 2008). In *Caenorhabditis elegans* or insects, pheromone production is amenable to peroxisomes (Joo *et al.*, 2010; Spiegel *et al.*, 2011). Also, industrial scale production of beta-lactam antibiotic penicillin relies on metabolic reactions catalysed in peroxisomes of filamentous fungi *Penicillium chrysogenum* (Kiel *et al.*, 2005b).

1.2.2 β-Oxidation of fatty acids

The key steps of lipid catabolism in peroxisomes are well conserved and I thus focus specifically on yeast *S. cerevisiae* in this section. A profound overview of fatty acid β-oxidation and related biochemical processes in mammalian cells is provided in Wanders and Waterham (2006a).

Yeast replenish the amount of fatty acids needed either through *de novo* synthesis or exogenous sources (Tehlivets *et al.*, 2007). Notably, an impaired fatty acid synthetase, the key enzyme in endogenous fatty acid synthesis, is compensated by uptake of external fatty acids (Dirusso *et al.*, 2000). In yeast cells, exogenous long-chain fatty acids (LCFA, Figure 1.1) are imported and concurrently activated with coenzyme A (CoA) by acyl-CoA synthetases Fat1, Faa1, Faa3 and Faa4 (Black and DiRusso, 2007). Acyl-CoA thioesters (acyl-CoA), products of the nucleotide dependent fatty acid activation reaction, shuttle towards the peroxisomal membrane and translocate into the peroxisomal lumen aided by heterodimeric ATP binding cassette (ABC) transporters Pxa1-Pxa2 (van Roermund *et al.*, 2012). In contrast, free medium-chain fatty acids (MCFC) are activated intra-peroxisomal through acyl-CoA synthetase Faa2 (Hettema *et al.*, 1996). The adenine nucleotide transporter Ant1 maintains the required pool of free ATP (Palmieri *et al.*, 2001).

The actual β-oxidation is divided into 4 reactions, progressing through dehydrogenation, hydrogenation, dehydrogenation and finally thiolytic cleavage (Figure 1.1, I-IV). In the initial step acyl-CoA is oxidized to trans-Δ2-enoyl-CoA, generating a double bond between the second and third carbon atom, catalysed by the acyl-CoA oxidase Fox1. Released electrons of this reaction are directly transmitted to oxygen to yield the toxic by-product H_2O_2, which in turn is degraded by catalase Cta1, thereby regenerating electron carrier $FADH_2$. Further processing of trans-Δ2-enoyl-CoA yields enantioselective L3-ketoacyl-CoA by Fox2, generating L3-hydroxyacyl-CoA as an intermediate. Concomitantly, electron acceptor NAD+ is reduced to NADH. The thiolase Fox3 performs thiolytic cleavage, the final step of the β-oxidation, where 3-ketoacyl-CoA is fragmented into acetyl-CoA and acyl-CoA shortened by two carbon units. Remaining acyl-CoA molecules undergo repetitive cycles of β-oxidation until the entire fatty acid chain is cleaved into acetyl-CoA. Fatty acids with an odd-number of carbon atoms are cleaved into acetyl-CoA and propionyl-CoA as final products. (Hiltunen *et al.*, 2003; Poirier *et al.*, 2006).

Acetyl-CoA moieties are essential metabolites for subsequent energy production. Acetyl-CoA units are either directed to the mitochondrial matrix by the carnitine acetyl transferase Cat2 to be subjected to the citric acid cycle (TCA) for subsequent ATP synthesis in mitochondria, or localized to both, the cytosol and peroxisome for biosynthesis of carbohydrates or amino acids throughout the glyoxylate cycle (Rottensteiner and Theodoulou, 2006).

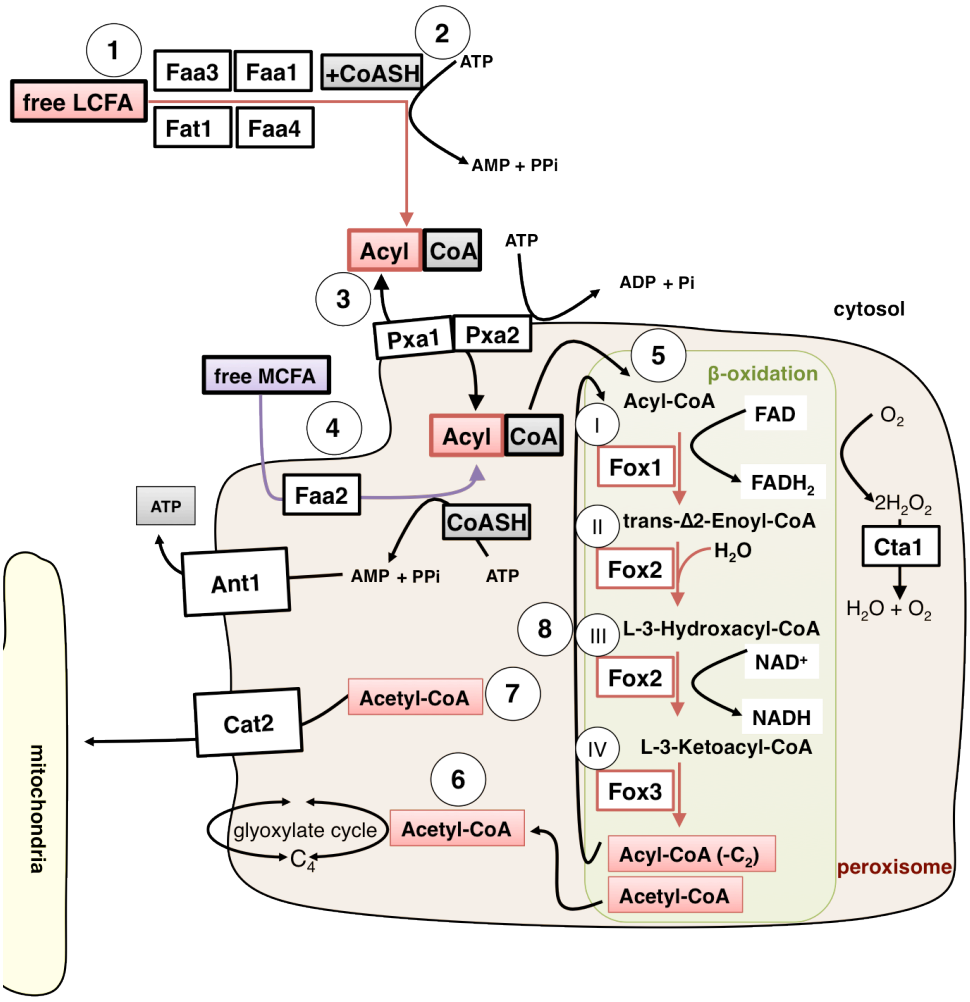

Figure 1.1 Peroxisomal β-oxidation in *S. cerevisiae*. Schematic overview of processes involved in *S. cerevisiae* lipid catabolism. **(1)** Transport of free long-chain fatty acids (LCFA) into the cytosol, handled by acyl-CoA synthetases Fat1, Faa1, Faa3 and Faa4. **(2)** Activation of LCFAs through ATP dependent transfer of coenzyme A (CoA) resulting in acyl-CoA intermediates. **(3)** LCFAs translocate into the peroxisomal lumen via heterodimeric ABC transporters Pxa1-Pxa2. **(4)** ATP consuming activation of medium-chain fatty acids (MCFA) through acetyl-CoA synthase Faa2, stimulated by Ant1. **(5)** Acyl-CoA intermediates, derived from LCFA or MCFA activation, undergo β-oxidation, which is divided into 4 reactions (Hiltunen *et al*., 2003; Poirier *et al*., 2006): **(I)** dehydrogenation by acyl-CoA oxidase Fox1, yielding harmful H_2O_2. Catalase Cta1 degrades H_2O_2, thereby regenerating electron carrier $FADH_2$. **(II)** Hydrogenation by Fox2. **(III)** Dehydrogenation by Fox2, electron acceptor NAD+ is reduced to NADH. **(IV)** Thiolytic cleavage by thiolase Fox3, yielding acetyl-CoA and acyl-CoA shortened by a two-carbon unit ($-C_2$). **(6)** Acetyl-CoA molecules enter glyoxylate cycle for biosynthesis of carbohydrates or amino acids. **(7)** Carnitine acetyl transferase Cat2 directs acetyl-CoA units to the mitochondria for ATP synthesis downstream of the TCA cycle (not shown). **(8)** Remaining acyl-CoA molecules undergo repetitive cycles of β-oxidation until the entire fatty acid chain is cleaved.

1.3 Peroxisome biogenesis - *S. cerevisiae* peroxins (Pex)

Work by Erdmann et al. (1989) on targeting signals of peroxisomal proteins in *S. cerevisiae* identified mutant yeast strains defective in proper assembly of functional peroxisomes. Those mutants grow normally on glucose but fail to metabolize oleic acid as the sole carbon source (onu: oleate-non-utilizing-phenotype). Moreover, peroxisomal matrix enzymes are mislocalised to the cytosol and detectable peroxisomes are significantly reduced as observed

by electron microscopy. Those phenotypes result from single gene mutations and corresponding mutants are termed *pex* (peroxisomal assembly) mutants and related gene products peroxins (Erdmann and Kunau, 1992; Distel *et al.*, 1996). Hence, peroxins (Pex) are indispensible for the accurate formation of peroxisomes. At present, 33 Pex proteins have been identified in yeast, regulating peroxisome homeostasis and adaption to cellular needs (Platta and Erdmann, 2007; Tower *et al.*, 2011). Distinct groups of Pex proteins are responsible for peroxisomal matrix protein import and membrane development. Considerably progress has been made unravelling the role and function of individual Pex proteins in peroxisome synthesis, which are outlined in the following sections.

1.3.1 Matrix protein import: translocation across the peroxisomal membrane

The peroxisomal proteome consists of up to 50 different matrix enzymes (Schluter *et al.*, 2010). However, peroxisomes do not enclose genomic DNA and distinct from other organelles, all matrix proteins are nuclear encoded and synthesized on polyribosomes in the cytosol (Lazarow and Fujiki, 1985). Hence, for constant flux of peroxisomal matrix proteins, target proteins have to be directed post-translationally into peroxisomes.

The majority of peroxisomal matrix proteins are fused to a C-terminal peroxisomal targeting sequence type 1 (PTS1), defined by a degenerate serine-lysine-leucine (SKL) motif (Brocard and Hartig, 2006). The soluble receptor protein Pex5 recognizes and binds PTS1 containing proteins (McCollum *et al.*, 1993; Van der Leij *et al.*, 1993; Szilard *et al.*, 1995; van der Klei *et al.*, 1995), associating into a mobile receptor-cargo complex (Figure 1.2). An alternative, less frequent import route is used by PTS type 2 (PTS2) proteins, which are detected by the cytosolic import receptor Pex7. The PTS2 is located at the N-terminus of corresponding matrix proteins and covers a non-canonical nonapeptide (Lazarow, 2006). In *S. cerevisiae*, stable interactions between Pex7 and target PTS2 proteins depend on additional peroxins, namely Pex18 and Pex21 (Schliebs and Kunau, 2006).

For cargo delivery it is hypothesized that only cargo-associated Pex5 or Pex7, respectively, are capable to shuttle towards the peroxisomal exterior, interacting with a membrane bound ternary docking complex consisting of peroxisomal membrane proteins Pex13, Pex14 and Pex17 (Rucktäschel *et al.*, 2011). It was reported that primary interactions of cargo-loaded PTS1 receptor Pex5 occur with Pex14, whereas PTS2 receptor Pex7 initially associates with Pex13 (Girzalsky *et al.*, 2010). Once assembled, PTS1 target proteins traverse across the membrane into the peroxisomal lumen. However, the detailed molecular mechanisms of cargo translocation still remain puzzling. Intriguingly, peroxisomes efficiently import large protein oligomers and even 9 nm gold particles (Walton *et al.*, 1995), although no translocon-like structure has been observed so far (Smith and Aitchison, 2009). Hence, the available data led

to several models, including the membrane invagination model (McNew and Goodman, 1996) and the transient pore hypothesis (Erdmann and Schliebs, 2005). The latter assumes that membrane bound Pex5/Pex14 temporarily constitute a protein conducting channel, specific for peroxisomal matrix protein translocation. Indeed, published studies support the model of a short-lived peroxisomal membrane translocon consisting of self-integrating Pex5/Pex14 moieties (Platta *et al.*, 2014).

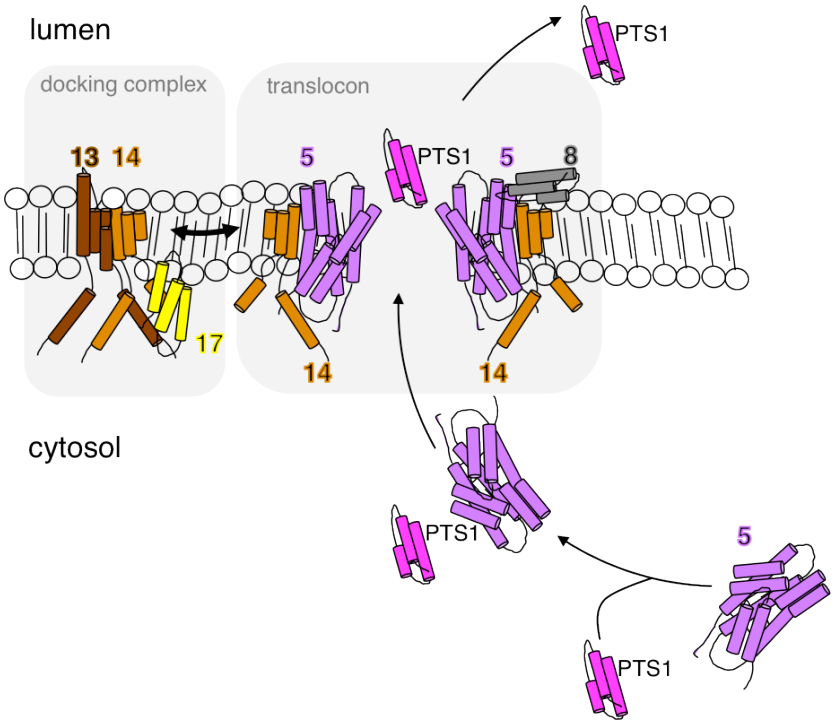

Figure 1.2 PTS1 import into peroxisomes. Soluble receptor Pex5 associates with the target PTS1 protein in the cytosol, subsequently shuttling towards the peroxisomal membrane. Cargo-loaded Pex5 interacts with membrane protein 14, which in turn constitutes the peroxisomal docking complex together with Pex13 and Pex17. PTS1 release presumably involves the formation of a transient translocon, comprising at least Pex5/Pex14 moieties. Association of Pex8 with Pex5 might support cargo release into the peroxisomal lumen.

Accordingly, the process of cargo protein release into the peroxisomal lumen remains unknown. However, it became evident that intraperoxisomal protein Pex8 associates with Pex5 downstream of the docking event, probably participating in cargo detachment (Rehling *et al.*, 2000). Furthermore, Rayapuram and Subramani (2006) report a connection of the docking complex to the heteromeric RING (really interesting new gene)- type complex, which is bridged by Pex8 (Figure 1.3). The trimeric RING-domain containing complex consists of Pex2, Pex10 and Pex12, each of which is a catalytically active E3 ligase (El Magraoui *et al.*, 2012), since mono- or polyubiquitination of unloaded Pex5 are mandatory for efficient receptor export (Platta *et al.*, 2004; Kragt *et al.*, 2005). Pex5 destined for protein degradation by the 26 S proteasome is polyubiquitinated by the RING-type E3 ligases Pex2/Pex10 and polyubiquitin chain attachment is supported by ubiquitin activating (E1-) enzyme Uba1 (Hicke

et al., 2005) and ubiquitin-conjugating (E2-) enzyme Ubc4 (Kiel *et al.*, 2005a). Reasons for 26S degradation of Pex5 are either an impaired export machinery or faulty receptor proteins. In contrast, monoubiquitination of Pex5 is somewhat distinct, as the ubiquitin attachment site comprises a conserved cysteine instead of a common lysine, which is recognized by E2 enzyme Pex4 and E3 ligases Pex10/Pex12 (Platta *et al.*, 2007; Williams *et al.*, 2007). Pex4 anchors to the peroxisomal membrane via association with the membrane protein Pex22 (Williams *et al.*, 2012). The single step ubiquitination of Pex5 is decisive for subsequent receptor recycling, recovering Pex5 for succeeding rounds of peroxisomal matrix protein import (Figure 1.3).

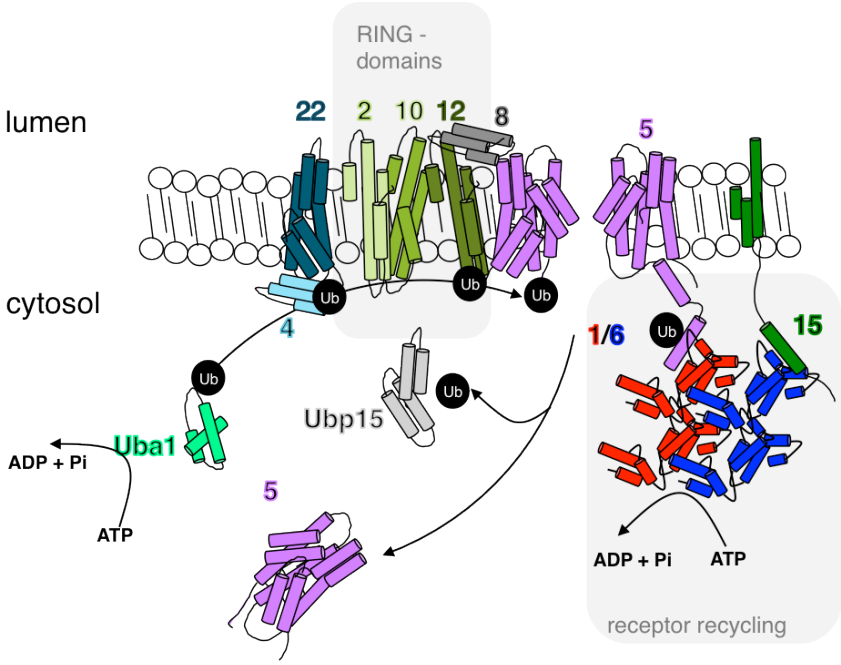

Figure 1.3 Ubiquitin dependent export of PTS1 receptor Pex5. Subsequent to PTS1 cargo release, Pex5 is monoubiquitinated (Ub) through the sequential action of ubiquitin-activating E1 enzyme Uba1, ubiquitin-conjugating E2 enzyme Pex4 and E3 ubiquitin ligase Pex12. ATP dependent receptor release is completed through AAA+ proteins Pex1/Pex6. Proteins Pex1/Pex6 anchor to the peroxisomal membrane via interactions with integral transmembrane protein Pex15. Ubiquitin dehydrolase Ubp15 removes monoubiquitin from Pex5 prior to new rounds of PTS1 import.

The export of either mono- or partially polyubiquitinated, cargo-free Pex5 from the membrane is an ATP consuming mechanism and relies on the soluble AAA+ proteins Pex1/Pex6 (Platta *et al.*, 2005). The heteromeric complex associates with integral membrane protein Pex15 via Pex6 at the cytosolic side of the peroxisomal membrane (Birschmann *et al.*, 2003; Rosenkranz *et al.*, 2006). However, the detailed mechanism of energy consuming receptor release and interactions of Pex5 with the ATPase complex Pex1/Pex6 is still under debate. Available data is summarized and discussed in more detail in section 1.6. Subsequent to Pex5 export and prior to a new import cycle, ubiquitin markers have to be enzymatically cleaved. Recently, the deubiquitinating enzyme Ubp15 has been identified as the hydrolase consecutively removing

single ubiquitin moieties from Pex5 in *S. cerevisiae* (Debelyy *et al.*, 2011).
Intriguingly, studies of *S. cerevisiae* PTS2 co-receptor Pex18 revealed an identical mono- and polyubiquitination pattern (Hensel *et al.*, 2011), while no evidence on Pex7 ubiquitination, degradation or release exists. The current knowledge on the detailed mechanism of cargo-release and PTS2 receptor export remains fragmentary.
Switching from a soluble to a membrane-integrated state is a remarkable feature of the PTS1 receptor Pex5 and distinct from other organelles like mitochondria or the endoplasmatic reticulum (ER). Furthermore, energy consuming processing of ubiquitinated Pex5 by AAA+ proteins Pex1/Pex6 might be the driving force for concomitant cargo translocation along the transient pore, summarized in the export-driven-import model (Schliebs *et al.*, 2010). Strikingly, similar mechanisms involving recognition and ATP dependent membrane release of ubiquitin labelled substrates by an AAA+ complex exist in cellular pathways like ERAD (endoplasmatic-reticulum-associated-degradation).

1.3.2 Peroxisomal membrane development

Mutations in *PEX* genes that compromise matrix protein import results in organellar remnants, which still recruit peroxisomal membrane proteins (‘ghosts’, Schrader and Fahimi, 2008). Hence, underlying mechanisms of matrix protein import and development of peroxisomal membranes are distinct from each other.
In analogy to peroxisomal matrix proteins, the majority of peroxisomal membrane proteins (PMPs) are translated on free polyribosomes in the cytosol and post-translationally inserted into the membrane (Rucktäschel *et al.*, 2011). Class I PMPs comprise an internal membrane-targeting signal (mPTS), which is recognized by the cytosolic import receptor protein Pex19 (Jones *et al.*, 2004; Rottensteiner *et al.*, 2004). The mPTS is not strictly conserved, covering a transmembrane domain that assists membrane insertion and a Pex19 binding stretch (Girzalsky *et al.*, 2010). Additionally, farnesylation of Pex19 is an essential prerequisite for precise mPTS recognition and protein stability (Rucktäschel *et al.*, 2009). In human skin fibroblasts, Pex19-cargo complexes are subsequently recruited to the peroxisomal membrane via docking to membrane protein Pex3 (Fang *et al.*, 2004). Studies in CHO cells imply that insertion of target PMPs into the peroxisomal membrane is ATP dependent (Matsuzono and Fujiki, 2006) Analysis of PMP import in yeast *Pichia pastoris* suggest that the structural integrity of membrane protein complexes is achieved through chaperone-like functions of Pex19 (Snyder *et al.*, 2000). However, underlying molecular mechanisms are still focus of research.
Class II PMPs (e.g. Pex3) do not encompass an intrinsic mPTS and traffic to the peroxisomal membrane via the ER (Hettema *et al.*, 2014). Signal sequences of Pex3, required for ER

shuttling, are identified (Fakieh *et al.*, 2013) and insertion into the ER membrane involves the Sec61 translocation machinery and the GET pathway, similar to secretory proteins (Schuldiner *et al.*, 2008; Thoms *et al.*, 2012). Target PMPs are exported in a vesicle-mediated transport relying on Pex19, cytosol and ATP (Lam *et al.*, 2010; Agrawal *et al.*, 2011) resulting in fully functional peroxisomes (van der Zand *et al.*, 2010).

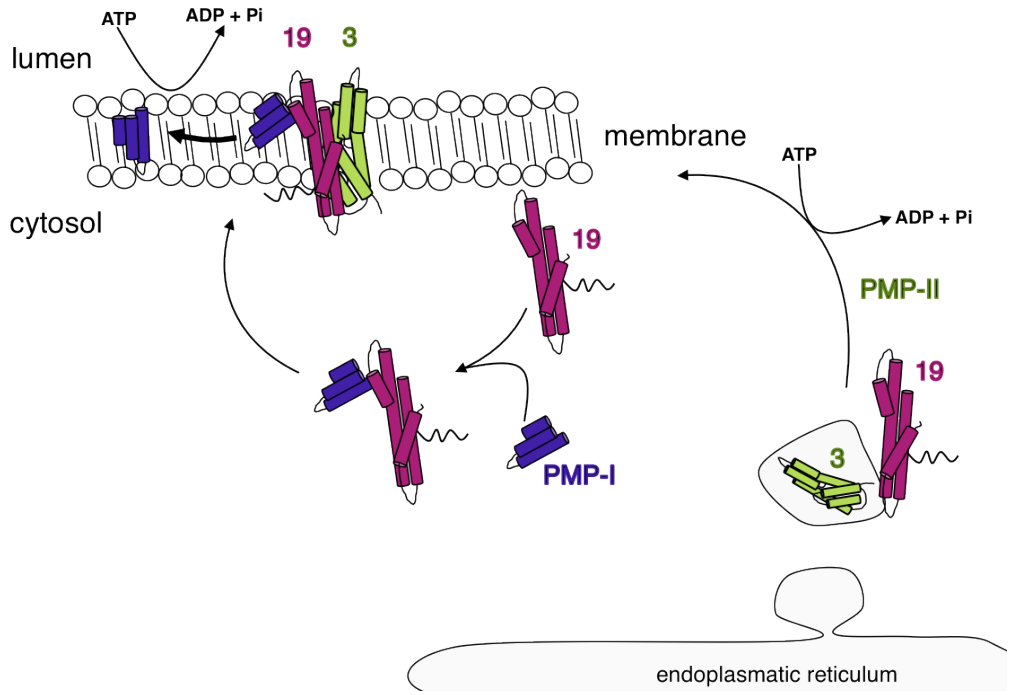

Figure 1.4 Import of peroxisomal membrane proteins. Class 1 peroxisomal membrane proteins (PMP-I) are recognized and bound by Pex19 (19) in the cytosol and shuttled towards the peroxisomal membrane. After docking to membrane protein Pex3, PMP-I are inserted into the peroxisomal membrane. Class 2 peroxisomal membrane proteins (PMP-II) traverse to peroxisomes via the endoplasmatic reticulum. Vesicle transport through the cytosol is assessed in the presence of Pex19 and ATP.

1.4 Pex1 and Pex6 are AAA+ proteins

Functional Pex1 and Pex6 were one of the first proteins identified to be essential for peroxisomal biogenesis in *S. cerevisiae* (Erdmann *et al.*, 1991; Voorn-Brouwer *et al.*, 1993). Strong sequence homology of yeast Pex1/Pex6, cell division protein p97 (yeast Cdc48) or vesicle fusion protein NSF (yeast Sec18), suggested a novel family of ATPases, commonly termed AAA family (ATPases with diverse functional activities, Kunau *et al.*, 1993). Members of the AAA family feature a conserved nucleotide binding domain comprised of up to 230 amino acids, covering a Walker A and Walker B motif, which are indispensible for ATP binding and hydrolysis (Walker *et al.*, 1982). As revealed by multiple sequence alignments, Pex1 and Pex6 group into the class of type II AAA+ proteins, featuring two consecutive nucleotide binding domains (D1 and D2, Figure 1.5 A), flanked by less conserved

N- and C-terminal stretches (Patel and Latterich, 1998; Neuwald *et al.*, 1999). In contrast to type II AAA+ proteins p97/Cdc48, only the D2 domain of either Pex1 or Pex6 are evolutionary conserved among related AAA+ proteins (Beyer, 1997). Beyer (1997) also shows that despite degeneration of Pex1/Pex6 D1 domains, non-canonical motifs for either nucleotide binding and/or hydrolysis can be found in this domain. This is in line with publications showing that orthologs of the D1 domains of Pex1 or Pex6 are less conserved (19-28 %) compared to the D2 domains (29-52 %), implying a greater significance of the second AAA+ domain. An additional region of high sequence conservation, which is typically found in all AAA+ proteins, called the second region of homology (SRH), was identified in the Pex1 D2 domain, highlighting the close sequence based relationship of the peroxins to type II AAA+ proteins p97 and NSF or ClpA and ClpB - type proteins (Ogura *et al.*, 2004).

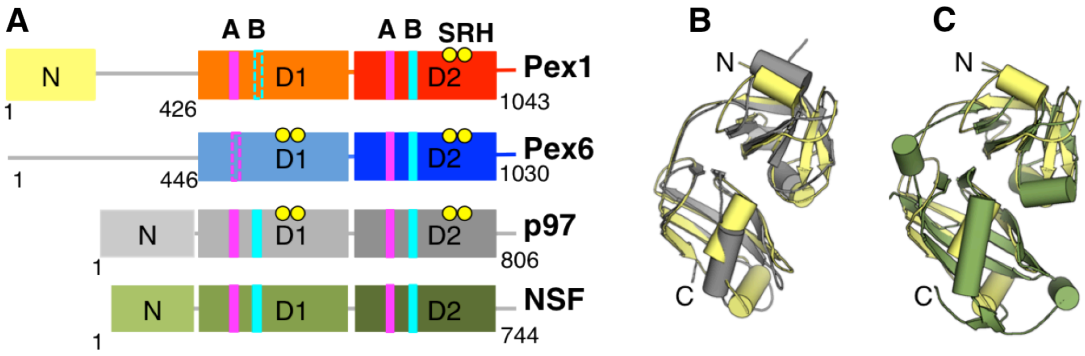

Figure 1.5 *S. cerevisiae* Pex1/Pex6 domain organization and crystal structure of murine Pex1 N-terminal domain. (A) Schematic domain structure representation of full-length Pex1 and Pex6 protomers in comparison with p97 and NSF (N, N-terminal domain; D1/D2, AAA+ domain 1/2). Conserved structural motifs and residues of the AAA+ domain are indicated as follows: Walker A (A, magenta bars), Walker B (B, turquoise bars), second region of homology (SRH) comprising arginine finger residues (yellow dots). Non-canonical Walker A and B motifs are indicated as dotted lines. (B) Ribbon diagram shows kidney shaped fold of Pex1 N domain (yellow, pdb-ID: 1WLF). Superposition with mammalian p97 N domain (grey, pdb-ID: 3qq7) or (C) mammalian NSF N domain (green, pdb-ID: 1qcs) gives a similar overall folding topology.

Structural studies of active type II AAA+ proteins p97 or NSF revealed a hexameric domain arrangement assembled around a central cavity with similar overall dimensions (Lenzen *et al.*, 1998; Zhang *et al.*, 2000; Lee *et al.*, 2003a). Global nucleotide induced conformational changes, observed in crystal structures and cryo-EM reconstructions (Pye *et al.*, 2006; Zhao *et al.*, 2012) suggest that AAA+ proteins use the energy of ATP hydrolysis to act on distinct substrates in the cell. The sequence homology of Pex1/Pex6 to p97 and NSF indicates a similar mechanism during cycles of ATP binding and hydrolysis. However, thus far structural analyses of Pex1 and Pex6 AAA+ proteins led to the crystal structure of only the N-terminal 180 amino acids of murine Pex1 (Shiozawa *et al.*, 2004), resembling the N domains of p97 and NSF (Figure 1.5 B, C). The extreme N-terminus of Pex1 depicts a double ψ-barrel fold,

which consists of two distinct subdomains, accommodating a shallow groove. The corresponding indentation in p97 and NSF N-termini allows specific adaptor protein binding (Yu *et al.*, 1999; Dreveny *et al.*, 2004). A comparable function could be assumed for Pex1 NTD, however structural or biochemical evidence is missing. Notably, in p97 and NSF the distance between N and D1 domains ranges between 30-60 amino acids (Shiozawa *et al.*, 2004). In contrast, up to 250 amino acids link the crystalized N-terminal part of Pex1 to its D1 domain.

1.5 Pex1 and Pex6 form an ATP-dependent heteromeric complex

ATP dependent *in vivo* and *in vitro* interaction of Pex1 and Pex6 was initially described in yeast *Pichia pastoris* (Faber, 1998) and verified in *S. cerevisiae* (Birschmann *et al.*, 2005) and *Hansenula polymorpha* (Kiel *et al.*, 1999), in plants (Goto *et al.*, 2011) and humans (Tamura, 1998). Pex1/Pex6 complex formation in *S. cerevisiae* was revealed by co-immunoprecipitation and yeast-two-hybrid analysis, excluding homo-oligomerisation of the two peroxins (Birschmann *et al.*, 2005). The study further implies that the interaction occurs via the less conserved first AAA+ domain of Pex1 or Pex6 and strictly depends on nucleotide binding to the Pex1 D2 domain (Figure 1.6). In the context of peroxisomal biogenesis, the authors show in oleate growth assays of Pex1/Pex6 Walker mutants, that nucleotide binding and hydrolysis in Pex1 D2 domains is essential for complex function *in vivo*. This is in line with previous studies emphasizing ATP binding and hydrolysis in the Pex6 D2 domain for unrestricted growth of *S. cerevisiae* under oleic acid conditions (Birschmann *et al.*, 2003). Respective Pex1/Pex6 Walker or null mutants encompass peroxisomal remnants (‘ghosts’) that partially contain peroxisomal membrane proteins but mislocalise matrix proteins to the cytosol (Birschmann *et al.*, 2005).

Since functional type II AAA+ proteins assemble into higher oligomers (Ye *et al.*, 2004), the capability of *S. cerevisiae* Pex1/Pex6 to form higher molecular weight complexes was recently characterized by analytical size exclusion chromatography (Saffian *et al.*, 2012). The authors demonstrate that in the presence of ATP, Pex1 and Pex6 form heterohexameric complexes with a 1:1 stoichiometry. Furthermore, ATP depletion through apyrase treatment results in complex disassembly and verifies the importance of nucleotide for complex stability. In analogy to Birschmann et al. (2005), Pex1 and Pex6 do not form homohexamers, only gel filtration fraction corresponding to Pex1 homotrimers could be observed. Finally, impaired ATPase activity upon N-ethylmalemide treatment verified that nucleotide binding to the Pex1 D2 domain is indispensible for complex formation *in vivo* and *in vitro* (Saffian *et al.*, 2012).

In terms of complex formation, consequences of nucleotide binding and hydrolysis in mammalian Pex1/6 complexes differs from the results obtained for the yeast orthologs

(Tamura *et al.*, 2006). Complex formation requires nucleotide binding to both, Pex1/Pex6 D1 and D2 domains and hydrolytic activity in the second AAA+ domain of Pex1. Furthermore, Tamura et al. (2006) characterized the complementation activity of Pex1/Pex6 Walker mutants and similar to *S. cerevisiae* Pex1/Pex6, functional D2 domains are mandatory for peroxisome biogenesis in mammalian cells. Additionally, ATP binding to the mammalian Pex6 D1 is required for fully functional peroxisomes. Equivalent to yeast mutants, aberrant mammalian Pex1 or Pex6 results in peroxisomal remnants and accumulation of peroxisomal matrix proteins in the cytosol, as observed by electron microscopy of CHO cells (Tsukamoto *et al.*, 1995; Tamura *et al.*, 1998). Notably, in humans mutations in either the *PEX1* or the *PEX6* gene are the most common cause for serious peroxisomal biogenesis disorders (Geisbrecht *et al.*, 1998).

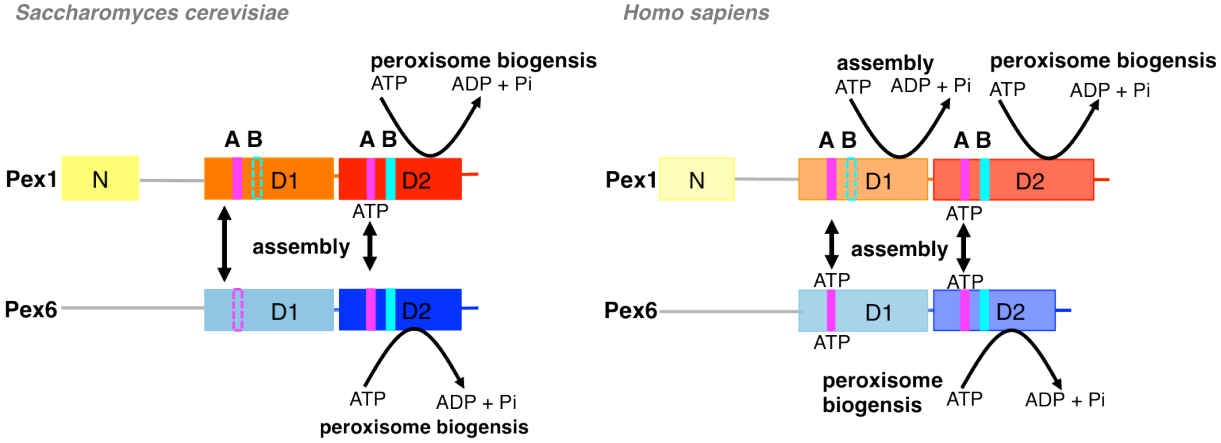

Figure 1.6 Comparison of ATP dependent functions of *S. cerevisiae* and human Pex1 and Pex6 proteins. Assembly of *S. cerevisiae* Pex1/Pex6 is mediated through Pex1 or Pex6 D1 domains, accompanied by ATP binding to the Pex1 D2 domain. Functional complexes in yeast require ATP binding and hydrolysis in Pex1/Pex6 D2 domains (left). Complex assembly of human Pex1/Pex6 relies on hydrolytic activity in Pex1 D1 and nucleotide binding to Pex1 D2 and Pex6 D1/D2 domains. Peroxisome biogenesis in humans is maintained through ATP binding to Pex6 D1 and nucleotide hydrolysis in Pex1/Pex6 D2 domains (right).

To date, only a few heterohexameric AAA+ protein complexes have been identified. Besides Pex1/6, DNA helicases Ruvb1/Ruvb2 (Lakomek *et al.*, 2015), proteasomal Rpt ATPases (Bar-Nun and Glickman, 2012) and the mitochondrial Yta10/Yta12 complex (Augustin *et al.*, 2009) assemble into active AAA+ type I and type II heterohexamers. While for most of those AAA+ complexes structural analyses are available (Lee *et al.*, 2011; Lander *et al.*, 2012), revealing significant ATP dependent conformational dynamics, comparable studies for full-length Pex1/6 do not yet exist.

1.6 Scope of Pex1/6 at the peroxisomal membrane

The dual localization of the Pex1/6 complex, switching between the cytosol and the outer peroxisomal membrane (Rosenkranz *et al.*, 2006), points towards certain molecular dynamics and structural flexibility. The authors suggest that the Pex1/6 complex assembles in the cytosol and navigates to the peroxisomal exterior upon interaction with integral membrane protein Pex15. The latter is exclusively localized to the peroxisomal membrane (Elgersma *et al.*, 1997) directing most of its protein sequence towards the cytosol, whereas the C-terminus faces the peroxisomal lumen (Figure 1.3). Birschmann et al. (2003) demonstrated direct association of the Pex15 cytosolic domain with the Pex6 N-terminus, including a dual role of nucleotide binding and hydrolysis, most likely regulating attachment and release of the Pex1/6 complex from the peroxisomal membrane. The study suggests that nucleotide binding to Pex6 D1 stimulates interaction with Pex15, whereas hydrolysis activity in Pex6 D2 triggers detachment of the Pex1/6 complex. Notably, communication of the AAA+ complex with Pex15 solely occurs via Pex6 and is independent of Pex1. Obviously, recruitment of the Pex1/6 complex depends on nucleotide occupancy and hydrolytic activity of Pex6 AAA+ domains and an N-terminal conformation allowing flexible alteration between a membrane bound and an unbound arrangement of Pex1/6.

Interaction with Pex15 links Pex1/6 complexes to the import of peroxisomal matrix proteins during which Pex1/6 relocates the cargo-free PTS1 receptor Pex5 to the cytosol (see section 1.3.1). Earlier reports could show that the cellular distribution and localisation of human Pex5 is ATP dependent (Dodt and Gould, 1996). Follow up studies demonstrated that docking of cargo-associated Pex5 with the peroxisomal membrane is ATP independent, whereas recycling of Pex5 requires ATP (Gouveia *et al.*, 2003). Subsequently, yeast and human Pex1 and Pex6 were connected to the extraction of Pex5 from peroxisomal membranes (Miyata and Fujiki, 2005; Platta *et al.*, 2005). Approaches to delineate the role of *S. cerevisiae* Pex1/6 during recycling of Pex5 included *in vitro* export systems (Platta *et al.*, 2005). The authors found ubiquitination of Pex5 at the peroxisomal membrane as crucial feature for Pex1/6 dependent receptor export (Figure 1.3). Furthermore, ATP binding and hydrolytic activity in D2 domains of both, Pex1 and Pex6, are essential for Pex5 dislocation (Platta *et al*., 2005). Otherwise, ubiquitinated Pex5 stays associated to the membrane. Since compromised ATP hydrolysis in Pex1 D2 does neither affect assembly with Pex6 nor interferes with Pex15 mediated linkage to the outer peroxisomal membrane, hydrolytic function might be attributed specifically to Pex5 release. Thus, the energy of ATP hydrolysis generated in Pex1/6 complexes is believed to structurally remodel Pex5 in order to liberate the receptor from its membranous environment (Grimm *et al.*, 2012). As demonstrated in pull down assays, Pex1/6 co-purifies a multicomponent assembly, comprised of Pex15, Pex5, Pex8 and factors of the

docking and RING-domain containing subcomplexes (Rosenkranz *et al.*, 2006). However, direct interaction between the Pex1/6 complex and Pex5 has not been observed so far. Hence, either adaptor proteins or post-translational modifications (e.g. ubiquitination) might initiate and control Pex5 export (Kiel *et al.*, 2005a; Kragt *et al.*, 2005).

Concomitantly to or downstream of Pex5 release deubiquitinating (DUB) enzyme Ubp15 removes mono-ubiquitin moieties from Pex5 (Debelyy *et al.*, 2011). The authors show that connection of Ubp15 to the export process occurs through binding to the Pex6 D1 domain. Intriguingly, comparable interactions have been observed for AAA+ protein p97/Cdc48 and DUB enzymes VCIP135/Otu1, which modulate ubiquitin chains on substrate proteins for either recycling or proteasomal degradation (Jentsch and Rumpf, 2007; Meyer *et al.*, 2012).

Although polyubiquitination of aberrant Pex5 is attributed to different enzymes, previous studies suggest that Pex1/6 complexes also enhance export of polyubiquitinated Pex5 for subsequent targeting to the proteasome (Platta *et al.*, 2004; Kiel *et al.*, 2005a). Hence, the purpose of mono- or polyubiquitination of Pex5 can be separated in an essential intrinsic step of peroxisomal matrix protein import or in a quality control process through the proteasome-ubiquitin system (Thoms and Erdmann, 2006).

ATP consumption by Pex1/6 complexes supplies the overall energy required for the mechanical relocation of Pex5 to the cytosol, intimately linking import and export activities at the peroxisomal membrane. In order to gain further insight into the molecular mechanism of Pex1/6 complexes in action, structural studies of the AAA+ assembly could be of great significance.

1.7 Peroxisomal biogenesis disorders (PBDs)

To date, a remarkable number of yeast *pex* mutants, deficient in assembling functional peroxisomes, have been identified through genetic phenotype complementation approaches (Platta and Erdmann, 2007). This led inevitably to the determination of human Pex homologs using homology probing (Gould and Valle, 2000) or cloning of mammalian cDNA, functionally complementing phenotypes of peroxisome-deficient CHO cells (Fujiki *et al.*, 2006). As mentioned previously, peroxisomes host a plethora of essential ana- and catabolic reactions, which are crucial for cell survival from yeast to men (see section 1.2.1). Hence, malfunctioned peroxisome synthesis caused by defects in metabolic enzymes or biogenesis factors leads to organellar dysfunction in humans. Correspondingly, a heterogeneous group of severe, autosomal recessive disorders has evolved. As depicted in Figure 1.7, those diseases are clinically classified into two groups: (1) peroxisomal biogensis disorders and (2) isolated peroxisomal enzyme deficiencies (Steinberg *et al.*, 2006; Wanders and Waterham, 2006b).

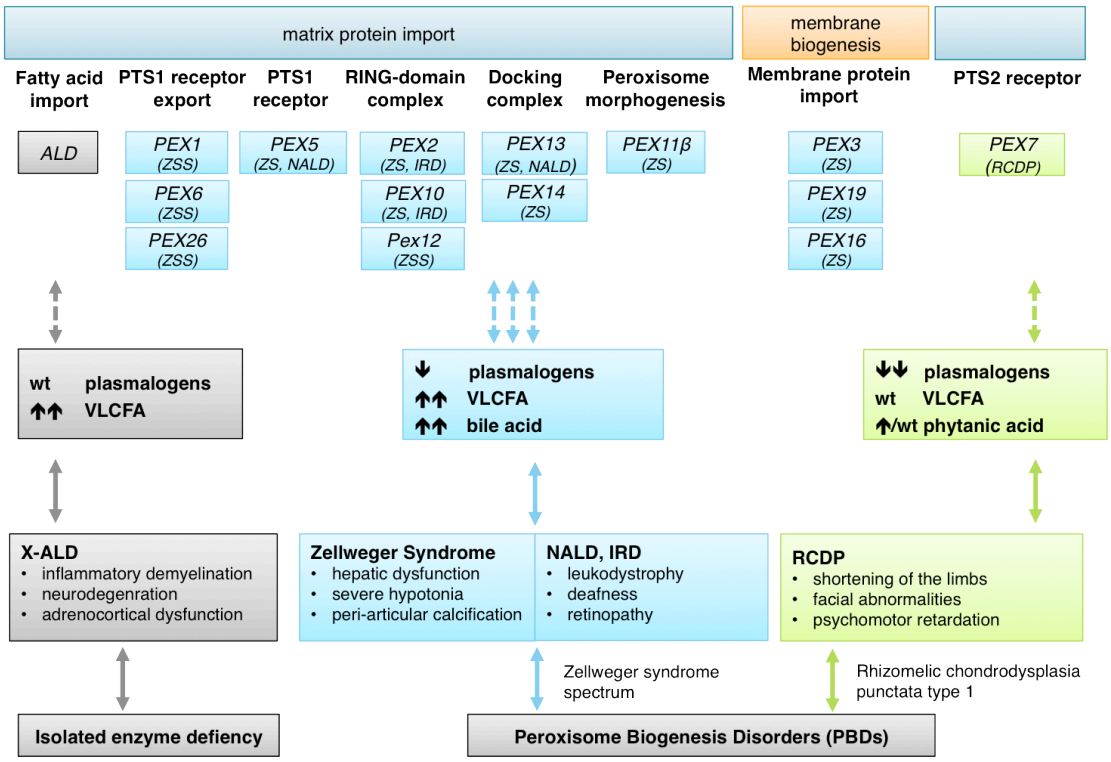

Figure 1.7 Overview of peroxisomal biogenesis disorders (PBDs). The diagram summarizes *PEX* genes corresponding to their cellular tasks, which are known to be aberrant in peroxisomal biogenesis disorders. Resulting clinical phenotype(s) of mutated *PEX* genes is given below (ZSS: Zellweger syndrome spectrum; ZS: Zellweger syndrome; NALD: neonatal adrenoleukodystrophy; IRD: infantile Refsum disease; RCDP: rhizomelic chondrodysplasia punctata). Biochemical markers linked to X-ALD (X-linked adrenoleukodystrophy), Zellweger syndrome, NALD, IRD or RCDP are shown as elevated (↑), decreased (↓) or wild type (wt) levels (VLCFA: very long-chain fatty acids). Specific clinical phenotypes of either X-ALD, the Zellweger syndrome spectrum or rhizomelic chondrodysplasia punctata type 1 are given in insets. Colour code is as follows: genotypes, biochemical or clinical phenotypes linked to X-ALD (grey insets), genotypes, biochemical or clinical phenotypes linked to ZS, NALD or IRD (light blue), genotypes, biochemical or clinical phenotypes linked to RCDP (light green).

Among single enzyme defects, mutations in the *ALD* gene, coding for human ABC transporter protein ALDP, are most frequently, causing X-linked adrenoleukodystrophy (Mosser *et al.*, 1993; Gartner, 2000). It mainly affects peroxisomes of the nervous system and the adrenal glands, where ADLP-dependent ABC transporters fail to actively supply peroxisomes with fatty acids. This in turn results in accumulation of saturated VLCFA in the plasma of adrenal cortex and inflammatory myelination defects (Berger and Gärtner, 2006).

Defects in peroxisomal biogenesis disorders (PBDs) trace back exclusively to mutations in the *PEX* gene family and a total of 14 complementation groups (CGs), covering 14 distinct human *PEX* genes, have been identified (Fujiki *et al.*, 2014). PBDs group in two subtypes, namely Zellweger syndrome spectrum (ZSS) and Rhizomelic chondrodysplasia punctata (RCDP) type 1 (Figure 1.7, Waterham and Ebberink, 2012).

RCDP patients suffer from a mutation in their *PEX7* gene (Braverman *et al.*, 2002; Motley *et al.*, 2002) that encodes the PTS2 receptor protein (see section 1.3.1). Thus, import of PTS2

type matrix proteins is impaired. Amongst others, metabolic consequences comprise increased levels of VLCFA, deficient ether lipid synthesis or impaired phytanic acid breakdown (Hoefler *et al.*, 1988). Hence, for diagnostic purposes levels of VLCFA, plasmalogens and phytanic acid could be determined either in patient's blood plasma or in established fibroblast cell lines. However, RCDP type 1 results in significant clinical phenotypes including shortening of proximal front bones (rhizomelia), abnormal facies or growth and psychomotor retardation (Wardinsky *et al.*, 1990). Since life expectancy ranges from 1 year up to young adulthood, RCDP could be considered as a milder form of peroxisomal biogenesis disorders.

Mutations in the remaining 13 PEX genes cause fatal diseases, which are biochemically and phenotypically distinct from RCDP. Those are collectively grouped into the Zellweger syndrome spectrum. The latter comprises three clinical disorders with highly similar phenotypes. Those are the Zellweger syndrome (ZS), neonatal adrenoleukodystrophy (NALD) and infantile Refsum disease (IRD), with ZS being the most and IRD the least severe disorder (Waterham and Ebberink, 2012)

At least 70 % of all ZSS patients harbour a mutation in *PEX1* (Steinberg *et al.*, 2006). The human AAA+ protein is a functional ortholog of *S. cerevisiae* Pex1, thus essential for peroxisomal matrix protein import and Pex5 export upon interaction with human Pex6 (Dodt and Gould, 1996; Tamura, 1998). Hence, protein import into peroxisomes is compromised and peroxisomal matrix proteins are mislocalised to the cytosol. Up to 90 different mutations have been identified in human *PEX1* (Ebberink *et al.*, 2011). However, two altered alleles are most frequently found in ZSS patients: I700fs and G843D (Reuber *et al.*, 1997; Collins and Gould, 1999). The I700fs allele is related to decreased mRNA levels resulting in a complete loss of *PEX1* function (null allele). In contrast, *Pex1*G834D results in a temperature-sensitive phenotype with limited binding of *Pex1*G834D to human Pex6 (Imamura *et al.*, 1998). Notably, respective patients are typically mildly affected. Clinical phenotypes strongly depend on the corresponding genotypes, since patients homozygous for *Pex1*I700fs typically do not survive the first year of life (Poll-The *et al.*, 2004), whereas *Pex1*G843D hetero- or homozygosity displays intermediate or mild clinical phenotypes (Majewski *et al.*, 2011). *PEX1* deficiency affects matrix protein import and thus, β-oxidation of (VLC) fatty acids and specifically bile acid intermediates. Consequently, elevated levels of VLCFA or bile acid serve as diagnostic disease markers in customized screens (Johnson *et al.*, 2001). Based on phenotypic heterogeneity, pathologies of *PEX1* mutations cover the whole spectra of ZSS (ZS, NALD, IRD), including profound hypotonia, hepatic malfunction, deafness, degeneration of myelin and respiratory complications (Figure 1.7).

Deficiencies in human *PEX6* are the second most common cause for ZSS disorders (Waterham and Ebberink, 2012). However, there is no evidence for a common defect in Pex6 and mutations occur along the entire *PEX6* coding sequence, accumulating in exon 1

(Ebberink *et al.*, 2010). Notably, *PEX6* mutations, which were identified in 21 ZSS patients, imply modifications causing premature stop codons (Steinberg *et al.*, 2004). Moreover, in studies of *PEX6* mutant CHO cell lines, a temperature-sensitive phenotype was observed, possibly reflecting a similarly mild clinical progression as for *Pex1*G834D (Imamura *et al.*, 2000). The metabolic consequences of *PEX6* defects reflect those described for *PEX1* mutations. Hence, for diagnostic purposes levels of VLCFA, plasmalogens and bile acid could be determined either in patient's blood plasma or in established fibroblast cell lines. Patients with an aberrant *PEX6* develop clinical features associated to ZS and NALD, which are craniofacial abnormalities, leukodystrophy, dysfunction of neuronal migration or seizures and spasticity (Figure 1.7).

Besides *PEX1* and *PEX6*, additional mutations in *PEX* genes associated with either an import defect (*PEX5*, *PEX26*, *PEX2*, *PEX10*, *PEX12*), reduced peroxisomal proliferation (Pex11β) or impaired membrane development (*PEX3*, *PEX19*, *PEX16*) have been identified and linked to ZSS (Fujiki *et al.*, 2014).

1.8 The molecular functions and structures of AAA+ protein complexes

The family of AAA (ATPases associated with divers cellular activities) proteins was found based on sequence homology of the nucleotide binding regions of their early members, including Pex1/Pex6, p97, NSF and TBP-1 (Erdmann *et al.*, 1991; Kunau *et al.*, 1993). AAA proteins are P-loop NTPases and unifying signature sequences are the Walker A and Walker B motif, which interact with incoming nucleotides (Walker *et al.*, 1982). Following systematic sequence analyses and structural comparison of proteins homologous to the AAA family resulted in an extended class of evolutionary related AAA proteins, designated AAA+ superfamily (ATPases associated with various cellular activities; Neuwald *et al.*, 1999). Despite functional specialisation, a common theme of AAA+ proteins includes assembly into large, macromolecular machines, structurally remodelling proteins or oligonucleotides with mechanical force derived from ATP utilization (Tucker and Sallai, 2007).

1.8.1 Topology of the nucleotide binding domain

In AAA+ proteins, nucleotide binding takes place at a homologous protein domain that is present once in type I AAA+ proteins, whereas type II AAA+ proteins consist of two nucleotide binding domains (Figure 1.8 A; Patel and Latterich, 1998). It was shown that the preceding N-terminal domains of some AAA+ complexes engage with adaptor proteins (Birschmann *et al.*, 2003; Dreveny *et al.*, 2004). The ATPase domain is composed of an α/β core domain, followed by a small C-terminal, α-helical subdomain (Figure 1.8 B, C; Erzberger

and Berger, 2006.). The large N-terminal α/β core features a central Rossmann fold, including five parallel β-sheets, which sequentially arrange in a 5-1-4-3-2 topology (Hanson and Whiteheart, 2005). The Rossmann fold comprises the Walker A motif, also called phosphate binding (P)-loop, which is formed by the consensus sequence GXXXXGK[T/S] (Walker *et al.*, 1982). The Walker A lysine is essential for nucleotide binding, coordinating the γ phosphate group of bound ATP thereby promoting catalysis (Ye *et al.*, 2004). Upon exchange to alanine, ATP binding to the ATPase domain is abrogated (Matveeva *et al.*, 1997; Babst *et al.*, 1998). Notably, Walker A mutations can also affect hexamerisation in type II AAA+ proteins (Schirmer *et al.*, 1998; Mogk *et al.*, 2003). The Walker B motif of AAA+ proteins contains two acidic amino acids, preceded by several hydrophobic residues (hhhhDE, Walker *et al.*, 1982). At the nucleotide binding pocket, Walker B aspartate coordinates the Mg^{2+} ion, whereas glutamate primes a water molecule for the subsequent nucleophilic attack on the ATP γ phosphate resulting in ATP hydrolysis (Iyer *et al.*, 2004). It was reported, that conservative mutations within the Walker B motif (D→N or E→Q) typically allow ATP binding but impair nucleotide hydrolysis (Weibezahn *et al.*, 2003; Dalal *et al.*, 2004). Hence, AAA+ proteins captured in an ATP bound state *in vitro* likely reflects the substrate-engaged state *in vivo*, which can be very useful to investigate the functions of AAA+ complexes.

Zhang and Wigley (2008) demonstrated in a comprehensive analysis of AAA+ crystal structures that binding of ATP induces a switch in the Walker B glutamate from an active into an inactive state (glutamate switch). The authors propose a model in which hydrogen bonds of a neighbouring β2 asparagine attract the glutamate, thereby withdrawing the acidic residue from the nucleotide-binding pocket. Thus, ATP hydrolysis would not occur until interactions with the substrate are fully established.

Studies of Walker B mutations in mammalian NSF revealed significant differences between amino acid changes in either the D1 or D2 domain (Whiteheart *et al.*, 1994). While alterations in the D1 domain drastically reduce ATP turnover, equivalent mutations within the D2 domain only slightly disturbs hydrolytic activity. Thus, the authors concluded a separation of function between D1/D2 domains, divided into an oligomerisation domain (D2) and a hydrolysis active domain (D1), which was also discovered for other type II ATPases in subsequent studies (Schlee *et al.*, 2001; Nishikori *et al.*, 2011). However, the responsibility of individual AAA+ domains concerning catalytic activity and oligomerisation varies among AAA+ proteins. While murine p97 D1 domain is crucial for ATP dependent hexamerisation (Wang *et al.*, 2003), the D2 is the major site of p97 ATPase activity (Song *et al.*, 2003). Within the central Rossmann fold the Walker A and Walker B motif locate at the N-terminal end of α1 and in β3, respectively (Figure 1.8 B, C).

Additionally, a conserved sensor motif (sensor 1) was identified C-terminally of the Walker

motifs positioned in the connecting loop between β4 and α4, likely participating in intra-subunit communications and nucleotide hydrolysis (Guenther *et al.*, 1997; Hattendorf and Lindquist, 2002). In crystal structures of AAA+ proteins, polar sensor 1 residues (TN) align between the Walker A and Walker B motif, oriented towards the nucleotide binding pocket (Wendler *et al.*, 2012). Sensor 1 mutations eliminate enzymatic activity of corresponding AAA+ proteins (Zhao *et al.*, 2010). The location of the sensor 1 motif designates the beginning of another highly conserved stretch, named the second region of homology (SRH, Lupas and Martin, 2002).

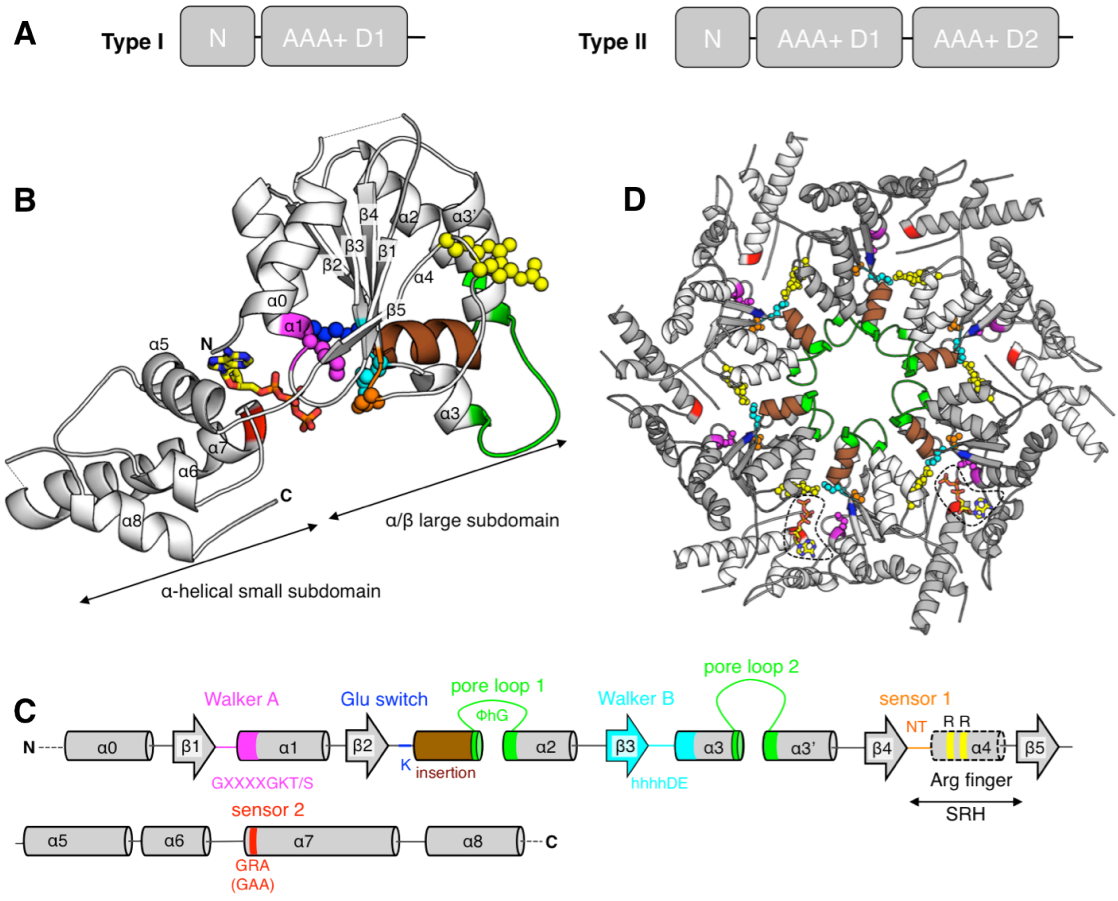

Figure 1.8 Organization and structure of the AAA+ nucleotide-binding domain. (A) Domain organization: Type I AAA+ proteins have one nucleotide-binding domain (AAA+ D1) while type II AAA+ proteins comprise two ATPase domains in one polypeptide chain (AAA+ D1/D2), each preceded by a N-terminal domain. (B) Crystal structure of an individual p97 D2 AAA+ protein domain (pdb-ID: 3CF3). Highly conserved structural elements are indicated according to the colour code in (C). As a member of the classic AAA clade, p97 contains an alanine instead of an arginine within its sensor 2 motif and the conserved glutamate switch aspartate is replaced by lysine. Nucleotide (ATP) derives from an FtsH crystal structure (pdb-ID: 2CEA). (C) Secondary structure according to the p97 crystal structure in (A), showing the position of key residues and corresponding consensus sequences. (D) p97 D2 domain depicted as full hexamer. Individual AAA+ subunits are colored alternately white and grey with functional key residues highlighted as in (B). Two ATP molecules, highlighted by black dashed lines, exemplify positions of nucleotide.

Besides the sensor 1 motif, the SRH contains conserved arginine residues, termed arginine fingers, which contribute to overall ATPase activity and complex stability of functional AAA+ oligomers (Ogura *et al.*, 2004). In AAA+ assemblies arginine fingers stabilize the emerging negative charge upon ATP hydrolysis in opposing AAA+ protomers, sustaining the organization of ATP binding pockets at subunit interfaces (Karata *et al.*, 1999). While two arginine fingers are present in classic AAA proteins, only one is conserved throughout the superfamily of AAA+ proteins (Wendler *et al.*, 2012). Those arginine residues are situated between α4 and β5 of the large, central α/β subdomain (Figure 1.8 B, C).

Likewise, the small α-helical domain, C-terminally of the Rossmann fold, contains a conserved arginine residue, described as sensor 2 motif (Muller and Schulz, 1992). In classic AAA proteins this arginine residue is replaced by an alanine (Neuwald *et al.*, 1999). The sensor 2 residues (GAR) are positioned in α7 and contribute to ATP hydrolysis. Thus, mutations disturb nucleotide turnover, sometimes related to compromised ATP binding (Ogura *et al.*, 2004). Surprisingly, mutational studies in ClpX demonstrated that the region around the sensor 2 motif in helix α7 is essential for substrate unfolding (Joshi *et al.*, 2003). Correspondingly, domain motions of the C-terminal, helical subdomain relative to the large α/β core domain around the connecting hinge have been confirmed in subsequent crystal structures of ClpX (Glynn *et al.*, 2009).

AAA+ proteins have been analysed extensively in structural studies, revealing examples of pentameric (Simonetta *et al.*, 2009), hexameric (DeLaBarre and Brunger, 2003) and heptameric (Lee *et al.*, 2003b) arrangements of identical subunits in AAA+ holoenzymes. Upon oligomerisation, ATP biding sites are positioned at the interfaces between individual AAA+ subunits and most, if not all AAA+ oligomers feature a central pore (Figure 1.8 D). Furthermore, it was reported that substrate interactions occur via conserved pore loops, which line the central channel of AAA+ complexes (Yamada-Inagawa *et al.*, 2003; Lum *et al.*, 2004; Siddiqui *et al.*, 2004). Thus, substrate processing is inevitably linked to the assembly of individual AAA+ subunits into active oligomers. Many AAA+ proteins comprise an aromatic-hydrophobic-glycine (ϕhG) pattern in the substrate-binding loop region 1, positioned before helix α2. Additionally, substrate interacting residues line pore loop region 2, arranged in helix α3 (White and Lauring, 2007). Upon hexamerisation, substrate-binding pore loops face towards the symmetry axis of the AAA+ complex (Figure 1.8 D). It was reported that in AAA+ translocase ClpX or chaperone ClpB those central pore residues are crucial for an unfolding-coupled translocation of substrate proteins (Weibezahn *et al.*, 2004; Martin *et al.*, 2008). However, details concerning underlying molecular mechanisms are still fragmentary.

1.8.2 From structure to mechanism

Established through comprehensive analyses of sequence-based relationships and juxtaposition of available crystal structures of the AAA+ core domains, AAA+ proteins are classified in distinct clades (Iyer *et al.*, 2004; Ammelburg *et al.*, 2006; Erzberger and Berger, 2006; Wendler *et al.*, 2012). AAA+ assemblies group into 4 basic clusters: the PACTT group/PSI superclade (including H2-insert, PS-II insert and HCLR clade), the extended AAA group/classic clade, the HEC group (including clamp loader and initiator clade) and the helicase superfamily III.

Pex1/Pex6 AAA+ proteins belong to the extended AAA group, together with other type I or type II ATPases, like p97/Cdc48, NSF/Sec18, ClpA and ClpB-type of proteins, bacterial protease FtsH, proteasomal Rpt proteins, Rubisco activase or members of the katanin family (Erzberger and Berger, 2006). AAA+ modules of the classic group have two arginine fingers but lack a canonical sensor 2 motif (Figure 1.8 B-D; Wendler *et al.*, 2012). Members of the classic clade function in a variety of cellular tasks, including peroxisome biogenesis (Pex1, Pex6; Erdmann *et al.*, 1991, Voorn-Brouwer *et al.*, 1993), ER-associated degradation (ERAD) of misfolded or damaged proteins (p97/Cdc48; Meyer and Weihl, 2014), homo- and heterotypic membrane fusion (NSF/Sec18; Wilson *et al.*, 1989, Püschel *et al.*, 1994), microtubule-severing in mitosis/meiosis or flagellar physiology (katanin; Quarmby, 2000), protein disaggregation (Hsp104/ClpB; Sanchez and Lindquist, 1990), or protein proteolysis (ClpAP or FtsH, Figure 1.9; Ogura and Wilkinson, 2001).

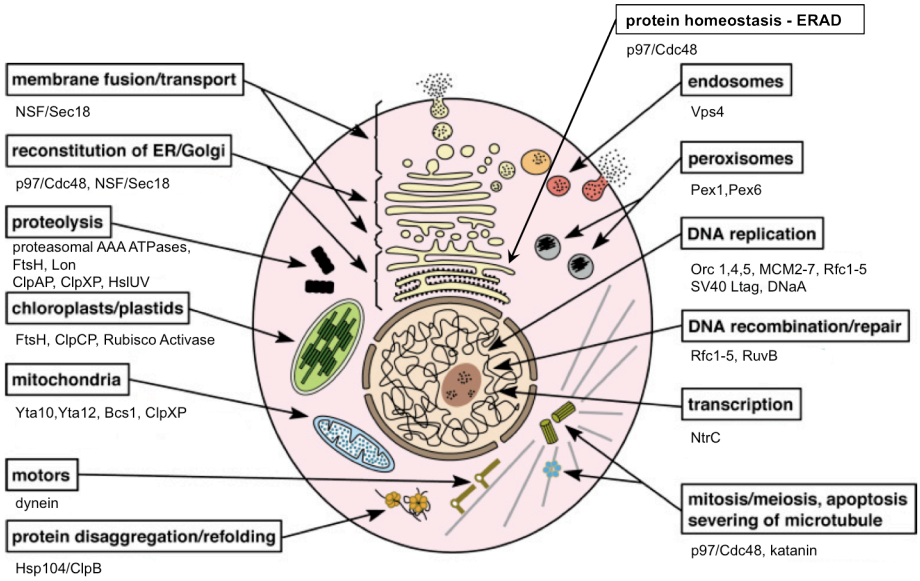

Figure 1.9 Functions and subcellular localization of AAA+ proteins. Representation of a schematic eukaryotic cell, including cell compartments and multiprotein complexes (adapted from Ogura and Wilkinson, 2001). Canonical functions of individual AAA+ proteins are indicated, including prokaryotic members.

Despite variegated subcellular localizations and low functional similarities, AAA+ complexes generally consume ATP to power reactions, which are certainly linked to substantial conformational remodelling of substrate proteins (Tucker and Sallai, 2007). Proficient enzymatic processivity of AAA+ proteins depends on oligomerisation into ring shaped assemblies, most frequently hexamers (Singh and Maurizi, 1994; Whiteheart *et al.*, 1994; Krzewska *et al.*, 2001; Mogk *et al.*, 2003; Greenleaf *et al.*, 2008). Negative stain and cryo electron microscopy (EM) studies demonstrated that AAA+ proteases ClpA and ClpX translocate target proteins through their central pore towards the peptidase chamber of ClpP for final protein degradation (Ortega *et al.*, 2000; Ishikawa *et al.*, 2001). Since early crystal structures of related AAA+ protein NSF or p97 depicted narrow central pores (Lenzen *et al.*, 1998; Zhang *et al.*, 2000), which would restrict the entry to the inner channel of even smallest folded proteins, biochemical studies investigated and verified the capacity of ClpA and ClpX to mechanically unravel fully folded substrate structures (Hoskins *et al.*, 1998; Singh *et al.*, 2000). Substrate unfolding is linked to another characteristic feature shared among ATPases of the extended AAA group. Those members contain a small helical insertion before helix α2 within the AAA core domain (Erzberger and Berger, 2006), which is directed towards the central axis in hexameric complexes (Figure 1.8 B-D). This accessory, clade specific element was shown to be crucial for substrate specific enzymatic activity of hexameric AAA+ complexes ClpA and p97 (Hinnerwisch *et al.*, 2005; DeLaBarre *et al.*, 2006). Indeed, the α-helical insertion connects to or includes residues of pore loop 1, which contains a highly conserved axial aromatic-hydrophobic-glycine pattern ([Y/F/W][V/F/I]G) in many AAA+ proteins and protrudes from every AAA+ subunit into the central pore (Martin *et al.*, 2008). Comparative structural studies of bacterial protease HslU by Wang *et al*. (2001) proposed for the first time that a conserved tyrosine residue in pore loop 1 transmits nucleotide dependent movements of the hexameric AAA+ ring to the substrate protein, resulting in an unfolding-coupled translocation mechanism. The authors suggest that HslU threads target substrates through the central pore concurrently unfolding target protein structures. Follow-up studies on HslU (Park *et al.*, 2005) and related prokaryotic proteases ClpX (Siddiqui *et al.*, 2004; Martin *et al.*, 2008) or FtsH (Yamada-Inagawa *et al.*, 2003) confirmed that conserved axial pore residues are associated with substrate binding and/or threading coupled to ATP turnover. Likewise, biochemical analyses could show that hexameric type II AAA+ oligomers ClpB or Hsp104 actively translocate substrate molecules through their central pore (Weibezahn *et al.*, 2004; Tessarz *et al.*, 2008). Furthermore, mutations of those tyrosines within substrate binding loop regions in ClpB/Hsp104 compromise substrate recognition and processing, hinting at a substantial contribution of those residues in translocation (Lum *et al.*, 2004; Weibezahn *et al.*, 2004; Tessarz *et al.*, 2008).

Cross-linking studies of type II AAA+ protein ClpA have demonstrated that substrate proteins

directly engage with tyrosines of three substrate-binding loop regions, arranged along the pore of ClpA D1 and D2 (Hinnerwisch *et al.*, 2005). The authors show that particularly mutations of the functional tyrosine in the ClpA D2 domain allow direct binding of substrate protein concomitantly blocking translocation and unfolding of the polypeptides. Hence, Hinnerwisch and colleagues suggest that the attachment of substrate proteins depends on interaction with all three axial pore loops but translocation is driven by out of plane movements of the more active D2 domain along the central axis upon ATP hydrolysis.

Also, p97 actively interacts with target molecules via substrate-binding loop 2 in the D1 domain (Figure 1.10; DeLaBarre *et al.*, 2006). Furthermore, the authors demonstrated that non-conservative mutations of aromatic residues within pore loops of p97 D1 or D2 significantly affected p97 function in ERAD. Reminiscent of ClpA, a functional aromatic residue of p97D2 undergoes large conformational changes along the pore axis upon ATP hydrolysis, highlighted by structural comparison of ADP and AMPPNP bound p97 crystal structures (DeLaBarre *et al.*, 2006), However, a threading mechanism has not yet been shown for p97. Furthermore, DeLaBarre and colleagues propose that target polypeptides cannot enter the narrow central pore of the p97 D1 domain.

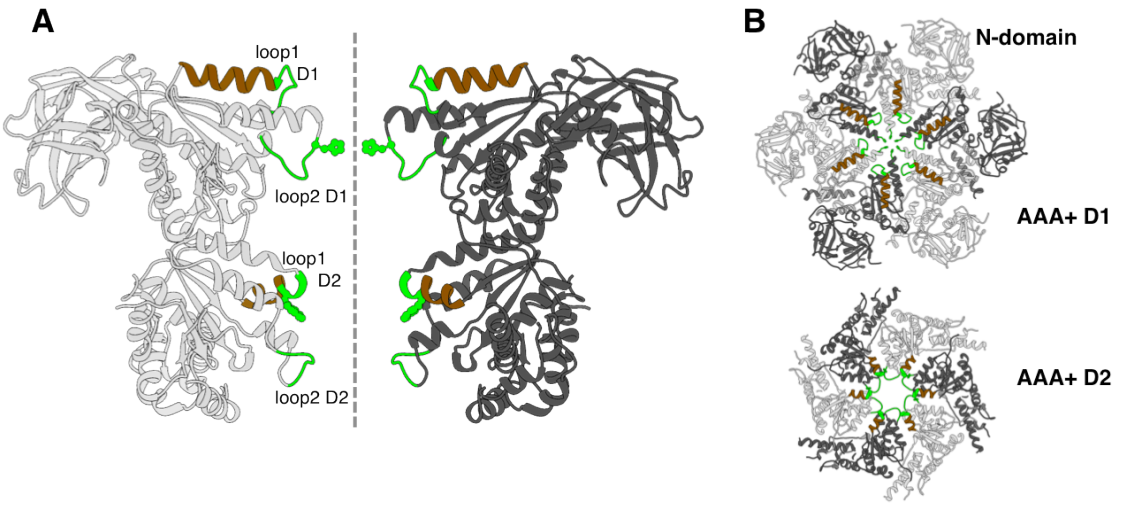

Figure 1.10 Localisation of substrate-interacting pore loops in p97. (A) Side view cartoon representation of p97 (pdb-ID: 3CF3). Two opposing protomers of the p97 hexamer are shown. Pore facing loops are highlighted in green and grey dashed line indicates central symmetry axis. Structural elements of p97 are colored according to Figure 1.8. Aromatic residues $p97^{H317}$ and $p97^{W551}$ are depicted as green spheres. (B) Cartoon representation of p97 D1 and D2 cross-section views (pdb-ID: 3CF3). Aromatic residues $p97^{H317}$ and $p97^{W551}$ are shown as green sticks.

Subsequent structural characterisations of p97 led to a model in which the energy of nucleotide hydrolysis is transmitted via long-range conformational changes from D1 and D2, respectively, to the N-terminal domains, which interact with substrate proteins (Davies *et al.*, 2008). In contrast, recent cryo-EM studies propose a threading mechanism for Cdc48, the archeal ortholog of p97 (Barthelme *et al.*, 2014).

Movements of substrate-binding elements are likely connected to the hydrolytic activity in individual AAA+ subunits. Four models of ATP turnover have been proposed in order to describe the coordination of hydrolysis cycles among hexameric AAA+ arrangements and thus substrate translocation: stochastic, rotational, sequential or synchronized/concerted ATP hydrolysis (Figure 1.11 A, Lyubimov *et al.*, 2011). Differences in nucleotide occupancy coupled to the arrangement of ATPase sites visualized through structural studies support one mode of "firing" or another.

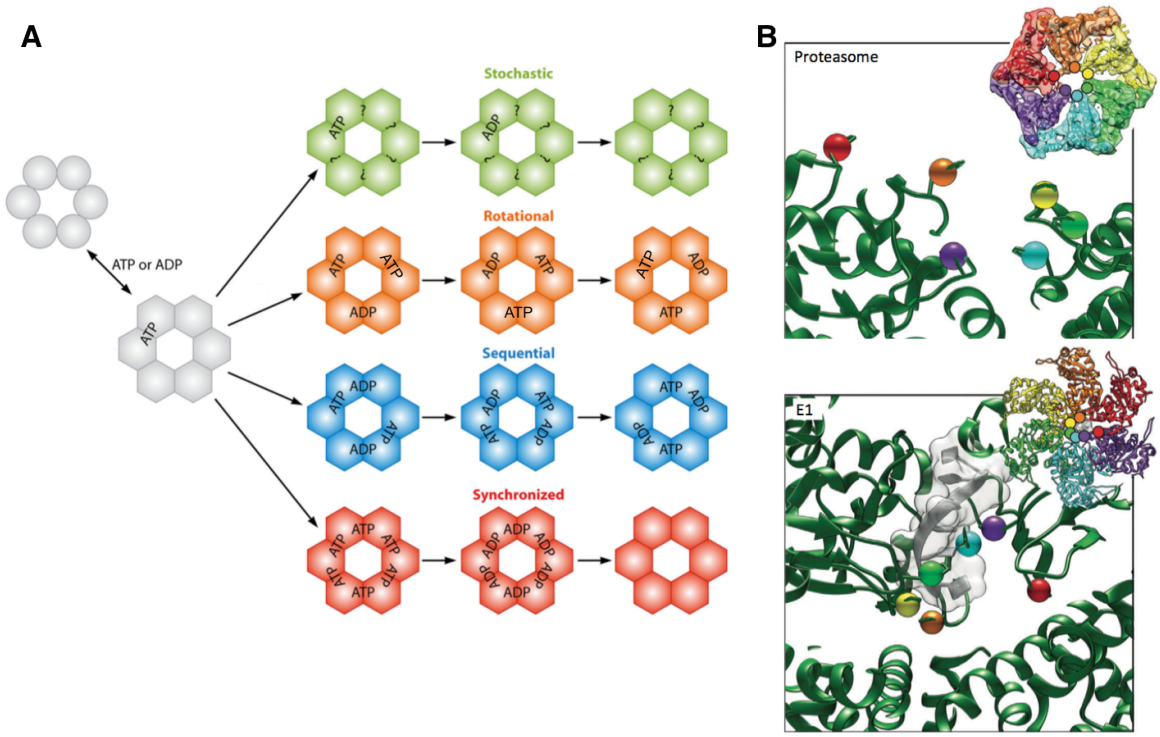

Figure 1.11 Models for coordination of NTP hydrolysis and nucleotide dependent arrangement of poor loops in AAA+ hexamers. (A) In the stochastic/probabilistic model, ATP binding (ATP) and hydrolysis (ADP) occurs in monomers independent of residual protomers (?). In the rotational model, only three subunits are active at different stages of the reaction cycle. Sequential nucleotide binding and hydrolysis occurs at six active ATPase sites proceeding from one neighbouring protomer to the next along the ATPase ring. Synchronized ATP binding and hydrolysis happens at all ATPase sites at the same time (adapted from Bush and Dixon, 2012). (B) Exposure of asymmetrically arranged pore or DNA-binding loop residues in either the base subunits of the substrate-bound 26S proteasome or the E1 helicase bound to DNA (adapted from Nyquist and Martin, 2014).

In the presence of different nucleotides, virtually all crystal structures of p97 show a homogeneous nucleotide occupancy in the hexamer (Zhang *et al.*, 2000; Huyton *et al.*, 2003; Davies *et al.*, 2008). p97 assembles in symmetric ring structures featuring a tight arrangement of AAA+ domains (Figure 1.10 B). Hence, a concerted model for ATP hydrolysis can be assumed, in which all protomers bind and hydrolyse nucleotide simultaneously. Notably, in the presence of the transition state analogue ADP-AlFx, p97 shows an unequal nucleotide loading in the D2 domain (DeLaBarre and Brunger, 2005). While the D1 domain is

permanently occupied by ADP (Huyton *et al.*, 2003), ATP binding and hydrolysis in p97 D2 could rather follow a rotary sequence.

In line with concerted nucleotide binding and hydrolysis in p97, structural and biochemical data available for related AAA+ proteins NSF and SV40 Ltag propose a concerted mechanism of nucleotide turnover (Gai *et al.*, 2004; Zhao *et al.*, 2012). Accordingly, it was suggested that ATP binding and hydrolysis mainly levers substrate-interacting loops locally up and down the central ring axis without significantly changing the relative orientations of the protein domains (Gai *et al.*, 2004; DeLaBarre and Brunger, 2005). In contrast, Wendler *et al.* (2009) could show that hydrolysis competent Hsp104 forms hexameric complexes enclosing a large central cavity, deviating from the inter-locked arrangement observed in crystal structures of related AAA+ proteins, indicating remarkable conformational switching dynamics while cycling through different nucleotide states. Accordingly, these and related cryo-EM studies of NSF (Chang *et al.*, 2012) or p97 (Rouiller *et al.*, 2002) revealed a global conformational flexibility of the AAA+ subunits in the hexamer during the ATPase cycle, inducing nucleotide dependent domain movements of entire AAA+ sites within one ring and/or relative to the second ring.

Sub-stoichiometric or mixed nucleotide occupancy of AAA+ domains has been observed in structural studies of homohexameric AAA+ proteases HslU and ClpX or enhancer binding protein PspF (Bochtler *et al.*, 2000; Wang *et al.*, 2001; Martin *et al.*, 2005; Stinson *et al.*, 2013), suggesting rather a rotational or sequential model for the ATPase cycle. Notably, Stinson *et al*. (2013) also provide structural and biochemical data supporting a stochastic/probabilistic mechanism for ATP turnover and function in ClpX, in which hydrolysis events would occur independently at individual protomers.

Despite full nucleotide loading, asymmetric arrangements of individual AAA+ domains within hexameric assemblies of protease FtsH (Suno *et al.*, 2006), papillomavirus E1 helicase (Enemark and Joshua-Tor, 2006; Sanders *et al.*, 2007) or related RecA-like protein T7 gp4 helicase (Singleton *et al.*, 2000) have been observed, further supporting rotational or sequential rounds of NTPase activity and indicating a preferred order of nucleotide states.

Additionally, crystal structures of ClpX and HslU demonstrate that individual ATPase domains hold a certain degree of freedom, allowing the small α-helical subdomains to move flexibly relative to the corresponding central α/β large subdomain around the connecting hinge (Wang *et al.*, 2001; Glynn *et al.*, 2009). Thus, protomer interfaces change during the ATPase cycle, likely allowing directed intersubunit communication in order to coordinate accurate substrate processing. Similar results were obtained in symmetry-free cryo-EM reconstructions of Hsp104, depicting altered subunit interfaces resulting in protomer conformations that suggest varying nucleotide states within the homohexamer, hinting at sequential ATP consumption (Wendler *et al.*, 2009). However, as most type I or type II AAA+ complexes are homo-oligomers, the characterization of inter-domain and intra-domain

communication between AAA+ domains has been difficult to address. Primary studies are reported on the heterohexameric type I AAA+ Yta10/Yta12 complex (Augustin *et al.*, 2009). The authors show that the protomers arrange in an alternating fashion, allowing mutational studies in only a subset of AAA+ domains and thus, examining possible protomer-protomer communications. Their results demonstrate that the nucleotide state of one subunit type (Yta12) influences ATP turnover in adjacent subunits (Yta10). Augustin *et al*. (2009) propose a model in which regulated ATP hydrolysis in adjoining Yta10/Yta12 subunits results in a rotational power stroke of pore loop 1, unfolding and translocating the polypeptide through the pore by rotational substrate hand-off. However, whether such mechanism applies to related AAA+ proteins has to be examined further.

Still, it is not known whether substrate-interacting pore loops move only locally in order to thread the substrate along the pore or nucleotide dependent movements of entire subunits participate in the translocation process. Single particle analyses of actively translocating 26S proteasomes or functional NSF complexes demonstrate that the AAA+ rings accommodate a distorted symmetry (Matyskiela *et al.*, 2013; Zhao *et al.*, 2015), resulting in a spiral arrangement of individual subunits (Figure 1.11 B). This domain organization is assumed to be functionally relevant for substrate processing. Comparable arrangements have been found in the E1 helicase and the RecA-type Rho or DnaB helicases (Nyquist and Martin, 2014). Single molecule studies on the translocation process of hexameric ClpX and pentameric ϕ29 packaging motor suggests that the hydrolysis cycle follows radially around the spiral staircase accompanied by prompt large-scale conformational changes of entire ATPase subunits, thereby escorting the substrate downwards the pore (Moffitt *et al.*, 2009; Aubin-Tam *et al.*, 2011; Maillard *et al.*, 2011; Chistol *et al.*, 2012). Subsequently, AAA+ domains would occupy the initial spiral arrangement ready for the next round of substrate translocation.

1.9 Aim of this study

AAA+ proteins Pex1 and Pex6 from yeast *S. cerevisiae* form nucleotide dependent heterohexameric complexes (Saffian *et al*., 2012). Pex1/6 use the energy from ATP turnover to dislocate the import receptor Pex5 from the peroxisomal membrane back to the cytosol (Platta *et al*., 2005). According to the export driven import model, ATP dependent release of Pex5 by Pex1/6 is coupled to cargo translocation across the peroxisomal membrane and thus sustains the overall energy requirement of matrix protein import into peroxisomes (Schliebs *et al*., 2010). Previous studies established that functional D2 domains of Pex1 and Pex6 are essential to act on Pex5 and maintain peroxisome biogenesis (Birschmann *et al*., 2003; Birschmann *et al*., 2005; Platta *et al*., 2005). Proteins from the AAA+ family typically assemble into large, macromolecular protein complexes, structurally remodelling their substrate proteins using the energy from ATP consumption (Tucker and Sallai, 2007). It was shown for several AAA+ proteins that substrate processing involves a threading mechanism through the central pore of assembled complexes (Weibezahn *et al.*, 2004; Hinnerwisch *et al.*, 2005; Martin *et al.*, 2008; Tessarz *et al.*, 2008). However, details concerning the functional mechanism or structural architecture of AAA+ complex Pex1/6 are still fragmentary.

In this study, we solve the three-dimensional structure of the Pex1/6 complex from *S. cerevisiae* using negative stain electron microscopy (EM). In order to obtain satisfactory protein concentrations for structural analysis part of this study includes developing a strategy for the overexpression of recombinant Pex1 and Pex6 in *S. cerevisiae.* Our comprehensive EM analysis of Pex1/6 complexes in the presence of different nucleotides resolves intermediate steps of the ATPase cycle of Pex1/6, revealing energy creating conformational states, which could fit the model of Pex5 dislocation *in vivo*. Additionally, the overall architecture gives an explicit overview of substrate or adaptor interactions sites and their spatial arrangement around or within the AAA+ assembly. Structural analyses in combination with biochemical assays of Pex1/6 Walker B complexes demonstrate that the ATPase sites within the complex are functionally non-redundant and provide a profound insight on cooperativity or protomer-protomer communication within the Pex1/6 complex.

Our data provide a model, which might apply to the function and mechanism of Pex1/6 complexes in the human system. Hence, the here presented study could be of fundamental relevance in order to understand the molecular consequences of Pex1/6 dysfunction and thus, help to develop future therapeutic treatments for Zellweger patients.

2 Material and Methods

Unless stated otherwise, chemicals were of *pro analysis* quality and purchased from either Carl Roth GmbH + Co. KG (Karlsruhe), Fluka/Sigma Aldrich Chemie GmbH (Seezen), Merck (Darmstadt), Invitrogen GmbH (Karlsruhe), Roche Diagnostics GmbH (Mannheim) or VWR International GmbH (Darmstadt). Yeast and bacterial media components and supplements were purchased from ForMedium (Norfolk, UK). Liquid media were autoclaved 20 minutes at 120°C before use.

2.1 Oligonucleotides, plasmids, strains and culture conditions

2.1.1 Oligonucleotides

Oligonucleotides used in this study were purchased from Metabion International AG (Martinsried) and are listed in Table 2.1-2.4.

Table 2.1 Primers used in this study generating *PEX1*/*PEX6* galactose overexpression plasmids.

Name	Sequence (5' -> 3')	Restriction site(s)
PEX1-fwd	CGAACCAAGCTTATGACGACGA CCAAGAGGTTG	HindIII
deltaN-R189-PEX1-fwd	AAAAAAGCTTATGCGTTTGGTG AAGGCTGAG	HindIII
PEX1-rev	GCCGACTCTCCCTTATGGGATCC CAAC	BamHI
PEX6-Topo-fwd	AAAAGGTACCATGAAGGCATCG CTTACGTTT	KpnI
His_6-PEX6-Topo-fwd	AAAAGGTACCATGCATCATCAT CATCATCATAAGGCATCGCTTA CGTTT	KpnI
PEX6-Topo-rev	AAAAGGATCCAGCACCTTCAAA ATTAGC	BamHI
Spacer-TEV-ProtA-fwd	GATTCGGATCCGATTATGATATT CCAACTACT	BamHI
Spacer-TEV-ProtA-rev	TCCGCGGGGAAGTCAACCTGAG GATCCGCCG	BamHI
PEX1-D2-E798Q-fwd	CTATTTTTTGACCAATTCGATTC GATCGCGCCA	PvuI
PEX1-D2-E798Q-rev	TGGCGCGATCGAATCGAATTGG TCAAAAAATAG	PvuI
PEX6-D2-E832Q-fwd	TGTGTCATATTTTTTGATCAAAT CGATTCAGTAGCA	BclI
PEX6-D2-E832Q-rev	TGCTACTGAATCGATTTGATCAA AAAATATGACACA	BclI

Table 2.2 Primers used generating *PEX1*/*PEX6* plasmids for oleate growth assays.

Name	Sequence (5' -> 3')	Restriction site(s)
Prom-PEX1-Topo-fwd	AAAATCTAGATAATTCTATGTA ACCTCGATGGC	SacI
Prom-PEX1-Topo-rev	AAAACTCGAGTCAGGATCCCAT AAGGGAGAGTCGGCTACCAAT	BamHI and XhoI
Prom-PEX6-Topo-fwd	AAAATCTAGAAAGAACTTTATA TATCATGTAGC	XbaI
Prom-PEX6-rev	AAAAGGTACCTTAAGCACCTTC AAAATTAGC	KpnI
PEX1-D1-Y488A-fwd	CACATCTTCGTTAAAGCTGCAG ATTGTGAAACATTGC	PstI
PEX1-D1-Y488A-rev	GCAATGTTTCACAATCTGCAGC TTTAACGAAGATGTG	PstI
PEX1-D1-H495A-fwd	GCGGATTGTGAAACGCTAGCTG AGACATCAAATTTA	NheI
PEX1-D1-H495A-rev	TAAATTTGATGTCTCAGCTAGC GTTTCACAATCCGC	NheI
PEX1-D2-F771A-fwd	CAGAGATTTTAAACAAGGCGAT CGGTGCCAGCGAACA	PvuI
PEX1-D2-F771A-rev	TGTTCGCTGGCACCGATCGCCTT GTTTAAAATCTCTG	PvuI
PEX1-D2-R855K-fwd	TTAAGACCGGGAAAGCTTGACA AAAGTGTGATCTGT	HindIII
PEX1-D2-R855K-rev	ACAGATCACACTTTTGTCAAGC TTTCCCGGTCTTAA	HindIII
Pex1-D2-D797N-fwd	ATTCTATTTTTTaACGAGTTCGA TTCgATcGCGCCAAAG	PvuI
Pex1-D2-D797N-rev	CTTTGGCGCgATcGAATCGAACT CGTtAAAAAATAGAAT	PvuI
PEX6-D1-Y528A-fwd	ACATCTAAGATTATTGGCGCCA TTAGGGCTAAATGTG	NarI
PEX6-D1-Y528A-rev	CACATTTAGCCCTAATGGCGCC AATAATCTTAGATGT	NarI
PEX6-D1-R607K-fwd	GATAACGTGCCCTCGAGCTTTA AATCACATATGAGA	XhoI
PEX6-D1-R607K-rev	TCTCATATGTGATTTAAAGCTCG AGGGCACGTT ATC	XhoI
PEX6-D1-R611K-fwd	GATCACATATGAAATTTGAGAT CTTAGTACCCGTTC	BglII

Name	Sequence (5' -> 3')	Restriction site(s)
PEX6-D2-Y805A-fwd	GAACTGTTGAATATGGCGATCG GTGAGAGTGAAGCTA	PvuI
PEX6-D2-Y805A-rev	TAGCTTCACTCTCACCGATCGCC ATATTCAACAGTTC	PvuI
PEX6-D2-R892K-fwd	GCACTACTAAGCCCGGGAAAAT TCGATAAATTGTTA	SmaI
PEX6-D2-R892K-rev	TAACAATTTATCGAATTTTCCCG GGCTTAGTAGTGC	SmaI

Table 2.3 Primers used in this study to verify *PEX1* and *PEX6* deletion strains.

Name	Sequence (5' -> 3')
PEX1-confirmationA	ATGAGTCCATAATACTGTACTGGCG
PEX1-D	TATATATGCAACTTCGGATTTCGTT
PEX6-confirmationA	TCACTTGGATGAAAAATTACTGAAA
PEX6-D	AAAAGGTGTTGCTTCATATACCATC

Table 2.4 *PEX1* and *PEX6* sequencing primers used in this study.

Name	Sequence (5' -> 3')
Sequ-PEX1-1-fwd	CCCCGGATCGGACTACTAG
Sequ-PEX1-2-fwd	GCATTAAGCTCTCATCTTTG
Sequ-PEX1-3-fwd	CCAGATCATGAAACTAAAT
Sequ-PEX1-4-fwd	GGCAATGATAATATAGAATA
Sequ-PEX1-rev	CTGTGGCCAAAACAG GATTG
Sequ-PEX6-1-fwd	GAACAATATACGCACCTCCC
Sequ-PEX6-2-fwd	GCAATCAAATTACAAAAATC
Sequ-PEX6-3-fwd	GCAACAAACAGACCAGACTT
Sequ-PEX6-rev	GGTACTACATTGTCTAATATG

2.1.2 Plasmids

Plasmids and corresponding sources are listed in Table 2.5 and Table 2.6.

Table 2.5 Plasmids used in this study for Pex1/6 overexpression.

Plasmid	Description	Source / reference
pRS425-Gal1	*GAL1, LEU2, 2µ, Amp^r*	gift from C. Enenkel
pYES2	*GAL1, URA3, 2µ, Amp^r*	Invitrogen
pGEX-4T3-GST-*PEX1*^{E798Q}	*Amp^r, pBR322, Ptac:GST- PEX1^{E798Q}*	Maria Walker
pRS425-*PEX1*-TEV-ProA	*Amp^r, LEU2, 2µ, GAL:PEX1-TEV-ProA*	This study
pRS425-*PEX1^{E798Q}*-His6-TEV-ProA	*Amp^r, LEU2, 2µ, GAL:PEX1^{E798Q}-His6-TEV-ProA*	This study
pRS425-ΔN-R189-*PEX1*-His6-TEV-ProA	*Amp^r, LEU2, 2µ, GAL: PEX1-Δ188-His6-TEV-ProA*	This study
TOPO pCR2.1-PEX6	*Amp^r, Kan^r, pUC, f1, LacZα::PEX6*	This study
TOPO pCR2.1-His6-PEX6	*Amp^r, Kan^r, pUC, f1, LacZα::His6-PEX6*	This study
TOPO pCR2.1-His6-Spacer-TEV-ProA	*Amp^r, Kan^r, pUC, f1, LacZα::His6-Spacer-TEV-ProA*	This study
pYES2-*PEX6*-TEV-ProA	*Amp^r, LEU2, 2µ, GAL:PEX6-TEV-ProA*	This study
pYES2-His6-*PEX6*-TEV-ProA	*Amp^r, LEU2, 2µ, GAL:His6-PEX6-TEV-ProA*	This study
pYES2-His6-*PEX6^{E832Q}*-TEV-ProA	*Amp^r, LEU2, 2µ, GAL:His$_6$-PEX6^{E832Q}-TEV-ProA*	This study

Table 2.6 Plasmids used in this study for Pex1/6 oleate growth assays.

Plasmid	Description	Source / reference
pRS316	*URA3, CEN/ARS, Ampr*	ATCC® 77145TM
TOPO pCR2.1-pPEX1	*Amp^r, Kan^r, pUC, f1, LacZα::pPEX1*	This study
TOPO pCR2.1-pPEX6	*Amp^r, Kan^r, pUC, f1, LacZα::pPEX6*	This study
pRS316-p*PEX1*	*Amp^r, URA3,CEN/ARS, PEX1:PEX1*	This study
pRS316-p*PEX6*	*Amp^r, URA3,CEN/ARS, PEX6:PEX6*	This study
pRS316-p*PEX1^{Y488A}*	*Amp^r, URA3, CEN/ARS, PEX1:PEX1^{Y488A}*	This study
pRS316-p*PEX1^{H495A}*	*Amp^r, URA3, CEN/ARS, PEX1:PEX1^{H495A}*	This study
pRS316-p*PEX1^{F771A}*	*Amp^r, URA3, CEN/ARS, PEX1:PEX1^{F771A}*	This study
pRS316-p*PEX1^{R855K}*	*Amp^r, URA3, CEN/ARS, PEX1:PEX1 ^{R855K}*	This study
pRS316-p*PEX1^{D797N}*	*Amp^r ,URA3, CEN/ARS,PEX1:PEX1 ^{D797N}*	This study

Plasmid	Description	Source / reference
pRS316-p*PEX6*^{Y805A}	*Amp*^{r}*, URA3, CEN/ARS, PEX6:PEX6*^{Y805A}	This study
pRS316-p*PEX6*^{R607K}	*Amp*^{r}*, URA3, CEN/ARS, PEX6:PEX6*^{R607K}	This study
pRS316 -p*PEX6*^{R611K}	*Amp*^{r}*, URA3, CEN/ARS, PEX6:PEX6*^{R611K}	This study
pRS316-p*PEX6*^{R892K}	*Amp*^{r}*, URA3, CEN/ARS, PEX6:PEX6*^{R892K}	This study

2.1.3 Bacterial strains and culture conditions

Escherichia coli (*E. coli*) strains (Table 2.7) are grown at 37°C in Luria Bertani (LB) liquid medium with shaking (150 rpm) or on solid LB agar plates for 16 hours (h), supplemented with appropriate antibiotics.

LB Medium 0.5 % (w/v) yeast extract
1.0 % (w/v) bacto trypton
0.6 % (w/v) NaCl
(1.5 % (w/v) agar for solid plates)

Ampicillin (amp, 100 mg ml^{-1}) or kanamycin (kan, 34 mg ml^{-1}) stock solutions are prepared in ethanol and sterile filtered (syringe-filter with 22 µm cut-off, Carl Roth GmbH + Co. KG). Antibiotics are added to a final concentration of either 0.1 mg ml^{-1} (amp) or 0.034 mg ml^{-1} (kan) in liquid medium. Agar plates contained a final concentration of 0.05 mg ml^{-1} amp.

Table 2.7 *E. coli* strains used in this study.

***E. coli* strain**	**Genotype**	**Source / reference**
Dh5α	*F*$^{-}$*, ø80dlacZΔM15, Δ(lacZYA-argF)U169, deoR, recA1, endA1, hsdR17(rk*$^{-}$*, mk*$^{+}$*), phoA, supE44, λ*$^{-}$*, thi-1, gyrA96, relA1*	(Sambrook *et al.*, 1989)
One Shot® TOP10	F´[*lac*Iq Tn*10* (TetR)] *mcr*A Δ(*mrr-hsd*RMS-*mcr*BC) φ80*lacZ*.M15Δ*lac*X74 *deo*R *rec*A1 *ara*Δ139 Δ(*ara-leu*)7697 *gal*U *gal*K *rps*L (Str^{R}) *end*A1 *nup*G	Invitrogen

2.1.4 Yeast strains and culture conditions

Yeast strains (Table 2.8) are grown at 28°C in YPD liquid medium with gentle shaking (120-130 rpm) or on solid YPD agar plates for 2-3 days. To select for auxotrophies, yeast strains are grown in either liquid complete medium (CM) while shaking (120-130 rpm) or on solid CM agar plates for 2-3 days, lacking appropriate amino acids.

YPD medium
1 % (w/v) yeast extract
2 % (w/v) bacto peptone
2 % (w/v) glucose
(2 % (w/v) agar for solid medium)

Complete medium (CM)
0.19 % (w/v) yeast nitrogen base (w/o AA and AS)
0.5 % (w/v) ammonium sulfate
2 % (w/v) glucose
0.065 % (w/v) drop out powder (-his, -ura, -leu),
0.3 % (v/v) 2 M NaOH

CM is selectively supplemented with 0.01 % (w/v) leucine, 0.003 % (w/v) uracil or 0.003 %(w/v) histidine. For induction of Pex1/6 protein expression glucose is replaced by 2 % (w/v) galactose.

Table 2.8 Yeast strains used in this study.

***S. cerevisiae* strain**	**Genotype**	**Source / reference**
WCGa	*MATa his3-11,15leu2-3, 112 ura3 can GAL*	(Heinemeyer *et al.*, 1994)
SC2044	*MATa ade2, arg4, leu2-3, 112 trp1-289 ura3-52; Nas6Tap URA3*	Euroscarf
Pex1-TEV-ProA + His6-*pex6*WB-TEV-ProA	*MATa his3-11, 15leu2-3, 112 ura3 can GAL,* [pRS425-*PEX1*-TEV-ProA], [pYES2-His6-*PEX6*^{E832Q}-TEV-ProA]	This study
pex1 WB -His6-TEV-ProA + Pex6-TEV-ProA	*MATa his3-11, 15leu2-3, 112 ura3 can GAL,* [pRS425-*PEX1*^{E798Q}-His6-TEV-ProA], [pYES2-*PEX6*-TEV-ProA]	This study
pex1 WB -His6-TEV-ProA + His6-*pex6*^{E832Q}-TEV-ProA	*MATa his3-11, 15leu2-3, 112 ura3 can GAL,* [pRS425-*PEX1*^{E798Q}-His6-TEV-ProA], [pYES2-His6-*PEX6*^{E832Q}-TEV-ProA]	This study
Δ188*PEX1*-His6-TEV-ProA + Pex6-TEV-ProA	*MATa his3-11, 15leu2-3, 112 ura3 can GAL,* [pRS425-ΔN-R189-*PEX1*-His6-TEV-ProA], [pYES2-*PEX6*-TEV-ProA]	This study
BY 4742	*MATa; his3D1; leu2D0; lys2D0; ura3D0*	Euroscarf
BY 4742Δ*pex1*	*MATa; his3D1; leu2D0; lys2D0; ura3D0; YKL197c::kanMX4*	Euroscarf

***S. cerevisiae* strain**	**Genotype**	**Source / reference**
BY 4742Δ*pex6*	*MATa; his3D1; leu2D0; lys2D0; ura3D0; YNL329c::kanMX4*	Euroscarf
Δ*pex1* + Pex1	*MATa; his3D1; leu2D0; lys2D0; ura3D0;YKL197c::kanMX4* , [pRS316-*PEX1]*	This study
Δ*pex1* + *pex1*^{Y488A}	*MATa; his3D1; leu2D0; lys2D0; ura3D0;YKL197c::kanMX4* , [pRS316-*PEX1*^{Y488A}*]*	This study
Δ*pex1* + *pex1*^{H495A}	*MATa; his3D1; leu2D0; lys2D0; ura3D0; YKL197c::kanMX4,* [pRS316-*PEX1*^{H495A}*]*	This study
Δ*pex1* + *pex1*^{F771A}	*MATa; his3D1; leu2D0; lys2D0; ura3D0; YKL197c::kanMX4,* [pRS316-*PEX1*^{F771A}*]*	This study
Δ*pex1* + *pex1*^{R855K}	*MATa; his3D1; leu2D0; lys2D0; ura3D0; YKL197c::kanMX4,* [pRS316-*PEX1*^{R855K}*]*	This study
Δ*pex1* + *pex1*^{D797N}	*MATa; his3D1; leu2D0; lys2D0; ura3D0; YKL197c::kanMX4,* [pRS316-*PEX1*^{D797N}*]*	This study
Δ*pex6* +Pex6	*MATa; his3D1; leu2D0; lys2D0; ura3D0; YNL329c::kanMX4*, [pRS316-*PEX6*]	This study
Δ*pex6* +*pex6*^{Y528A}	*MATa; his3D1; leu2D0; lys2D0; ura3D0; YNL329c::kanMX4*, [pRS316-*PEX6*^{Y528A}]	This study
Δ*pex6* +*pex6*^{Y805A}	*MATa; his3D1; leu2D0; lys2D0; ura3D0; YNL329c::kanMX4*, [pRS316-*PEX6*^{Y805A}]	This study
Δ*pex6* +*pex6*^{R607K}	*MATa; his3D1; leu2D0; lys2D0; ura3D0; YNL329c::kanMX4*, [pRS316-*PEX6*^{R607K}]	This study
Δ*pex6* +*pex6*^{R611K}	*MATa; his3D1; leu2D0; lys2D0; ura3D0; YNL329c::kanMX4*, [pRS316 -*PEX6*^{R611K}]	This study
Δ*pex6* +*pex6*^{R892K}	*MATa; his3D1; leu2D0; lys2D0; ura3D0; YNL329c::kanMX4*, [pRS316-*PEX6*^{R892K}]	This study

2.2 General cloning strategy for Pex1/6 overexpression constructs

The open reading frame of both, *PEX1* and *PEX6*, are amplified from WCGa genomic DNA by PCR. *PEX1* oligonucleotides produced HindIII/BamHI endonuclease cutting sites, whereas *PEX6* primer pairs added KpnI/BamHI restriction sites and free deoxyadenosines (dA) overhangs to 3' termini for subsequent TOPO TA cloning. Moreover, *PEX6* is amplified using oligonucleotides, which are designed to add a N-terminal hexahistidin (His6-) tag downstream of the KpnI recognition site. After digestion with appropriate restriction enzymes, resulting *PEX1* inserts are ligated into the multiple cloning site of plasmid pRS425-*GAL1*. *PEX6* fragments are inserted enzyme free into plasmid pCRTopo2.1. Restriction analysis of isolated plasmid DNA confirmed correct cloning of *PEX1*/*PEX6* fragments. After restriction digest of pCRTopo2.1-*PEX6* and pCRTopo2.1-His6-*PEX6* using KpnI/BamHI enzymes, resulting *PEX6* DNA inserts are ligated into the multiple cloning site of pYES2. Correct cloning of *PEX6* and His6-*PEX6* into pYES2 is confirmed by restriction analysis.

The nucleotide sequence of a *tobacco etch virus* (TEV) cleavable protein A tag, encoding a spacer sequence and a TEV cleavage site followed by two IgG binding domains, is amplified from SC2044 genomic DNA containing a TAP (tandem affinity purification, Puig *et al.*, 2001) fusion protein using primer pairs listed in Table 2.1. The protein A tag (ProA-) is inserted with complementary ends into the BamHI site of pRS425-*PEX1* and pYES2-(His6)-*PEX6*, resulting in plasmids named pRS425-*PEX1*-TEV-ProA, pYES2-PEX6-TEV-ProA and pYES2-His6-*PEX6*-TEV-ProA. Restriction analysis and Sanger sequencing confirmed correct cloning of Pex1/Pex6 expression constructs.

Side-directed mutagenesis PCR using custom primer pairs Pex1-D2-E798Q and Pex6-D2-E832Q altered double stranded DNA encoding Pex1 and Pex6 Walker B motifs. Self-complementary primers resulted in base pair exchange and thereof in translational amino acid exchange (*pex1*^{E798Q} and *pex6*^{E832Q}). Moreover, oligonucleotides introduced specific endonuclease recognition sequences for restriction analysis (PvuI and BclI) through nucleotide exchange, leaving the amino acid sequence unmodified. pYES2-His6-*PEX6*-TEV-ProA is used as wild type template for side-directed mutagenesis resulting in plasmid named pYES2-His6-*PEX6*WB-TEV-ProA (Figure 4.1). Several attempts to introduce mutations in *PEX1* using template plasmid pRS425-*PEX1*-TEV-ProA failed. Instead, manipulated *PEX1* is amplified from bacterial expression vector pGEX-4T3-GST-*PEX1*WB and cloned as HindIII/BamHI insert into plasmid pRS425-*GAL1*.

The N-terminal truncation mutant Δ188*PEX1* is produced by PCR amplification of genomic DNA encoding amino acids 189-1043 and ligated via HindIII/BamHI sites into plasmid pRS425-*GAL1*. Correct cloning of *PEX1*WB and Δ188*PEX1* into pRS425-*GAL1* is confirmed by restriction analysis. Pex1 expression constructs, carrying a mutation in the Walker B motif

or the N-terminal truncation, are fused to a C-terminal His6-tag followed by the TEV cleavable protein A tag. The affinity tag is obtained by restriction digest of plasmid pCRTopo2.1-His6-Spacer-TEV-ProA with BamHI and subsequent ligation into the BamHI cutting site downstream of *PEX1*WB or Δ188*PEX1*, resulting in expression vectors termed pRS425-*PEX1*WB-His6-TEV-ProA and pRS425-ΔN189-*PEX1*-His6-TEV-ProA. Restriction analysis and Sanger sequencing confirmed correct cloning of Pex1/Pex6 expression constructs.

2.3 General cloning strategy for Pex1/6 plasmids used in oleate assays

Plasmids used in oleate growth assays are generated by PCR amplification of *PEX1* and *PEX6* open reading frames from WCGa genomic DNA including upstream native promotor regions covering endogenous oleate response elements (ORE, Einerhand *et al.*, 1993). Resulting PCR fragments contained 3' overhangs including SacI/XhoI (p*PEX1*) and XbaI/KpnI (p*PEX6*) endonuclease recognition sites and free dA tails. After digestion with appropriate restriction enzymes, p*PEX1*/p*PEX6* inserts are inserted enzyme free into plasmid pCRTopo2.1. Subsequently, reactions are transformed into E. *coli* Dh5α and ampicillin resistant, single colonies are used to inoculate liquid medium supplemented with ampicillin. Restriction analysis of isolated, recombinant plasmid DNA confirmed correct cloning of p*PEX1*/p*PEX6* fragments. After restriction digest of pCRTopo2.1-p*PEX1* and pCRTopo2.1-p*PEX6* using SacI/XhoI and XbaI/KpnI enzymes, resulting DNA inserts are ligated into the multiple cloning site of plasmid pRS316.

Side-directed mutagenesis PCR using custom primer pairs listed in Table 2.2 altered double stranded DNA encoding Pex1 and Pex6 pore loop or arginine finger residues. Self-complementary primers resulted in base pair exchange and thereof in translational amino acid exchange (*pex1*^{Y488A}, *pex1*^{H495A}, *pex1*^{F771A}, *pex1*^{D797N}, *pex6*^{Y528A}, *pex6*^{Y805A}, *pex1*^{R855K}, *pex6*^{R607K}, *pex6*^{R611K}, *pex6*^{R892K}). Moreover, oligonucleotides introduced specific endonuclease recognition sequences for restriction analysis through nucleotide exchange, leaving the protein primary structure unmodified. Restriction analysis and Sanger sequencing confirmed correct cloning of Pex1/Pex6 constructs used for oleate growth assays.

2.4 Molecular biological techniques

Phusion Hot Start II High-Fidelity DNA polymerase (New England Biolabs, NEB Frankfurt) is used for PCR amplification of *PEX1*/*PEX6* genes from genomic or plasmid DNA, while *Pfu* DNA polymerase (Fischer Scientific GmbH, Schwerte) is used for DNA manipulation by side-directed mutagenesis. Restriction endonucleases and enzymes are purchased from either NEB or Fermentas (Fischer Scientific GmbH, Schwerte).

2.4.1 DNA amplification by polymerase chain reaction (PCR)

DNA amplification from genomic or plasmid DNA is performed in a volume of 50 µl using primers listed in Table 2.1-2.2 and the thermocycler (Biometra T1 Thermocycler Analytik Jena AG, Jena) protocol shown in Table 2.9.

PCR reaction:
1 µl yeast chromosomal DNA or 1 µl (1:10 dilution) plasmid DNA
10 µl 5x High Fidelity buffer (+ $MgCl_2$)
1 µl [25 µM] forward primer
1 µl [25 µM] reverse primer
1 µl [10 mM] dNTPs
0.5 µl [2U] Phusion Hot Start II High-Fidelity DNA polymerase
total volume 50 µl

Table 2.9 Thermocycler protocol for DNA amplification by PCR.

Temperature (°C)	Time (s)	Cycles
95	60	1
95	30	30
45-55	30	
72	30s/ 1kb	
72	300	1
4	∞	1

2.4.2 DNA manipulation by side-directed mutagenesis

Point mutations are introduced in the open reading frame of *PEX1*/*PEX6* by side-directed mutagenesis PCR. Primers are self-complementary containing the desired mutation and an endonuclease recognition site (Table 2.2-2.3). PCR reaction is performed in a volume of 50 µl with the thermocycler protocol listed in Table 2.10.

PCR reaction:
0.5 µl plasmid DNA
5 µl 10x Pfu buffer (+ $MgCl_2$)
1 µl [25 µM] forward primer
1 µl [25 µM] reverse primer
0.5 µl [10 mM] dNTPs
1 µl [2.5 U] *Pfu* DNA Polymerase
total volume 50 µl

Table 2.10 Thermocycler protocol for side directed mutagenesis

Temperature (°C)	Time (s)	Cycles
95	30	1
95	30	18
45-55	60	
68	120s/ 1kb	
68	60	1
4	∞	1

2 µl DpnI are added to 30 µl PCR reaction an incubated over night at 37°C to degrade methylated template DNA. 10 µl of DpnI treated and 10 µl of untreated PCR reaction are transformed into 50 µl *E. coli* Dh5α cells. Restriction analysis and Sanger sequencing (GATC Biotech GmbH, Konstanz) confirmed introduction of point mutations.

2.4.3 Purification of plasmid DNA and DNA fragments

Plasmid DNA is amplified by growth of *E. coli* Dh5α in 3 ml LB medium supplemented with appropriate antibiotics for 16 h with gentle shaking (Sambrook *et al.*, 1989) in a sterile capped glass tube. Plasmid DNA is purified via selective adsorption to silica membranes using the QIAprep Spin Miniprep kit (QIAGEN, Hilden) according to manufacturer's instructions. For purification and isolation of DNA fragments after separation through agarose gel electrophoresis the NucleoSpin® Gel and PCR Clean-up kit (Macherey-Nagel, Düren) is used according to manufacturer's instructions.

2.4.4 Restriction enzyme digestion

For restriction analysis, 3 µl purified plasmid DNA are cleaved in a volume of 20 µl using 2.5-10 U restriction enzyme according to manufacturer's instructions for 2 h at 37°C. In double digest reactions, DNA molecules are incubated with the first restriction enzyme for 2 h at 37°C followed by addition of the second restriction endonuclease and further incubation for 2 h at 37°C. DNA fragments amplified via PCR or isolated plasmid vector DNA for downstream cloning procedures are cleaved in a volume of 300 µl using 80 U restriction endonuclease over night at 37°C. Linearized vector DNA and complementary DNA insert are subsequently separated by agarose gel electrophoresis and isolated using the NucleoSpin® Gel and PCR Clean-up kit (Macherey-Nagel, Düren).

2.4.5 Dephosphorylation

To prevent self-ligation, phosphate groups at the 5' overhang of nonattached vector DNA are removed through treatment with Antarctic Phosphatase (NEB). 25 µl vector DNA are

incubated with 5 U of Antarctic Phosphatase in a volume of 50 µl for 30 minutes at 37°C according to manufacturer's instructions. The enzyme is inactivated by incubation for 15 minutes at 65°C and 4 µl of the reaction are visualized by agarose gel electrophoresis.

2.4.6 Ligation

Complementary ends of DNA fragments and linearized (dephosphorylated) vector DNA are ligated in a molar ratio of 1 : 3. The reaction is performed in a volume of 20 µl in the presence of 400 U T4 DNA ligase (NEB). After incubation for 30 minutes at RT, 5 µl reaction are transformed in 50 µl *E. coli* Dh5α cells. Restriction analysis and Sanger sequencing (GATC Biotech GmbH, Konstanz) confirmed successful cloning.

2.4.7 TOPO TA Cloning®

*PEX*1/*PEX*6 destined for TOPO TA Cloning® are amplified via PCR using oligonucleotides that produce 3' end deoxyadenosines (dA) of DNA inserts Table 2.1). Fresh PCR products are mixed with plasmid vector pCR®2.1–TOPO® which provides a complementary deoxythymidine (dT) tail for enzyme free cloning. TOPO® cloning reactions are performed using the TOPO TA Cloning® kit (Invitrogen, Karlsruhe) according to manufacturer's instructions. Restriction analysis confirmed successful cloning.

2.4.8 Agarose gel electrophoresis

The separation of DNA molecules for sizing and comparative quantification is performed on 0.8 % agarose gels using a horizontal electrophoresis system (peqlab PerfectBlue Gel System Mini M). The appropriate amount of agarose is diluted in 70 ml 1x TBE running buffer (90 mM Tris, 90 mM boric acid, 2 mM EDTA, pH 8.0), microwaved until the agarose is fully melted and supplemented with Stain G in a ratio 1 : 70,000 (Serva, Heidelberg). DNA samples and 0.5 µg DNA ladder (GeneRuler DNA Ladder Mix) are mixed with 5x gel loading dye (90 mM Tris, 90 mM boric acid, 2 mM EDTA, pH 8.0; 50 % (v/v) glycerol, 0.25 % (w/v) bromphenol blue) and separated by electrophoresis for 1 h at 100 V. Through binding of free DNA molecules, Stain G emits green fluorescent light when exposed to UV light. Emitted signals are detected using a SafeLab Imager gel documentation system (Intas, Göttingen) thereby visualizing DNA fragments on the agarose gel.

2.4.9 Transformation of RuCl competent *E. coli* cells

For transformation of competent *E. coli* cells, appropriate amount of plasmid DNA (see sections 3.2.3 and 3.2.7) is added to 50 µl *E. coli* Dh5α. After incubation on ice for 15 minutes, cells are heat shocked at 42°C for 2 minutes and subsequently chilled on ice for 2 minutes. Cells are supplemented with 450 µl LB medium and incubated for 1 h at 37°C with shaking before plated on selective LB agar plates and incubated at 37°C over night. For

further analysis, a single colony of transformants is used to inoculate liquid LB medium.

2.4.10 Transformation of *S. cerevisiae* by electroporation

Recombinant plasmid DNA is introduced into yeast cells by electroporation. 50 ml liquid YPD medium are inoculated with desired yeast strain and grown for 14 h at 28°C with shaking (120 rpm) until log phase (OD_{600} = 1.3-1.5, determined using a WPA CO8000 Cell density meter, Biochrom Ltd., Cambridge UK) in a sterile 100 ml Erlenmeyer flask. The culture is harvested by centrifugation for 5 minutes at 3000 rpm (3463 x g), 4°C in a sterile 50 ml tube. Subsequently, cells are resuspended in 10 ml cold sterile water and pelleted for 5 minutes at 3000 rpm (3463 x g), 4°C. The cell pellet is resuspended in 10 ml cold 1 M sorbitol. After a further centrifugation step, cells are transferred in 1 ml cold sorbitol (1 M) into a pre-chilled, sterile 1.5 ml microcentrifuge tube and pelleted for 2 minutes at 6000 rpm (8452 x g), 4°C. Next, the cell pellet is resuspended in an equal volume of cold sorbitol (1 M). 1 µl recombinant plasmid DNA (Table 2.5 and Table 2.6) is added to 40 µl of resuspended cells in a pre-cooled electroporation cuvette (2 mm electrode distance, Gene Pulser Cuvette, Bio-Rad Laboratories GmbH, München) and incubated for 5 minutes on ice. Electroporation is carried out using a Bio-Rad Gene Pulser (1500 V, 25 µF, 200 Ω, t = 4.6-4.7 µsec). Cells are recovered by adding 1 ml cold 1 M sorbitol to the cuvette. The cell suspension is transferred to a pre-chilled, sterile 1.5 ml microcentrifuge tube and pelleted for 2 minutes at 10000 rpm (14086 x g), 4°C. The pellet is resuspended in 50 µl 1 M sorbitol, spread onto agar plates supplemented with appropriate amino acids and incubated at 28°C for 3 days.

2.4.11 Extraction and purification of genomic or plasmid DNA from *S. cerevisiae*

For recovery of plasmid DNA from yeast or preparation of yeast genomic DNA, a single colony of transformants (see section 2.4.10) or desired strain (Table 2.8) is used to inoculate 5 ml YPD liquid medium in a sterile capped glass tube. Yeast cells are grown over night at 28°C to stationary phase while shaking (120 rpm). 3 ml overnight culture are pelleted 5 minutes at 5000 rpm (2372 x g) at RT in a sterile microcentrifuge tube. The cell pellet is resuspended in 250 µl Buffer P1 (component of the QIAprep Spin Miniprep kit, QIAGEN, Hilden) and 100 µl sterile glass beads (0.25-0.5 mm diameter, Carl Roth GmbH, Kalrsuhe) are added. Yeast cells are disrupted by vortexing at highest speed 7 times for 1 minute with a 1-minute break on ice between each run. Resulting cell lysate is transferred into a fresh 1.5 ml microcentrifuge tube. Further steps are carried out using buffers and silica columns included in the QIAprep Spin Miniprep kit (QIAGEN, Hilden). The cell lysate is mixed with buffer P2 and inverted 4-6 times. After addition of buffer N3, tubes are inverted 10 times and subsequently spun 12 minutes at 13000 rpm (16060 x g) at RT. The supernatant is transferred to a spin column and spun for 1 minute at 13000 rpm (16060 x g) at RT. Resulting flow-

through is discarded and spin column is washed using 750 µl PE Buffer and spun for 2 minutes at 13000 rpm (16060 x g) at RT. After discarding the flow-through, the column is centrifuged for 3 minutes at 13000 rpm (16060 x g) at RT. The spin column is placed in fresh microcentrifuge tube and bound plasmid DNA is eluted by adding 50 µl EB buffer and subsequent centrifugation for 2 minutes at 13000 rpm (16060 x g) at RT. Genomic DNA is stored at -20°C.

To recover plasmid DNA, 50 µl competent *E. coli* Dh5α cells are transformed with 5 µl recovered vector DNA as described in 2.4.9. For further analysis, a single colony of *E. coli* transformants is used to inoculate liquid LB medium.

2.4.12 Frozen stocks for long-term storage

Yeast strains are stored as glycerol stocks in 2 ml screwcap vials at -80°C. 1 ml of a late-log or early-stationary phase culture is mixed with 400 µl sterile 80 % glycerol and stored at -80°C.

2.5 Protein biochemistry

2.5.1 Overexpression of heterologous Pex proteins in *S. cerevisiae*

2.5.1.1 Protein test expression

Pex1 and Pex6 recombinant proteins are overexpressed in *S. cerevisiae* from 2 µ plasmids pRS425-*GAL1* or pYES2, fused to the *GAL1* promotor. To assay the expression of recombinant Pex1/Pex6 proteins, a time course experiment is performed. *S. cerevisiae* cells, co-transformed with pRS425-Pex1 and pYES-Pex6 overexpression constructs (Table 2.5), are grown in 30 ml CM medium lacking amino acid leucine and nucleobase uracil (CM –leu –ura) overnight at 28°C with shaking (130 rpm, GFL 3005). Next, 15 ml overnight culture are pelleted 3 minutes at 3000 rpm (3463 x g) in a sterile 15 ml tube and washed 2-3 times with 10 ml sterile water. Expression of recombinant Pex1/6 proteins is induced by resuspending the cells in 15 ml CM -leu -ura containing 2 % and incubated at 28°C with modest shaking (130 rpm). After indicated time points, up to 1 x 10^9 cells ml^{-1} are harvested by centrifugation for 3 minutes at 13000 rpm (16060 x g) and stored at -20°C. For subsequent Western blot analysis (2.5.11), proteins are precipitated as described in 2.5.2 and subjected to SDS-PAGE 2.5.9).

To further optimize Pex1/6 overproduction for preparative large-scale purification, protein expression is induced from yeast cultures with varying optical densities as indicated for 16 h at 28°C with modest shaking (130 rpm). Subsequently, 1 OD_{600} cells (~ 3 x 10^7 cells ml^{-1}) are harvested by centrifugation for 3 minutes at 13 000 rpm (16060 x g) and stored at -20°C. Proteins are precipitated as described in 2.5.2, resuspended in 40 µl 1x Laemmli buffer (4 % (v/v) 50 mM Tris-HCl pH 6.8, 5 % (v/v) glycerol, 0.4 % (w/v) SDS, 0.775 % (w/v) DTT,

0.004 % (w/v) bromophenol blue) and 20 µl are subjected to SDS-PAGE (see section 2.5.9) and Western blot (see section 2.5.11).

2.5.1.2 Protein expression for purification

Pre-cultures for preparative Pex1/6 overproduction are grown in 100 ml CM -leu -ura for 48 h at 28°C while shaking (130 rpm) in a sterile 300 ml Erlenmeyer flask. The pre-culture is used to inoculate 4 liters of fresh YPD medium (in two sterile 5 L Erlenmeyer flasks) to an OD_{600} = 0.5 and cells are allowed to grow to mid-log phase (OD_{600} = 3.0). Subsequently, cells are harvested by centrifugation for 10 minutes at 4000 rpm (3.501 x g), 4°C, using a SLC–6000 rotor (Sorvall RC Evolution centrifuge, Thermo Fisher Scientific, Inc., Waltham (MA), USA) and washed 3 times with 25 ml sterile water. Protein expression is induced by resuspending cell pellets in 4 L CM -leu -ura medium containing 2 % galactose (in two sterile 5 L Erlenmeyer flasks) for 16 h at 28°C with shaking (130 rpm). Cells are pelleted (SLC-6000, 10 minutes at 3.501 x g, 4°C) and washed with 25 ml cold water. Cell pellets (approximately 2 x 10 g wet weight) are flash frozen in liquid nitrogen and stored at -80°C.

2.5.2 Yeast cell lysis and protein precipitation according to Yaffe and Schatz, 1984

For analysis of protein expression in total yeast cell extracts, *S. cerevisiae* cell pellets (up to 1 x 10^9 cells ml^{-1}) are resuspended in 1 ml dH_2O, supplemented with 160 µl 1.85 M NaOH and 85 µl 2-mercaptoethanol and incubated for 10 minutes on ice. Next, disrupted cells are mixed with 160 µl 50 % trichloroacetic acid and incubated for 10 minutes on ice. Precipitated samples are pelleted by centrifugation at 13000 rpm (16016 x g) for 3 minutes, 4°C and washed with 500 µl ice-cold acetone (3 minutes at 16016 x g, 4°C). Resulting pellets are air – dried for 10-15 minutes and if not stated otherwise, resuspended in 150 µl 1 x Laemmli buffer and 15 or 20 µl are subjected to SDS-PAGE (see section 2.5.9) and Western blot (see section 2.5.11).

2.5.3 Mechanical yeast cell disruption using a bead beater

Unless stated otherwise, all protein purification procedures are carried out at 4°C with pre-cooled equipment. For affinity purification of native Pex1/6 complexes, harvested cells are mechanically disrupted using a Fastprep24 bench top homogenizer (MP Biomedicals, Santa Ana, (CA) USA). To this end, cell pellets (~10 g wet weight each) are thawed on ice and each pellet is resuspended 1:1 in Buffer A (20 mM HEPES pH 7.5, 100 mM NaCl, 10 mM $MgCl_2$, 10% glycerol, 2mM ATP, 0.5 mM DTT) containing 20U DNaseI, 1 mM PMSF, one complete EDTA-free mini protease inhibitor cocktail tablet. After adding 25 ml glass beads (0.25-0.5 mm diameter, Carl Roth GmbH, Kalrsuhe) to 20 ml cell suspension, cells are disrupted at 6.5 M/s for 30 s at RT. Runs are repeated 8-10 times, thereby cooling the samples between each run for 5 minutes on ice. Examining the samples using a light microscope monitored

lysis efficiency. Cell lysate is recovered by centrifugation for 3 minutes at 1000 rpm (219 x g), 4°C, through pricked holes at the bottom of the 50 ml tube into a fresh tube.

2.5.4 Equilibration of IgG Sepharose beads

250-300 µl IgG Sepharose 6 Fast flow beads (GE Healthcare Bio-Sciences AB, Uppsala, Sweden) are equilibrated in an Econo-Pac chromatography column (Bio-Rad Laboratories GmbH, München) with 15 column volumes (= equivalent to volume of packed bed) TST buffer (10 mM Tris-HCl pH 7.6, 150 mM NaCl, 0.05 % (v/v) Tween-20), 30 column volumes 0.5 M HAc pH 3.4 and 15 column volumes buffer B (20 mM HEPES pH 7.5, 100 mM NaCl, 10 mM MgCl2, 10 % (v/v) glycerol). After affinity purification and TEV cleavage, IgG beads are regenerated through washing with 10 column volumes 0.5 M HAc pH 3.4 and 30 column volumes TST buffer. IgG beads are stored at 4°C and reused up to three times.

2.5.5 Immunopurification of Pex1/6 protein A fusion proteins from *S. cerevisiae*

After mechanical cell disruption, cell lysate is cleared by centrifugation using a SS-34 rotor (Sorvall RC Evolution centrifuge, Thermo Fisher) for 30 minutes at 15000 rpm (25099 x g), 4°C. The supernatant is repeatedly applied (3 times) on equilibrated IgG Sepharose beads 2.5.4). Subsequently, the beads are washed with 15 column volumes buffer A, 15 column volumes Buffer A containing 500 mM NaCl followed by 15 column volumes Buffer A. TEV cleavage of immobilized proteins is performed for 1h 20 min at 20°C in 3 column volumes buffer A. Liberated Pex1/6 complexes are eluted by gravity flow and IgG beads are washed with 2 x 3 column volumes Buffer A to recover remaining complexes from the matrix. Pex1/6 containing fractions are pooled and subjected to analytical ultracentrifugation (see section 2.5.6)

2.5.6 Glycerol density gradient centrifugation

600 µl-1200 µl of eluted Pex1/6 complexes are separated from contaminants and TEV protease by centrifugation through a 10%-40 % glycerol gradient in Buffer A without glycerol or through a 20 %-50 % glycerol gradient in Buffer A, respectively. Proteins and molecular complexes migrated through centrifugation in a SW40 rotor (Beckman Coulter, Inc., Pasadena (CA), USA) at 40000 rpm for 16 h, 4°C. Gradients are formed in 14 x 95 mm poly clear centrifuge tubes (Seton Scientific, Petaluma, CA, US) using a BioComp Gradient Station (BioComp Instruments, Inc., Fredericton, NB, Canada). Separated proteins are fractionated (600 µl), 50-100 µl precipitated as described in 2.5.8, and analysed by SDS-PAGE or Western blot (see sections 2.5.9 or 2.5.11).

2.5.7 Protein concentration and buffer exchange

Concentration and buffer exchange of purified Pex1/Pex6WB^{ATP} complexes obtained after

glycerol density gradient centrifugation is performed using Amicon Ultra Centrifugal Filters (0.5 ml, 50 K MWCO, Millipore GmbH, Schwalbach). 300 µl protein complexes are concentrated by centrifugation (5 minutes, 8452 x g, 4°C) to a final volume of 100 µl. In order to reduce the amount of glycerol, concentrated samples are washed three times with 100 µl buffer A containing 10 % glycerol and three times with 100 µl buffer A containing 5 % glycerol.

2.5.8 Protein TCA precipitation

Pex1/6 protein samples are mixed with 100 µl 0.15 % (w/v) sodium desoxycholate and 100 µl 72 % (w/v) trichloroacetic acid (TCA) and incubated for 15 minutes at RT. Precipitated proteins are pelleted by centrifugation for 10 minutes at 13000 rpm (16060 x g) at 4°C. Protein pellets are washed with 500 µl ice-cold acetone and spun down (5 minutes, 16060 x g, 4°C). The protein pellets are air-dried, dissolved in 1 x Laemmli buffer and analyzed by SDS-PAGE or Western Blot (see sections 2.5.9 or 2.5.11).

2.5.9 Sodium dodecyl sulfate polyacrylamide gel electrophoresis (SDS-PAGE)

Analytical separation of proteins within an electrical current according to their molecular weight is performed using discontinuous SDS-PAGE (Laemmli, 1970). SDS-polyacrylamide gels are prepared as described in Table 2.11.

Table 2.11 Preparation of SDS-polyacrylamide gels (results in 2 gels)

Resolving gel solution	12 %	10 %	7.5 %	**Stacking gel solution**	
H_2O	3.5 ml	4 ml	4.85 ml	**dH_2O**	3.05 ml
1.5 M Tris-HCl pH 8.8	2.5 ml	2.5 ml	2.5 ml	**0.5 M Tris-HCl pH 6.8**	1.25 ml
10 % SDS	100 µl	100 µl	100 µl	**10 % SDS**	50 µl
30 % acrylamide	4 ml	3.3 ml	2.5 ml	**30 % acrylamide**	0.65 ml
10 % APS	100 µl	100 µl	100 µl	**10 % APS**	25 µl
TEMED	10 µl	10 µl	10 µl	**TEMED**	5 µl

The resolving gel is covered with 50 % isopropanol while the gel matrix polymerizes. Stacking and resolving gels are allowed to polymerize 30 minutes before electrophoresis.

Protein samples are mixed with either 4 x Laemmli buffer (16 % (v/v) 200 mM Tris-HCl pH 6.8, 20 % (v/v) glycerol, 1.6 % (w/v) SDS, 3.1 % (w/v) DTT, 0.016 % (w/v) bromophenol blue) or resuspended in 1 x Laemmli buffer, boiled for 5-10 minutes at 95°C, followed by a quick spin-down at 13000 rpm (16100 x g) for 25 s. Roti-Mark Standard (Carl Roth GmbH + Co. KG, Karlsruhe) and PageRuler Unstained Protein Ladder (Fischer Scientific GmbH, Schwerte) are used as protein molecular weight markers. The electrophoretic run is carried out using a Mini-Protean Tetra Cell system (Bio-Rad Laboratories GmbH, München) in the presence of 1x SDS–PAGE running buffer (25 mM Tris-HCl, 200 mM glycin, 0.1% (w/v) SDS) at 200 V for 55-75 minutes.

2.5.10 Coomassie blue staining of SDS-polyacrylamide gels

Coomassie Brilliant Blue integrates with nonpolar, cationic and hydrophobic amino acids of polypeptide side chains. Coomassie blue staining was used to visualize protein bands in SDS-polyacrylamide gels. For this purpose, protein bands are fixed and stained within the gel matrix by boiling the gel for 5 s in Coomassie solution (0.1 % (w/v) Coomassie R250, 10 % (v/v) acetic acid, 40 % (v/v) methanol) followed by 10 minutes incubation at RT, gently shaking. Subsequent incubation for 1 h in destain solution (45 % (v/v) methanol, 10 % acetic acid) removed background staining.

For protein identification, the SDS-polyacrylamide gels are stained with Coomassie Blue (see sections 2.5.10) and subsequent mass spectrometry was carried out by Thomas Fröhlich in the laboratory for functional gene analysis (LAFUGA, Gene Center Munich).

2.5.11 Western blot (semi-dry)

Western blot allows electrophoretic transfer of proteins from SDS-polyacrylamide gels to a (nitrocellulose) membrane and subsequent immunodetection of specific proteins (Towbin *et al.*, 1979). For this purpose, nitrocellulose membrane (0.45 µm pore size, Whatman, GE Healthcare) and filter papers are soaked quickly in blotting buffer (5 % (v/v) 10 x SDS running buffer [250 mM Tris, 2 M glycine], 20 %(v/v) methanol, 0.25 % (v/v) 20 % SDS). The SDS-polyacrylamide gel is placed on top of the nitrocellulose membrane and sandwiched between two pieces of filter paper on each side. Protein transfer is carried out at 400 mA and 30 V for 90 minutes using a semi-dry electroblotter (PEQLAB Biotechnologie GmbH, Erlangen). Transfer efficiency is verified by amido black staining of the nitrocellulose membrane. For this purpose, the membrane is soaked in 45 ml dH_2O mixed with 5 ml amido black staining solution (0.1 % (w/v) amido black, 40 % methanol, 10 % acetic acid) for 5 minutes at RT. For immunodetection, the membrane is washed thoroughly with dH_2O and blocked with 5 % (w/v) skim milk powder in dH_2O for 30 min at RT to avoid unspecific antibody binding. In order to detect His6 tagged proteins, the primary antibody (α-His

antibody from mouse, unconjugated, Dianova GmbH, Hamburg) is directly added to the blocking solution (1:1000 (v/v)) and incubated over night at 4°C with gentle shaking. Next, the membrane is washed three times with 10 ml TST buffer (50 mM Tris-HCl pH 7.4, 150 mM NaCl, 0.1 % (v/v) Tween 20) for 10 minutes at RT and subsequently incubated with the HRP-conjugated secondary α-mouse antibody (from rabbit, Dianova GmbH, Hamburg) 1:10000 (v/v) in 5 % (w/v) skim milk powder solution for 2 h at RT, gently shaking. Last, the membrane is washed three times with TST buffer for 10 minutes at RT and quickly rinsed with water. To detect HRP-conjugates the membrane is incubated for 1 minute in 10 ml ECL solution containing equal parts of solution A (100 mM Tris HCl pH 8.5, 90 mM coumaric acid, 250 mM luminol) and solution B (100 mM Tris HCl pH 8.5, 0.03 % H_2O_2). Emitted signals are detected on a X-ray film (Amersham Hyperfilm TM ECL, GE Healthcare, Little Chalfont, UK) and developed with an Optimax X-RAY Film Processor.

2.6 Oleate growth assays

Complementation assays are performed as described in (Birschmann *et al.*, 2005) with minor modifications as follows. *S. cerevisiae* cells expressing wild type, no or mutant Pex1 and Pex6 alleles (Table 2.8) are grown in 3 ml YPD in sterile capped glass tubes at 28°C for 16 h with shaking (120 rpm). Next, the optical density (OD_{600}) of yeast cultures is determined. Subsequently, 1 ml cells are pelleted by centrifugation at 5000 rpm (2372 x g) for 5 minutes at RT and washed with sterile water (5 minutes, 2372 x g, RT). Cell pellets are resuspended in 1 ml sterile water and a 10-fold serial dilution starting with 2 x 10^4 cells are spotted on agar plates containing 0.67 % (w/v) yeast nitrogen base (without ammonium sulfate and without amino acids), 0.2 % (v/v) oleic acid, 0.5 % Tween 20 (v/v), 0.3 % (w/v) yeast extract, 0.5 % (w/v) ammonium sulfate and suitable amino acids, adjusted to pH 6. Control plates include 0.2 % glucose instead of oleic acid. Oleate plates are incubated for 5-6 days and control plates for 3 days at 28°C.

2.7 Electron microscopy (EM) techniques and single particle analysis

2.7.1 Plasma cleaning of EM grids

Initially hydrophilic, carbon support films become gradually hydrophobic over time. Therefore, carbon coated EM grids are glow discharged prior to use allowing aqueous solutions to spread evenly onto the carbon film (Dubochet *et al.*, 1971). Carbon coated copper grids are glow discharged at pressure level of 2.2 x 10^{-1} Torr using a plasma cleaner (Harrick Plasma, Ithaca NY, USA). 400 Cu mesh continuous carbon grids (Quantifoil Micro Tools GmbH, Jena) for negative stain EM are treated with a plasma cleaner for 45 seconds.

2.7.2 Negative staining of purified Pex1/6 protein complexes

Standardized negative staining procedure was established by Brenner and Horne (Brenner and Horne, 1959), using solutions of soluble heavy metal salts, which form an amorphous stain around the biological sample examined.

Wild type Pex1/6 complexes, purified from *E. coli* (~ 50 µg ml^{-1}, kindly provided by Dr. D. Saffian and I. Grimm in collaboration with Prof. Ralf Erdmann's lab, Ruhr-Universität Bochum) are incubated with ATPγS (2.5 mM) or ATP (5 mM) and Pex1GST/Pex6 complexes with ADP (5 mM) in 20 mM Tris-HCl pH 7.5, 20 mM NaCl, 10 mM $MgCl_2$. To prepare the ADP-AlFx state, 2 mM $AlCl_3$ and 8 mM NaF were added to purified wild type Pex1/6 complexes diluted to concentrations stated above in 20 mM HEPES pH 7.5, 50 mM NaCl, 2 mM $MgCl_2$ and 2mM ADP (Chang *et al.*, 2012). 3.5 µl protein solution are applied on glow discharged 400 Cu mesh continuous carbon grids (Quantifoil Micro Tools GmbH, Jena) and incubated for 45 seconds. After draining of excessive sample solution, proteins are stained twice with 2% (w/v) uranyl acetate (Ted Pella, Inc., Redding CA, USA) for 15 seconds, redrained and immediately air-dried. Mutant Pex1/6 complexes $Pex1WB^{ATP}/6$, $Pex1/6WB^{ATP}$, $Pex1/6DWB^{ATP}$, separated by density gradient centrifugation, are stained on successive drops of uranyl acetate. Grids are incubated for ~10 s on each drop of uranyl acetate and blotted to near dryness, according to (Lander *et al.*, 2012). Separated Δ188Pex1/Pex6 complexes are incubated with ATPγS (2.5 mM) and stained accordingly.

2.7.3 Acquisition of electron microscopy images

For initial characterization of the presence, size and shape of negatively stained Pex1/6 complexes, single images are recorded on a FEI Morgagni electron microscope operated at 80 keV (FEI, Hillsboro OR, USA) equipped with a SIS Megaview 1K CCD camera using a nominal magnification of 60,000 x. Images for three-dimensional (3D) reconstructions are recorded using a Tecnai G2 Spirit transmission electron microscope, operating at 120 keV equipped with a 2048 x 2048 pixel CCD camera (FEI, Hillsboro OR, USA) under low-dose conditions (~18 $e^-/Å^2$). The micrographs are taken at a nominal magnification of 103,448 x and sampled at 2.9 Å per pixel at the specimen level. Defoci range from 350-1000 nm.

2.7.4 Image pre-processing and particle selection of negative stain images

The defocus and astigmatism of micrographs are determined using CTFFIND3 (Mindell and Grigorieff, 2003). Raw micrographs with more than 10 % astigmatism or uneven stain are excluded from further image processing procedures. CTF correction is done in SPIDER (Frank *et al.*, 1996; Shaikh *et al.*, 2008) through flipping the phases of negative CTF lobes of full electron images.

A total of 3895 (ATPγS), 2948 (ATP), 1488 (ADP), 2394 (ADP-AlFx), 2064 ($Pex1WB/6^{ATP}$),

2048 (Pex1/6WB^{ATP}), 2073 (Pex1/6DWB^{ATP}) and 400 (Δ188Pex1/6^{ATPγS}) particles are manually selected using the MRC program Ximdisp (Crowther *et al.*, 1996) or semi-automatically using FindEM (Roseman, 2004), for which class averages with distinct views of primary picked particles serve as template. Selected particles are extracted using a box size of 160 pixels. For initial single particle analysis of Pex1/6^{ATPγS} a box size of 128 pixels was used.

2.7.5 Multivariate statistical analysis (MSA) classification and multi-reference alignment of negatively stained single particles

Initial analysis of Pex1/6 single particles is done in IMAGIC-5 (van Heel *et al.*, 1996). Each datasets is normalized, masked and frequencies of single particles are band-pass filtered between 200 and 10 Å. Next, Pex1/6 particles are centered by iterative translational alignments to their rotationally averaged sum. Resulting class averages, containing 5-10 images, serve as references to further group particles with distinct features based on multivariate statistical analysis (MSA) followed by multi-reference alignment (MRA). Three to seven rounds of MSA and MRA classification generate homogeneous classes, showing related in plane but diverse out of plane orientations.

2.7.6 Determination of Euler angles (angular reconstitution)

Initial 3D reconstructions are created in IMAGIC-5 by angular reconstitution imposing 3-fold symmetry. To this end, Euler angles are assigned to a range of 2D projections showing distinct views, which are classified and averaged by MSA and MRA, see section 2.7.5). The common line approach in IMAGIC-5 allows to define orientational relationships between those class averages and thereof the calculation of an initial 3D EM density map. This 3D reconstruction is re-projected in Euler-angle directions and visual analogy between re-projections and input 2D projections serves as measure of the quality of the initial 3D model obtained.

2.7.7 Iterative refinement by projection matching

Low-resolution 3D reconstructions, obtained from angular reconstitution (2.7.6), are used as a reference for projection matching in SPIDER. Euler angles, rotation and shift parameters of negatively stained Pex1/6 particle images are refined iteratively. For each round, a stack of references projections is created according to α (psi) = 90°, β (theta) = 0-180° and γ (phi) = 0-120 (operation '*PF 3Q*') and aligned to Pex1/6 datasets (operation '*AP SH*'), thereby decreasing the angular step size of eulerian angle β from 8° to 4°. For asymmetric Pex1/6 3D reconstructions, Euler angle γ ranged from 0-360°. Defined Euler angles and parameters for translational and rotational cross correlation of Pex1/6 particles are stored separately and ~70 - 80 % of best-matched Pex1/6 projections are included in reconstruction of 3D volumes imposing 3-fold symmetry (operation '*BP RP*'). Single-particle reconstructions are loosely masked in IMAGIC-5 before they are subjected to new rounds of projection matching. After 6

to 14 rounds, ~ 90% of Euler angles are stable and aligned Pex1/6 particles are averaged and classified by MSA and MRA (2.7.5). Final 3D reconstructions are re-projected in Euler-angle directions and visual analogy between re-projections and class averages of aligned Pex1/6 projections serves as measure of the quality of the final 3D model obtained.

2.7.8 Resolution assessment: Fourier Shell Correlation (FSC)

To determine the resolution of final Pex1/6 3D reconstructions in SPIDER, each input dataset is split in two independent sets of Pex1/6 particles to calculate two separate 3D reconstructions (operation '*RF 3*'). The two half-reconstructions are compared and the correlation of every spherical shell at each frequency is calculated over the whole spectrum in Fourier Space and the final resolution estimated using 0.5 as correlation cut off.

2.8 Protein sequence analysis

2.8.1 Multiple sequence alignment

To highlight sequence homology between protein sequences, multiple primary sequences are aligned using the ClustalW algorithm (Larkin *et al.*, 2007; Goujon *et al.*, 2010). Output files are visualized and edited using Jalview 2.7 (Waterhouse *et al.*, 2009).

2.8.2 Protein homology structure prediction

Pex1 and Pex6 D1/D2 homology models are created using the HHpred server (Soding *et al.*, 2005) followed by model building using MODELLER (Sali and Blundell, 1993) based on known p97 crystal structures (pdb-ID: 3CF2, 3CF0, 3HU3).

2.8.3 Atomic structure fitting

The hexameric p97 crystal structure (pdb-ID: 3CF3) is automatically fitted using '*Fit in Map*', implemented in the USCF Chimera package (Pettersen *et al*., 2004). Homology models of Pex1 and Pex6 D1/D2 AAA+ domains are automatically fitted into the Pex1/6$^{ATP\gamma S}$ EM density map and optimized based on the best cross-correlation using '*Fit in Map*'. Testing several starting positions resulted in the same local optima of the models in the EM density map, indicating only one local minimum for each fit. Fitted Pex1/Pex6 D1 or D2 domains are symmetrized using '*pdbsymm*' in Situs (Wriggers, 2010). All EM reconstructions are aligned to the ATPγS bound map in Chimera. Map segmentation is done using Chimera. All figures are prepared using either Pymol (www.pymol.org) or Chimera. In case of C1 (symmetry free) 3D reconstructions, homology models of Pex1/6 ATPase domains are fitted automatically to each D2 domain individually.

3 Results

Part of this study included developing a strategy in order to establish the expression of recombinant yeast Pex1 and Pex6 in *S. cerevisiae.* Moreover, the yield of purified Pex1/6 proteins should be optimized to achieve satisfactory protein concentrations for structural analysis using negative stain EM and single particle analysis.

3.1 Overexpression of *S. cerevisiae* Pex1 and Pex6

The coding sequences of wild type and mutant yeast Pex1 and Pex6 are inserted into episomal plasmids pRS245-*GAL*1 and pYES2 under control of the inducible *GAL1* promotor (see section 2.2). The transcription of genes under control of the *GAL1* promoter is induced up to 1000-fold when cells are grown in medium containing galactose as the sole carbon source (Johnston and Davis, 1984). The levels of ectopically expressed Pex1/Pex6 should be substantially elevated compared to endogenous Pex1/Pex6 protein levels. Furthermore, recombinant Pex1/Pex6 are overexpressed from 2 µ plasmids pRS425-*GAL1* and pYES2, which are present in high copy numbers in the corresponding yeast cells. The yeast strain WCGa is transformed with Pex1 and Pex6 expression vectors for co-expression of protein A (ProA-) tagged Pex1/Pex6 and their mutant versions, respectively.

3.1.1 Test overexpression of wild type Pex1 and Pex6 proteins

To achieve co-expression of stable Pex1/Pex6 proteins in yeast, different conditions for the expression of soluble, C-terminally protein A tagged Pex1/Pex6 (Pex1-ProA/Pex6-ProA) are tested.

First, the efficiency of overexpression is assayed in cultures with different densities to see whether the growth phase of the yeast cells has an influence on the amount of expressed protein. Notably, the yield of expressed Pex1-ProA/Pex6-ProA depends on the density of the respective yeast culture (Figure 3.1 A). Ectopic expression of Pex1-ProA/Pex6-ProA in cells in early- and mid-log phase (OD_{600}= 0.7-2.9) is significantly higher compared to cells in late-log phase (OD_{600}= 5.9). To further optimize protein expression conditions for Pex1-ProA/Pex6-ProA, the co-expression of both proteins is followed over time after the addition of galactose. The expression of recombinant proteins is induced from cells grown to an OD_{600}= 3.0. As analyzed by Western blot, expressed Pex1-ProA/Pex6-ProA can be detected after 6 h up to 21 h of galactose exposure (Figure 3.1 B). Induction of Pex1-ProA/Pex6-ProA expression seems to be delayed in cells, which are grown in glucose-containing medium prior

to induction with galactose, similar to earlier publications (Adams, 1972).

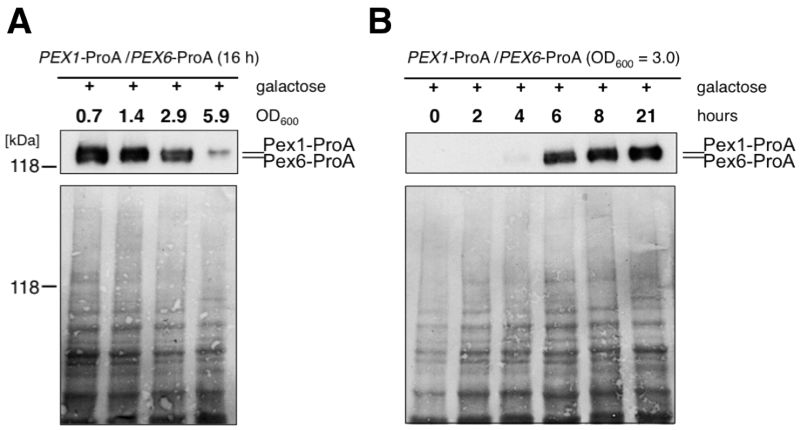

Figure 3.1 Pex1/6 overexpression depends on cell density and time. (A) Pex1-ProA/Pex6-ProA proteins are co-expressed for 16 h in yeast cultures with cell densities (OD_{600}) as indicated. (B) Pex1-ProA/Pex6-ProA co-expression followed over time. 1 OD_{600} cells (~3 x 10^7 cells ml^{-1}) are analysed per lane by Western Blot through detection of the protein A tag using α-mouse. Corresponding amido black staining is shown below.

Thus, for subsequent large-scale affinity purifications of recombinant Pex1/Pex6 proteins, cells are grown to mid-log phase (OD_{600} = 3.0) and induced with 2 % galactose for 16 h.

3.1.2 Test overexpression of modified Pex1 and Pex6 proteins

To dissect the influence of individual nucleotide binding pockets in Pex1/6 complexes, conserved residues within the Walker B motif of Pex1D2 or Pex6D2 are mutated. Typically, mutations in the Walker B consensus sequence block ATP hydrolysis but not ATP binding (Wendler *et al.*, 2012). Multiple sequence alignment shows that both, Pex1 and Pex6, harbour a highly conserved Walker B glutamate (Beyer, 1997), which is replaced by glutamine ($Pex1^{E798Q}$/$Pex6^{E832Q}$). Likewise to wild type Pex1/Pex6, the overexpression of recombinant Pex1/Pex6 Walker B (WB) proteins is tested. Recombinant Pex1WB-His6-ProA or His6-Pex6WB-ProA subunits are expressed in cells containing either the wild type or a mutant version of the respective other subunit.

Furthermore, a shortened version of Pex1 is generated to distinguish single protomers in Pex1/Pex6 assemblies using negative stain EM (see section 3.3.5). According to domain boundaries indicated in secondary structure predictions and to the existing crystal structure of the murine Pex1 N-terminal domain (pdb-ID: 1WLF; Shiozawa *et al.*, 2004), the first 188 amino acids of Pex1 are truncated and resulting ΔPex188-His6-ProA is co-expressed with full-length Pex6-ProA.

Respective yeast strains are tested for the ectopic co-expression of mutated or truncated Pex1/Pex6 proteins and assayed using immunoblotting. Pex1/Pex6 proteins are detected after

induction with 2 % galactose for 8 h (Figure 3.2) and indicated Pex1/Pex6 proteins are present in all strains tested. This result implies that neither point mutation nor N-terminal truncation alter the stability of the Pex1/Pex6 complex.

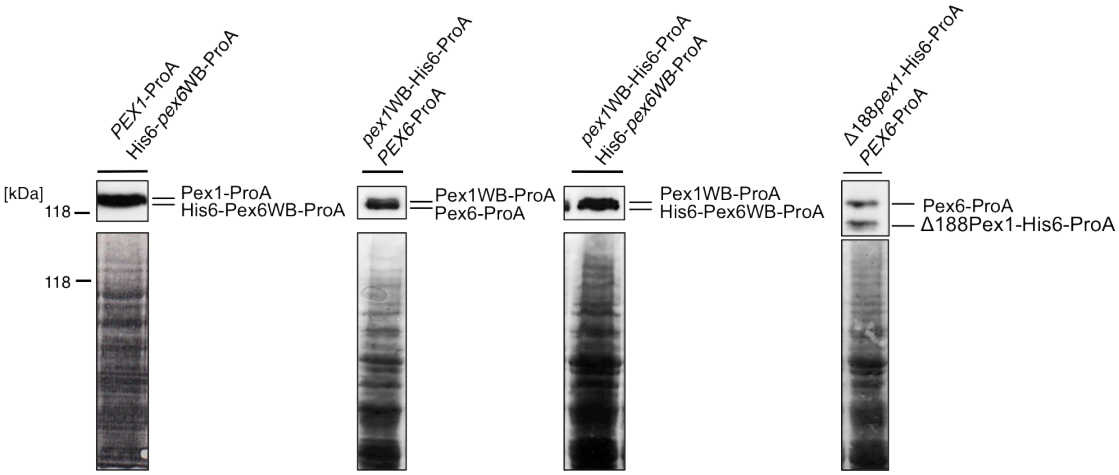

Figure 3.2 Pex1/6 overexpression strains. Pex1 and Pex6 proteins, fused to a C-terminal hexahistidin (His6-) protein A (ProA-) tag are expressed in the presence of galactose for 8 h. Up to 1 x 10^8 cells ml^{-1} are analysed by Western Blot through detection of the protein A tag using α-mouse antibodies. Corresponding amido black staining are shown below.

3.2 Purification of Pex1/6 complexes

3.2.1 Protein affinity purification of protein A tagged Pex1/Pex6

After optimization of Pex1/Pex6 co-expression conditions, a protocol for large-scale purification is established. Wild type Pex1/Pex6 proteins, both C-terminally fused to a TEV cleavable protein A tag, are isolated using IgG affinity chromatography in the presence of 2 mM ATP. As analysed by SDS-PAGE, TEV protease cleavage releases wild type Pex1 and Pex6 in stoichiometric amounts from the IgG matrix (Figure 3.3 A). The identity of purified Pex1 and Pex6 was additionally confirmed by mass spectrometry. Since the purification protocol is established for the isolation of Pex1/Pex6 wild type proteins, also mutated and truncated Pex1/Pex6 proteins are affinity-purified via their C-terminal protein A tag and released upon TEV cleavage (Figure 3.3 B-E).

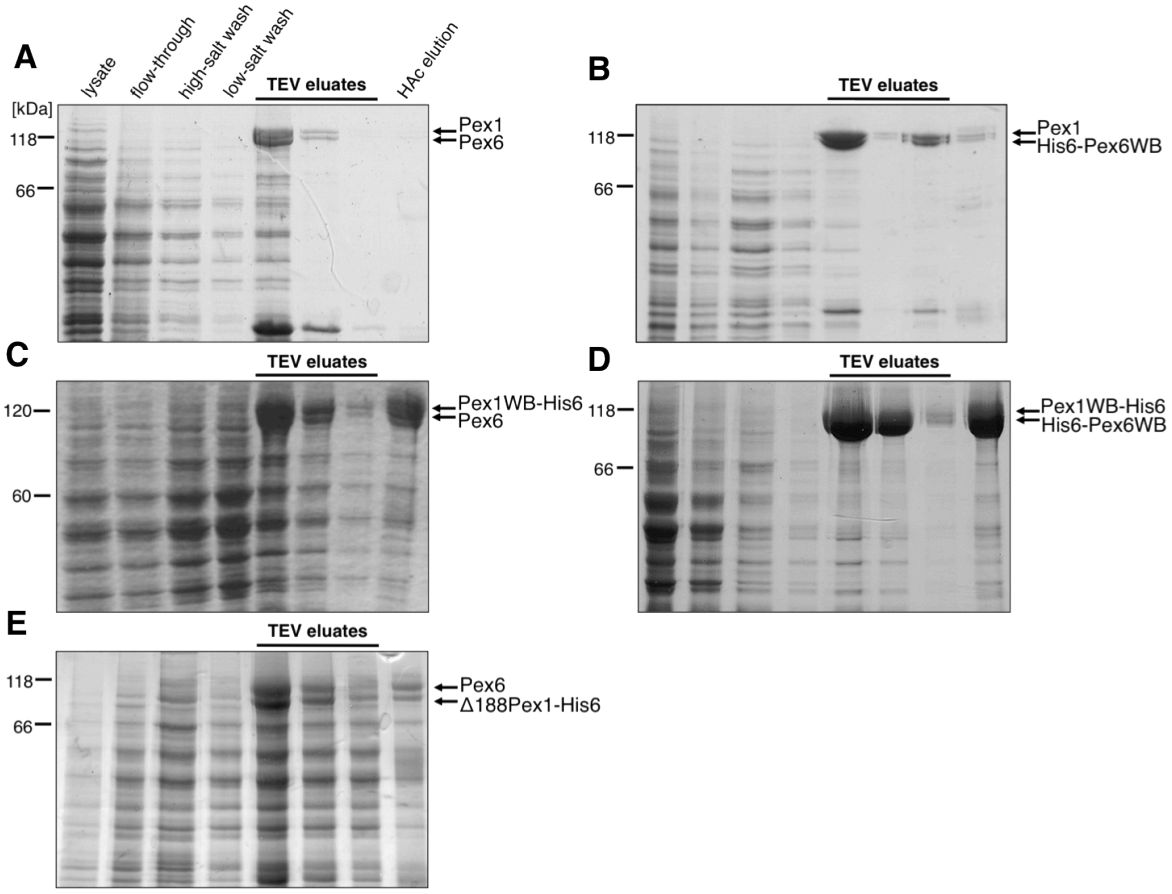

Figure 3.3 Protein A affinity purification of Pex1 and Pex6 proteins in the presence of 2 mM ATP. (A) and (B) 7.5 % SDS-PAGE or (C), (D) and (E) 10 % SDS-PAGE and Coomassie staining of fractions obtained through IgG affinity purification of Pex1/Pex6 proteins as indicated. High-salt wash was done using 500 mM NaCl, low-salt wash uing 100 mM NaCl. Pex1/Pex6 proteins are liberated by TEV protease cleavage in three fractions (TEV eluates) and remaining proteins are eluted from the affinity matrix using HAc pH 3.4 (HAc elution). All fractions are TCA precipitated and one-tenth in (A) and (B), one fifth in (C) and (D) or one-fourth in (E) of TEV eluates are analysed by SDS-PAGE.

3.2.2 Glycerol density gradient centrifugation of isolated Pex1/6 complexes

To further purify and detect whether eluted Pex1/Pex6 proteins assemble into a higher molecular weight complex in the presence of 2mM ATP, elution fractions are applied either on a linear 20 %-50 % or 10 %-40 % glycerol gradient, respectively, followed by ultracentrifugation. As analysed by SDS-PAGE (Figure 3.4 A) monodisperse Pex1/Pex6 or Pex1/His6-Pex6WB complexes migrated in stoichiometric amounts in the same higher molecular weight fractions (9-12, Figure 4.4 A), whereas TEV protease, unassembled Pex1/Pex6 proteins or putative Pex1 homotrimers are separated in lower molecular weight fractions (1-6, Figure 3.4 A).

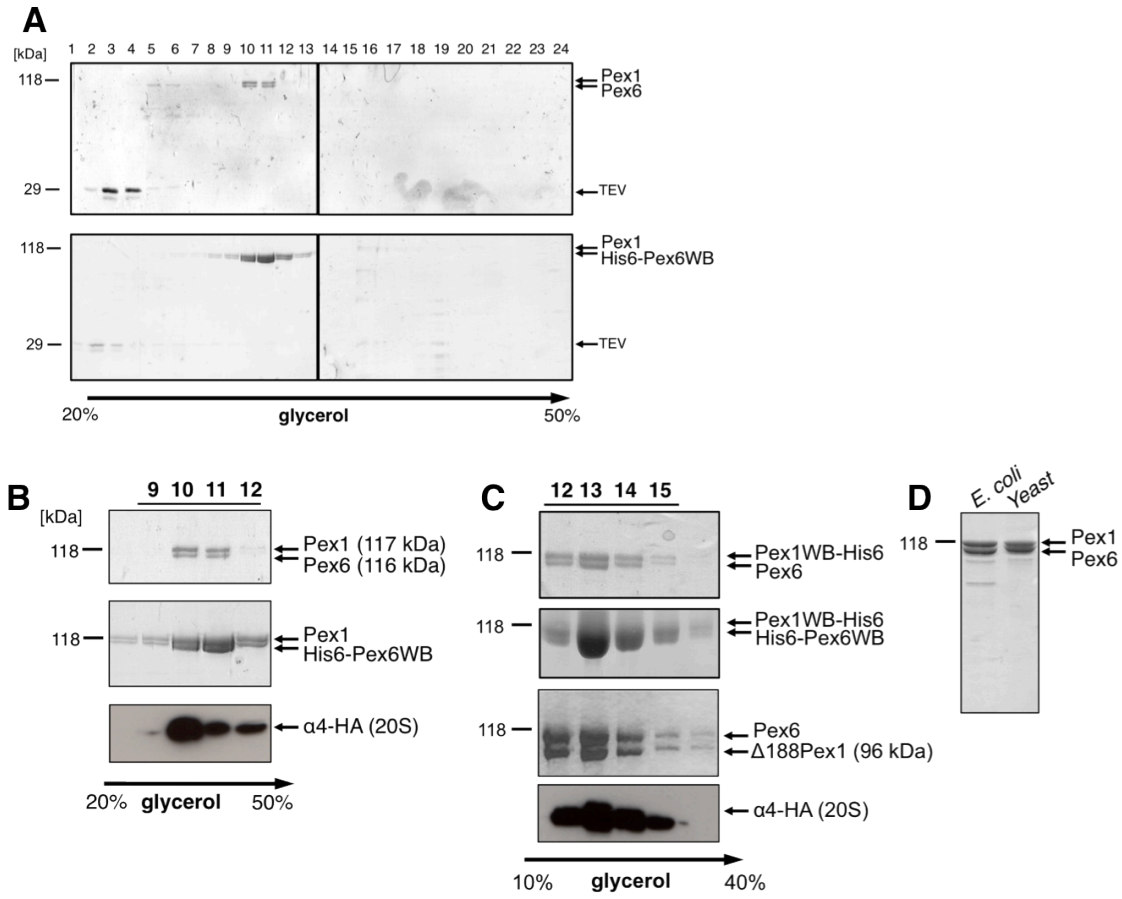

Figure 3.4 Glycerol gradient fraction analysis showing heterohexameric Pex1/6 assemblies compared to the 20S proteasome as size marker. (A) Glycerol gradient centrifugation fractions (1-24) of galactose induced wild type Pex1/Pex6 and mutated Pex1/His6-6WB purified from *S. cerevisiae* are TCA precipitated and analysed by 10 % SDS-PAGE. (B) and (C) show 10 % SDS-PAGE analysis of the migration behaviour of galactose induced wild type, mutated and truncated Pex1/6 complexes purified from *S. cerevisiae* as indicated, compared to peak fractions of similarly sized 20S proteasomes. 20S proteasomes are visualized by Western blot analysis through detection of HA-tagged α4 subunits using an α-HA antibody. (D) SDS-PAGE and Coomassie staining of purified Pex1/Pex6 originating from overexpression in *E. coli* (~5 µg, lane 1, provided by Dr. D. Saffian and I. Grimm from Prof. Ralf Erdmann's lab, Ruhr-Universität Bochum) or galactose induced Pex1/Pex6DWB co-expressed in *S. cerevisiae* (~5 µg, lane 2).

As reported previously, native Pex1/6 proteins form heterohexameric assemblies of ~ 698 kDa (Saffian *et al.*, 2012). Here, similarly sized yeast 20S proteasomes (~750 kDa, Groll *et al.*, 2000) serve as size marker for density gradient centrifugation. As judged from SDS-PAGE and immunoblotting, in the presence of ATP wild type Pex1/Pex6 (Pex1/6^{ATP}) and the Walker B complex Pex1/His6-Pex6WB (Pex1/6WB^{ATP}) migrate in the same fractions as the 20S proteasome (9-12, Figure 3.4 B). Thus, Pex1/6^{ATP} and Pex1/6WB^{ATP} predominantly assemble into complexes with the molecular size of heterohexamers.

Comparable results are obtained for complexes containing Pex1WB-His6/Pex6 (Pex1WB/6^{ATP}), Pex1WB-His6/His6-Pex6WB (Pex1/6DWB^{ATP}) and Δ188Pex1/Pex6^{ATP} after purification and analysis by glycerol gradient centrifugation. In the presence of ATP, all

Pex1/6 species migrated as higher molecular weight complexes similar to the 20S proteasome (12-15, Figure 3.4 C). Although Δ188Pex1/Pex6^{ATP} is estimated to assemble into a complex of ~ 638 kDa, it mainly migrates in the same higher molecular weight fractions as Pex1WB/6^{ATP} and Pex1/6DWB^{ATP} (13-15, Figure 3.4 C). Thus, differences in molecular weights of full-length and truncated Pex1/6 complexes cannot be distinctly resolved by glycerol gradient centrifugation. However, neither mutation of the D2 Walker B motif of Pex1 or Pex6, respectively, nor truncation of the first 188 amino acids of Pex1 interferes with native complex formation.

However, for subsequent structural analysis wild type Pex1/Pex6 proteins, which were heterogously expressed in *Escherichia coli* (*E. coli*), are obtained in collaboration with Prof. Ralf Erdmann's lab, Ruhr-Universität-Bochum (samples are kindly provided by Dr. D. Saffian and I. Grimm). When compared, Pex1/6 complexes isolated from either *E. coli* or yeast overexpression systems are purified to near homogeneity (Figure 3.4 D) and served as input for single particle electron microscopy (EM).

3.3 Structural characterisation of the Pex1/6 complex

So far, there is only little knowledge about the three-dimensional (3D) structure of yeast Pex1/6 complexes. To gain further insight into the architecture of the Pex1/6 AAA+ complex, we determine the structure of this type II AAA+ heterohexamer.. Moreover, this is the first comprehensive structural study of full-length Pex1/6 including structural and functional characterization of modified Pex1/6 assemblies.

3.3.1 Sequence similarity search

Earlier structural analyses of Pex1 and Pex6 AAA+ proteins lead to the crystal structure of the N-terminal 180 amino acids of murine Pex1 (Shiozawa *et al.*, 2004), showing strong architectural similarity to the N-terminal domains of type II AAA+ proteins p97/Cdc48 and NSF/Sec18 (Figure 1.5). Besides 3D analogy, multiple sequence alignments reveal hexameric p97/Cdc48 as closest homolog of Pex1 and Pex6 (Figure 3.5). The alignment profile shows that the D2 domains of both, Pex1 and Pex6 are well conserved. The D2 domains harbour the consensus sequence of the Walker A and the Walker B motif, two closely spaced arginine fingers and an aromatic-hydrophobic-glycine (F/YIG) pattern, corresponding to substrate-binding loop region 1 in related AAA+ proteins (Hinnerwisch *et al.*, 2005; Martin *et al.*, 2008). However, the D1 domains of Pex1/Pex6 are weakly conserved. While Pex1D1 displays a Walker A motif, the highly conserved glutamic acid of the Walker B motif is replaced by asparagine, presumably resulting in no or inefficient ATP hydrolysis. Amino acid residues

within the Pex6D1 Walker A motif deviate from the consensus sequence but allow either ADP or ATP binding (Birschmann *et al.*, 2003). Furthermore, Pex6D1 lacks the Walker B motif and neither Pex1 nor Pex6 contains well-conserved aromatic residues in the D1 pore loop region. Notably, the Pex6 D1 domain exhibits two poorly conserved arginine fingers, likely facilitating nucleotide dependent interactions with the neighbouring Pex1D1 domain.

Table 3.1 Output from Clustal W: Percent identity matrix. Sequences of yeast Pex1/6, p97 (Cdc48) and NSF (Sec18) homologs, Clp-type proteins (Hsp104, ClpB, ClpA) and SV40 large T antigen are aligned using ClustalW (Chenna et al., 2003); (Ec, *Escherichia coli*; sc, *Saccharomyces cerevisiae*; mm, *Mus musculus*; hs, *Homo sapiens*).

Protein name	mmp97	hsp97	Cdc48	Sec18	hsNSF	Hsp104	EcClpB	EcClpA	scPex1	scPex6	LTSV40
mmp97	**100.0**	100.0	69.73	22.86	23.87	11.02	10.89	9.52	21.47	21.51	8.45
hsp97	100.0	**100.0**	69.73	22.86	23.87	11.02	10.89	9.52	21.47	21.51	8.45
Cdc48	69.73	69.73	**100.0**	22.82	23.74	11.52	10.26	10.46	20.41	20.72	8.28
Sec18	22.86	22.86	22.82	**100.0**	45.27	11.48	10.82	11.16	13.21	11.55	8.35
hsNSF	23.87	23.87	23.74	45.27	**100.0**	10.78	10.96	10.86	12.79	12.43	8.21
Hsp104	11.02	11.02	11.52	11.48	10.78	**100.0**	43.95	35.86	9.12	8.34	7.58
EcClpB	10.89	10.89	10.26	0.82	10.96	43.95	**100.0**	40.88	8.16	10.25	8.48
EcClpA	9.52	9.52	10.46	11.16	10.86	35.86	40.88	**100.0**	8.73	8.76	8.68
scPex1	21.47	21.47	20.41	13.21	12.79	9.12	8.16	8.73	**100.0**	18.39	7.85
scPex6	21.51	21.51	20.72	11.55	12.43	8.34	10.25	8.76	18.39	**100.0**	6.17
LTSV40	8.45	8.45	8.28	8.35	8.21	7.58	8.48	8.68	7.85	6.17	**100.0**

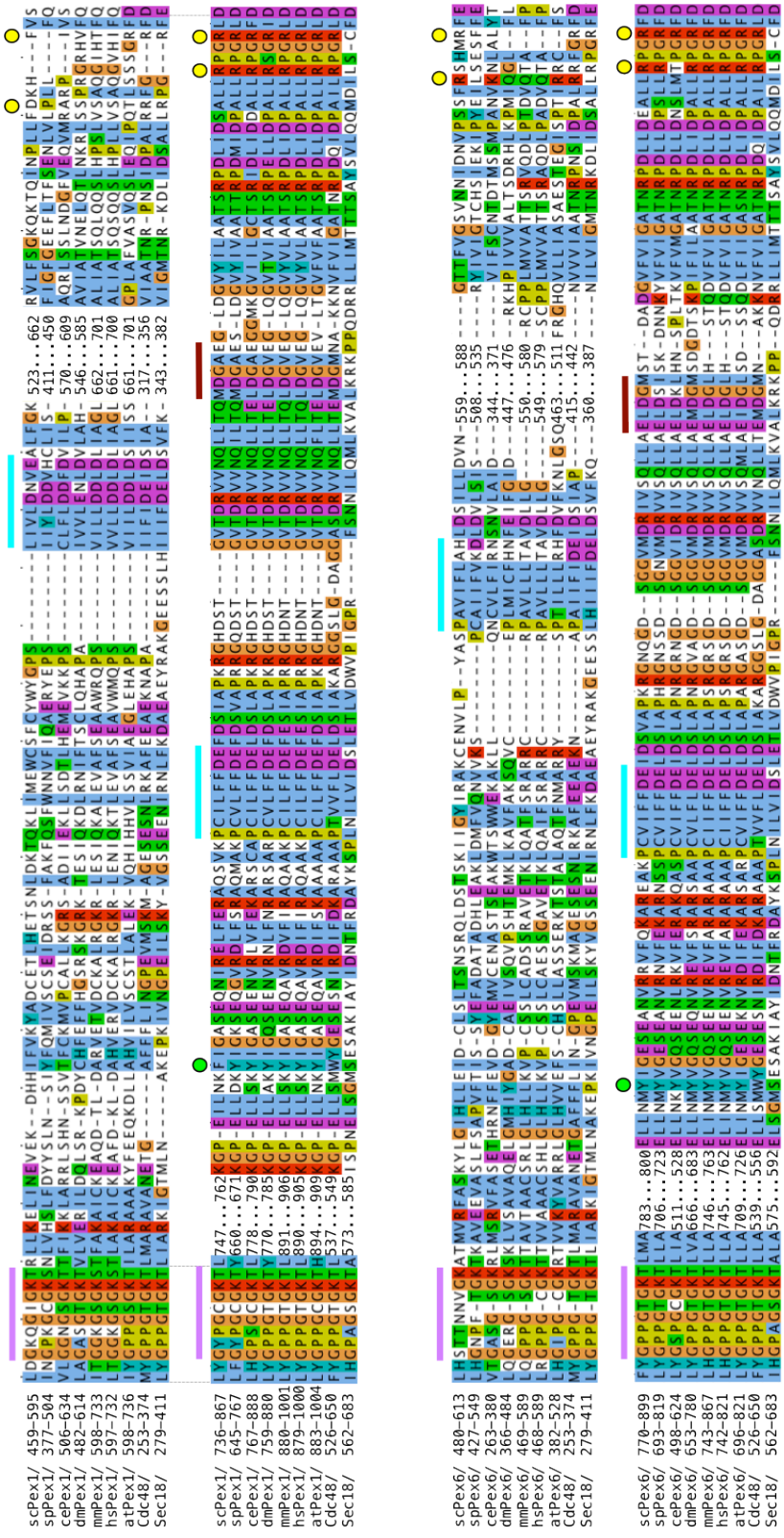

Figure 3.5 Multiple sequence alignment. Sequences of Pex1/6 homologs (sc, *Saccharomyces cerevisiae*; sp, *Schizosaccharomyces pombe*; ce, *Caenorhabditis elegans*; dm, *Drosophila melanogaster*; mm, *Mus musculus*; hs, *Homo sapiens*; at, *Arabidopsis thaliana*) and yeast Cdc48 (p97) and Sec18 (NSF) are aligned using ClustalW (Chenna et al., 2003) and visualized with JalView (Clamp et al., 2004). Canonical AAA+ elements are indicated as follows: Walker A (magenta bar), Walker B (turquois bar), substrate-binding loops (green dots), arginine fingers (yellow dots) and residues within ISS motif (brown bar).

3.3.2 Electron imaging and reference-free 2D analysis of Pex1/6$^{ATP\gamma S}$ complexes

To dissect the shape of Pex1/6 complexes, wild type proteins (provided by Dr. D. Saffian and I. Grimm, lab of Prof. Ralf Erdmann, Ruhr-Universität Bochum) are imaged with negative stain transmission EM. To this end, a solution of a soluble heavy metal salt serves as stain, which forms an amorphous cast around the complexes examined (Brenner and Horne, 1959). An aqueous solution of ~50 µg ml^{-1} wild type Pex1/6 proteins, incubated with the slowly hydrolysable ATP analogue ATPγS, is spread on a continuous carbon film and covered with an even, air-dried layer of uranyl acetate. As shown in Figure 3.6 A, a population of symmetric particles is homogeneously distributed across the carbon film. Remarkably, Pex1/6$^{ATP\gamma S}$ particles show predominantly the shape of an equilateral triangle, although the peroxisomal complex was expected to resemble the overall shape of hexameric p97. A negative stain data set is collected for detailed structural analysis of Pex1/6 in the presence of ATPγS, resulting in 3895 randomly oriented particle images. Single particles are aligned and classified based on the cross-correlation of similar features using multivariate-statistical analysis (MSA) and multi-reference alignment (MRA). Resultant class averages from reference-free alignment show a trimeric symmetry in top view classes and a double tier like shape capped by additional density in side view classes (Figure 3.6 B).

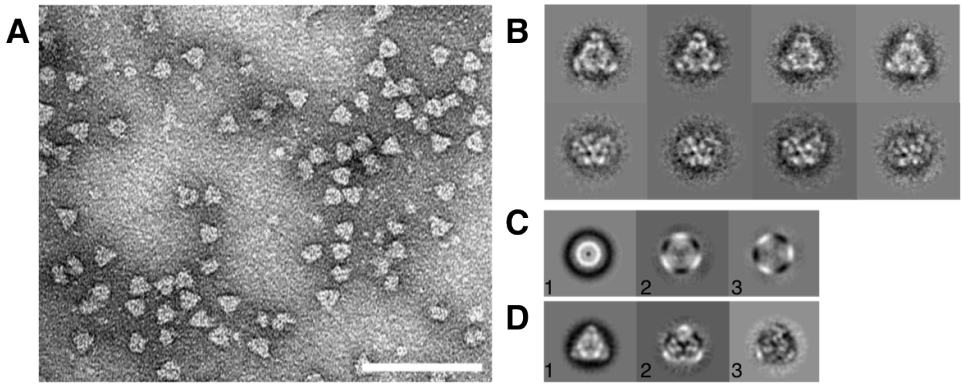

Figure 3.6 Wild type Pex1/6 $^{ATP\gamma S}$ complex analysed by negative stain. (A) Raw negative stain electron micrograph of purified wild type Pex1/6 complexes (~ 50 μg ml^{-1}) incubated with ATPγS, microscope was run at 80 keV. Scale bar, 100 nm. (B) Representative class averages, derived from multivariate statistical analysis, show characteristic top (upper row) and side views (lower row) of the Pex1/6$^{ATP\gamma S}$ complex. Each class represents an average of five to ten images. Box size, 128 pixels. (C) First three eigenimages obtained after translational (upper row) or translational and rotational (lower row) alignment.

To further exploit the degree of symmetry of Pex1/6$^{ATP\gamma S}$ complexes, the variance of the data set is assessed through multivariate statistics. Initial eigenimages, obtained after statistical analysis of centred Pex1/6$^{ATP\gamma S}$ particles, show the total sum of the data set (Figure 3.6 C, 1). Subsequent eigenimages display a trimeric symmetry as major density variation in the data set

(Figure 3.6 C, 2-3). However, alignment of rotational orientations shifts major variance towards main eigenimages, which clearly displays a central hexameric ring structure surrounded by a trimeric distributed density (Figure 3.6 D, 1). This indicates a central portion of Pex1/6 particles with a higher symmetry level. The density in subsequent eigenimages 2 and 3 are related to the shape of side views of Pex1/6$^{ATP\gamma S}$ complexes within the data set (Figure 3.6 D).

3.3.3 Domain topology of Pex1/6 complexes

In order to define the domain topology of the double-layered complex, a data set of Pex1/6 complexes with Pex1 C-terminally fused to a GST-tag (Pex1GST/Pex6, provided by Dr. Saffian), assembled in the presence of ATPγS, is acquired. 1500 raw particle images are aligned and averaged by MSA and MRA. When compared to wild type Pex1/6$^{ATP\gamma S}$ complexes without GST, resultant 2D side view classes display an additional blurry density emerging from to bottom layer of the Pex1GST/Pex6 complex (Figure 3.7 A, B). Furthermore, subtraction of Pex1GST/Pex6$^{ATP\gamma S}$ from Pex1/6$^{ATP\gamma S}$ side view class averages shows main density difference beneath the lower tier of the complex that is explained by the GST moiety emerging from the Pex1 C-terminus (Figure 3.7 C, D). Thus, the layer connected to the GST density comprises the D2 domain of Pex1/6, whereas the distal layer constitutes the D1 domain. Accordingly, AAA+ domains D1 and D2 are stacked on top of one another in the central portion of the Pex1/6 complex, whereas the density at the complex periphery is most likely attributed to the Pex1/6 N-termini.

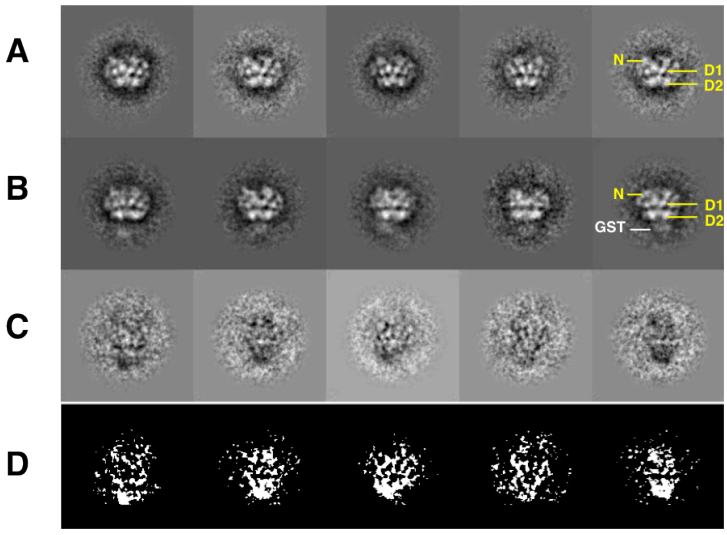

Figure 3.7 Pex1/6 domain allocation. (A) Side view class averages of Pex1/6$^{ATP\gamma S}$ and Pex1GST/Pex6$^{ATP\gamma S}$ (B) complexes followed by difference images (C) between (A) and (B). Binarised difference images are shown in (D).

3.3.4 Negative stain structure of the Pex1/6$^{ATP\gamma S}$ wild type complex

Subsequent to 2D analysis of Pex1/6$^{ATP\gamma S}$ particle images, class averages with characteristic views of Pex1/6 complexes (Figure 3.6 B) are used as input for initial model building using angular reconstitution in IMAGIC. After determination of particle orientations and Euler angle assignment, an initial 3D reconstruction is calculated, imposing 3-fold symmetry. Class averages, showing good visual similarity between input 2D projections and re-projections are used to get a consistent, initial low-resolution Pex1/6$^{ATP\gamma S}$ 3D map. The initial model is refined iteratively against 3895 raw particle images until the final 3D reconstruction converged, imposing C3 symmetry. The resultant negative stain EM map shows the structure of the yeast Pex1/6 complex in the presence of nucleotide at a resolution of 21 Å with overall dimensions of ~ 158 Å in diameter and ~ 117 Å in height (Figure 3.8 A-C). When viewed from the top, Pex1/6 assemble into a trimeric shaped complex with a double-layered side view. The centre of the 3D reconstruction has 6-fold symmetry, although 3-fold symmetry is used throughout model building and refinement.

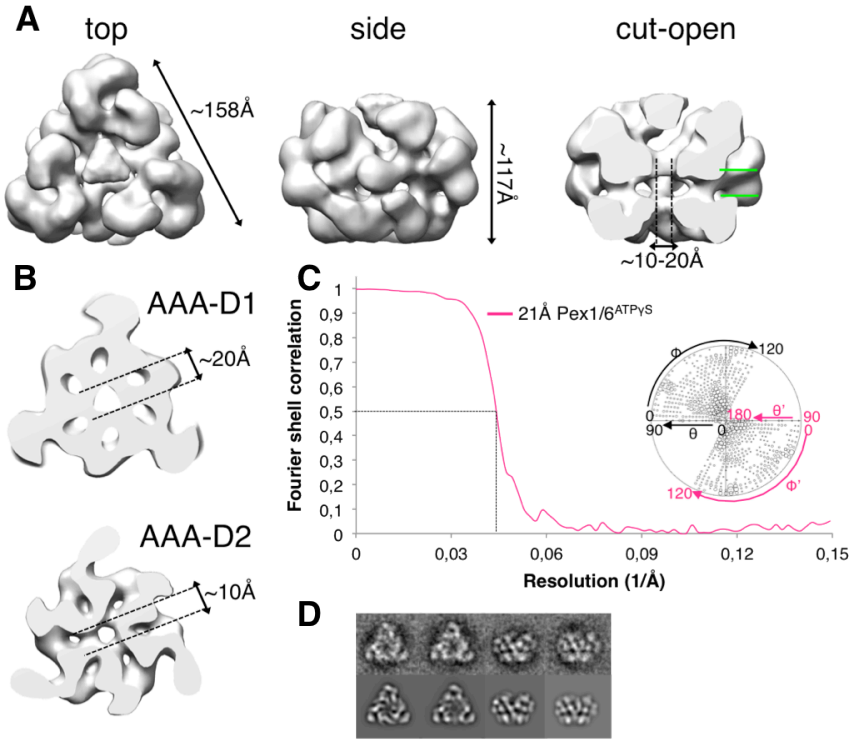

Figure 3.8 Final EM reconstruction of Pex1/6 incubated with ATPγS. (A) Surface representation of the final wild type Pex1/6$^{ATP\gamma S}$ negative stain 3D map shown as top, side and cut-open view (B) Cross-section of AAA-D1 and AAA-D2 domains. Green lines indicate cross-section viewing planes for D1/D2 domains. (C) Fourier Shell Correlation (FSC) curve of the final 3D reconstruction at the 0.5 cut-off criterion. The graph show the FSC plotted against spatial frequency [1/Å]. Inset: Euler plot for the Pex1/6$^{ATP\gamma S}$ dataset after final refinement with projection matching. The polar (θ) and azimuthal (Φ) directions are indicated (directions for mirrored particles, θ' and Φ', are indicated in pink). The C3 symmetry axis is placed in the centre of the Euler plot circle. (D) Representative class averages derived from multivariate statistical analysis show characteristic top and side views of Pex1/6$^{ATP\gamma S}$ (upper row) and corresponding re-projections of the final 3D reconstruction in the Euler-angle directions assigned to the class averages (lower row). Each class contains an average of five to ten images.

The cut-open side view shows a central channel traversing the complex from the D1 to the D2 domain, respectively, its diameter ranging from 10 Å (D2) up to 20 Å (D1). Additional density emerges from the top of the double tier, extending to the complex vertices, defining the trimeric appearance of the AAA+ complex. Furthermore, a small density appears at the channel entrance on the apical surface of D1. Class averages, obtained by MSA after the last round of refinement, are in very good agreement with resultant re-projections of the final 3D reconstruction (Figure 3.8 D), proving the quality of the final 3D volume.

3.3.5 Pex1 and Pex6 protomer positioning within the AAA+ complex

In order to trace Pex1 and Pex6 protomers within the AAA+ complex, truncated Pex1/6 complexes, missing the first 188 amino acids at the Pex1 N-terminus (Δ188Pex1/Pex6), are compared to full-length Pex1/6. Equally to wild type complexes, purified Δ188Pex1/Pex6 are assembled through incubation with ATPγS and negatively stained as described for Pex1/6$^{ATP\gamma S}$ (Figure 3.9 A). After acquiring a negative stain data set of ~ 3000 raw particle images, only the best 400 2D projections are used for final 3D reconstruction. Preferred top view orientation of most Δ188Pex1/Pex6$^{ATP\gamma S}$ complexes severely disturbed alignment and reconstruction procedures. Consequently, the amount of images displaying top view particles is reduced to ensure that the remaining 400 projections are distributed evenly across the Euler sphere. After initial model building using IMAGIC-5, the resulting 3D map is refined iteratively using projection matching in SPIDER, imposing C3 symmetry. The final 3D reconstruction of the Δ188Pex1/Pex6$^{ATP\gamma S}$ complex at 29 Å resolution, depicts a trimeric shape with two distinct layers in side views and indicates a central 6-fold symmetry (Figure 3.9 B, C). The cut-open side view shows a central channel protruding from the D1 to the D2 domain, respectively, the diameter extending from 26 Å (D2) up to 40 Å (D1). When compared to the cut-open side view of the wild type Pex1/6$^{ATP\gamma S}$ complex, the density on the symmetry axis above the central pore of the D1 domain is clearly missing and the central channel of Δ188Pex1/Pex6$^{ATP\gamma S}$ complex is accessible (Figure 3.9 B, orange circle). Notably, although overall dimensions of ΔPex188/Pex6$^{ATP\gamma S}$ are similar to wild type Pex1/6$^{ATP\gamma S}$, the truncated complex is less structured in the D1 and D2 ring. However, class averages and corresponding re-projections of the final 3D reconstruction show a satisfactory visual similarity, proving the quality of the final EM density map (Figure 3.9 A, inset).

Additionally, subtraction of EM density maps Δ188Pex1/Pex6$^{ATP\gamma S}$ from wild type Pex1/6$^{ATP\gamma S}$ reveals missing density in every second subunit that cannot be explained by conformational rearrangements of Δ188Pex1/Pex6$^{ATP\gamma S}$ D1/D2 domains (red circle, Figure 3.9 D, E). Hence, Pex1 N-termini reside on top of the complex whereas Pex6 N-termini are mainly placed at the periphery of the central AAA+ core (Figure 3.9 C). Accordingly, single D1 and D2 domains

can now be assigned to either Pex1 (D1 orange, D2 red) or Pex6 (D1 pale blue, D2 blue). Thus, the Pex1/6 complex consists of an alternating order of Pex1 and Pex6 subunits and assembles as a trimer of dimers.

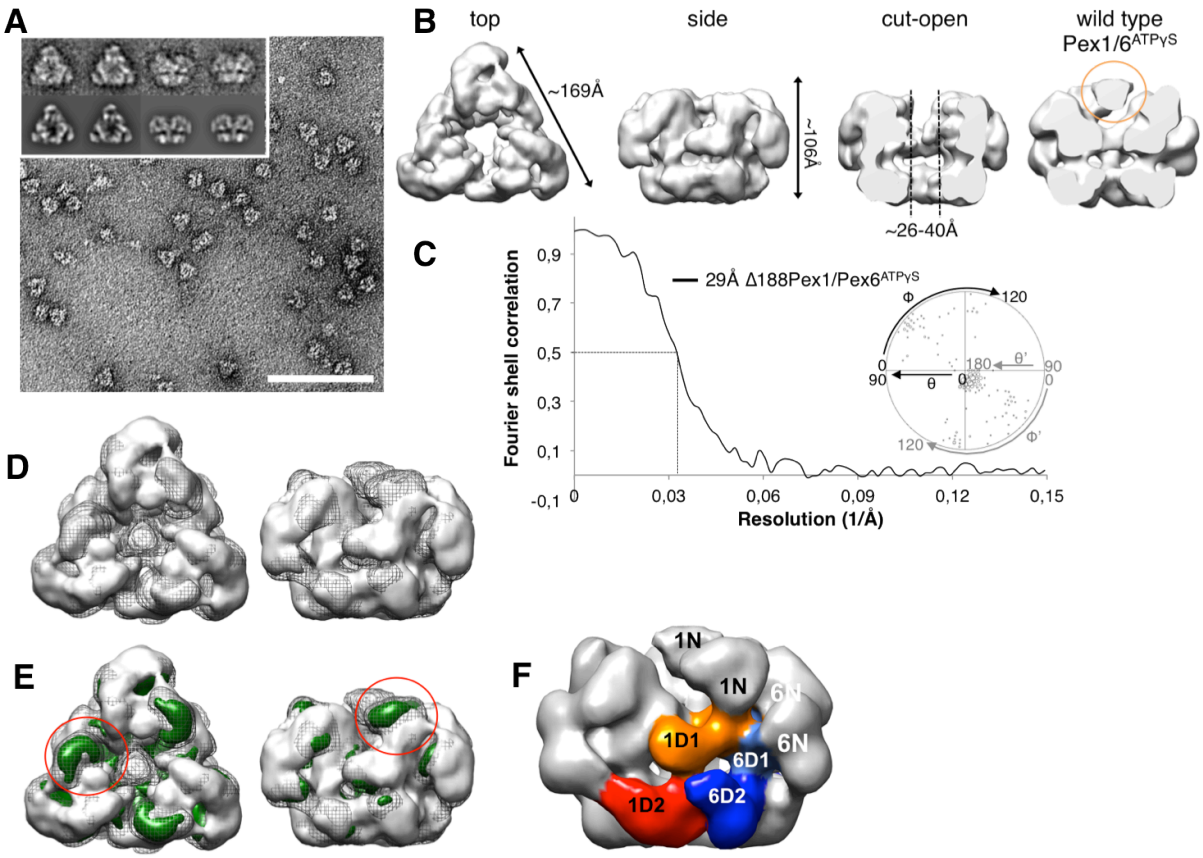

Figure 3.9 Negative stain 3D reconstruction of Δ188Pex1/Pex6 incubated with ATPγS for Pex1/Pex6 protomer assignment. (A) Raw negative stain electron micrograph of purified Δ188Pex1/Pex6^{ATPγS} complexes (~ 40 μg ml^{-1}), microscope was run at 80 keV. Scale bar, 100 nm. Representative class averages derived from MSA show top and side views of Δ188Pex1/Pex6^{ATPγS} complexes (inset, upper row) and corresponding re-projections of the final 3D reconstruction (inset, lower row). Each class contains an average of five to ten images. (B) Top, side and cut-open view of final Δ188Pex1/Pex6^{ATPγS} 3D map compared to the side cut-open view of the final Pex1/6^{ATPγS} 3D reconstruction, with the N-terminal density on the symmetry axis encircled in orange. (C) FSC curve of the final 3D reconstruction at the 0.5 cut-off criterion. The graph show the FSC plotted against spatial frequency [1/Å]. Inset: Euler plot for the Δ188Pex1/Pex6^{ATPγS} dataset after final refinement with projection matching. The polar (θ) and azimuthal (Φ) directions are indicated (directions for mirrored particles, θ' and Φ', are indicated in grey). The C3 symmetry axis is placed in the centre of the Euler plot circle. (D) Top and side views of surface representations of Δ188Pex1/Pex6^{ATPγS} hexamers (grey surface) overlaid with full-length Pex1/6^{ATPγS} hexamers (dark grey mesh). (E) The difference map between Pex1/6^{ATPγS} and Δ188Pex1/Pex6^{ATPγS} hexamers is shown in green. Difference density is encircled in red. (E) Surface representation of Pex1/6^{ATPγS} with Pex1 and Pex6 protomers highlighted according to their domain structure. The colour code is as follows: Pex1D1 (1D1, orange), Pex1D2 (1D2, red) and Pex6D1 (6D1, pale blue), Pex6D2 (6D2, blue). N-terminal domains of Pex1 (1N) and Pex6 (6N) are coloured grey.

3.3.6 3D comparison of Pex1/6 and p97

With the protomer allocation established and as a result of the close sequence based relationship of yeast Pex1 and Pex6 to p97, appearance and dimensions of the Pex1/6$^{ATP\gamma S}$ 3D reconstruction are compared to a low-pass filtered p97 crystal structure bound to ADP (pdb-ID: 3CF3, Davies *et al.*, 2008; Figure 3.10 A). Although additional p97 X-ray structures with the D2 domain bound to different nucleotides exist (pdb-ID: 3CF2 ADP-AlFx; pdb-ID: 3CF1 AMP-PNP), the crystal structures show only minor deviation from 6-fold rotational symmetry. Thus, p97 bound to ADP is selected as template for structural comparison and as described below, is used as atomic structure for initial fitting of the Pex1/6$^{ATP\gamma S}$ EM density map.

The width and height of the central Pex1/6 AAA+ double-layer are in good agreement with p97 (Figure 3.10 A). Similarly, Pex1/6$^{ATP\gamma S}$ D1 and D2 domains exhibit hexameric symmetry, which is typical for type II AAA+ assemblies and also applies to other complexes whose structure have been determined by cryo-EM (Rouiller *et al.*, 2002; Wendler *et al.*, 2007; Chang *et al.*, 2012). In contrast, the asymmetric distribution of Pex1/6 N-terminal domains is a unique feature and has not been observed so far for other AAA+ proteins. The first 180 amino acids of murine Pex1 show a strong structural homology to p97 and NSF (Shiozawa *et al.*, 2004), but Pex1 and Pex6 N-termini are 400 amino acids long and twice as large as the N-termini of their homologs (Figure 1.5). Consequently, the overall dimension differs because the N-terminal Pex1/Pex6 densities contribute to the overall height of the complex. p97 structures with elevated N-terminal domains are available but most structures, mainly those solved by X-ray crystallography, show p97 N-termini coplanar with the D1 layer (DeLaBarre and Brunger, 2003; Huyton *et al.*, 2003; Davies *et al.*, 2005; DeLaBarre and Brunger, 2005). Besides differences in the N domains, the D1 ring of the Pex1/6$^{ATP\gamma S}$ complex is somewhat wider compared to the compact appearance of p97 D1. The central channel in Pex1/6 D1 opens up to 20 Å and the axial pore extends to the bottom of the D2 domain (Figure 3.10 A, B) similar to EM structures of ClpA- and ClpB- type AAA+ hexamers (Wendler *et al.*, 2009; Effantin *et al.*, 2010). The latter thread substrate proteins through their open central pore, a mechanism that seems not to apply to the tightly packed arrangement of p97. However, dramatic conformational changes of p97 are so far only captured by SAXS and cryo-EM studies (Rouiller *et al.*, 2002; Davies *et al.*, 2005; Yeung *et al.*, 2014), whereas crystallographic constraints might determine domain orientations in p97 X-ray structures. For subsequent atomic structure fitting, homology models of Pex1/Pex6 single D1 and D2 domains are created based on the aforementioned p97 crystal structures neglecting the N-terminal domains. Without the N terminal domains, hexameric p97 (pdb-ID: 3CF3) readily fits the density of the D2 layer of Pex1/6$^{ATP\gamma S}$ complex, confirming that the stain does not significantly alter the Pex1/6$^{ATP\gamma S}$ complex integrity and all AAA+ domains are well resolved

in the negative stain reconstruction at 21 Å resolution (Figure 3.10 C, left). Furthermore, the good agreement of the fit in the D2 domain determines unambiguously the handedness of the Pex1/6 complex. The homology models of the Pex1/6 D1 and D2 ATPase domains are placed as rigid bodies into the EM density using the automated fitting procedure in UCSF Chimera. Several starting positions are tested and all ended in the same fit of the D1/D2 ATPase domains. Subsequently, docked models are symmetrized and resulting pseudo-atomic models

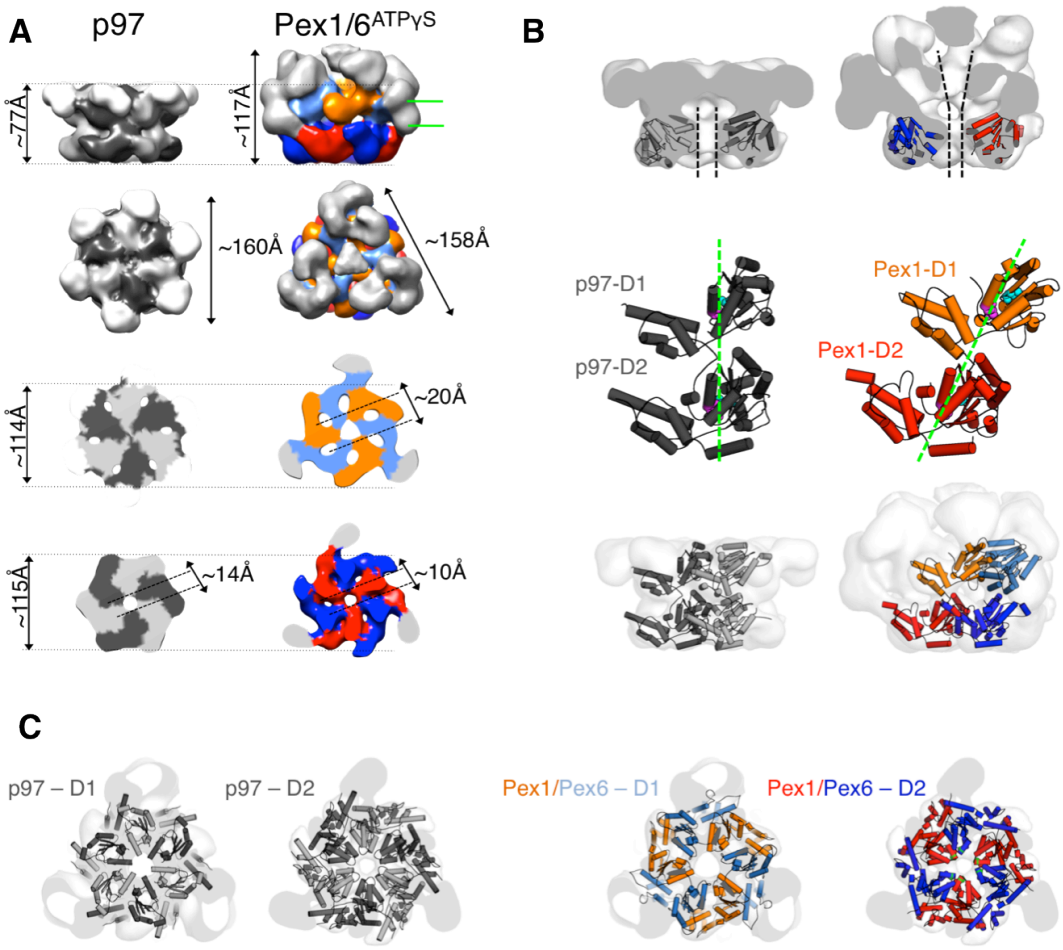

Figure 3.10 Pex1/6^{ATPγS} EM reconstructions compared to low-pass filtered p97 and rigid body fitting to the Pex1/6 3D volume. (A) Pex1/6^{ATPγS} EM density map as side, top and cross-section views of D1 and D2 rings. Equivalent views of p97 (pdb-ID: 3CF3) filtered to 20Å are shown for comparison. p97 single subunits are coloured alternately light and dark grey. Cross-section viewing planes are indicated by green lines. (B) Cut-open side views of the low-pass filtered p97 crystal structure with p97 D2 placed into the EM density map and of Pex1/6^{ATPγS} map with fitted Pex1D2 and Pex6D2 homology models. Black dotted lines indicate the central channel (upper row). Cartoon representation of a p97 protomer without N domains and of a Pex1 protomer homology model, seen from the side of the complex. Domain offset between Pex1D1 and Pex1D2 is indicated by green dotted lines. Walker A, Walker B motifs are shown as spheres and coloured as in Figure 1.5 (middle row). Side view of a p97 dimer fitted as rigid body into low-pass filtered p97 crystal structure and Pex1/6 heterodimer docked to Pex1/6^{ATPγS} 3D map. Domains are coloured as in Figure 3.9 F (lower row). (C) D1 and D2 cross-section views of p97 (pdb-ID; 3CF3) docked into the Pex1/6^{ATPγS} map (left). Rigid body fitting of the Pex1/6 homology model into the ATPγS EM map as indicated. Domains are coloured as in Figure 3.9 F. Pore facing aromatic residues Pex1^{F771} and Pex6^{Y805} are depicted as green spheres.

fit both tiers of the Pex1/6$^{ATP\gamma S}$ complex very well (Figure 3.10 C, right), revealing densities for 12 individual ATPase domains. Notably, the resulting arrangement of the D1 and D2 ring differs strongly between p97 and the Pex1/6 complex. While D1 and D2 domains are symmetrically stacked on top of each other in the p97 crystal structure, the D1 domains in Pex1/6 hexamers are rotated anticlockwise by ~ 30° relative to the D2 domain (Figure 3.10 B, middle row). This is also the reason for the low correlation between the p97 D1 ring and the Pex1/6 D1 ring when the p97 hexamer is fitted to the Pex1/6 hexamer (Figure 3.10 C, left). Consequently, the arrangement of D1 and D2 AAA+ rings in Pex1/6 is structurally closer to the one of type II AAA+ proteins ClpA and Hsp104 (Guo *et al.*, 2002; Wendler *et al.*, 2007; Effantin *et al.*, 2010) than to the one of p97.

3.3.7 EM reconstructions of Pex1/6 in ADP-AlFx, ATP and ADP states

In order to dissect conformational states of Pex1/6 throughout ATP binding and hydrolysis, the hexameric assembly is reconstructed with saturating quantities of different nucleotides (see section 2.7.2). Wild type Pex1/6 is incubated with either the transition state analogue ADP-AlFx or ATP and the previously mentioned Pex1GST/Pex6 complexes are incubated with ADP. Subsequently, samples are negatively stained according to Pex1/6$^{ATP\gamma S}$ and imaged by EM (Figure 3.11, A-C). A negative stain data set is acquired for every nucleotide state resulting in 2394 (Pex1/6$^{ADP\text{-}AlFx}$) 2948 (Pex1/6^{ATP}) and 1488 (Pex1/6^{ADP}) raw particle images. After classification by MSA and MRA, initial 3D models are build in IMAGIC-5 by angular reconstitution and further refined in SPIDER throughout repetitive cycles using projection matching, imposing 3-fold symmetry. Final EM density maps of the Pex1/6 complexes in different nucleotide states at resolutions of 23 Å-24 Å (Figure 3.11 D, E), retain distinct trimeric symmetry and double-layered side views (Figure 3.12). The overall dimensions for all reconstituted complexes are similar and mainly the orientation of the N-terminal domains contributes to differences in height (117 Å-103 Å) and width (158 Å-164 Å). Aside from the loosely packed D2 layer of Pex1/6^{ADP}, the central AAA+ core of all complexes shows clear C6 symmetry and well-resolved densities for ATPase domains. Again, upon hexamerisation Pex1/Pex6 N-terminal densities emerge apical from the D1 layer, sitting on the top and at the vertices of Pex1/6 complexes. Particularly, in the presence of ADP, D1 domains rotate away from the central symmetry axis providing a platform for a continuous N-terminal density distribution at the rim of the D1 domain. This constitutes an entrance to a large cavity in D1, extending up to 48 Å in diameter. Among all nucleotide states, Pex1/6^{ADP} displays the largest axial pore and has the most relaxed appearance. Addition of ATP alters the complex towards a more compact conformation, indicating nucleotide binding.

In contrast to Pex1/6 captured in the presence of ADP, the overall shape of Pex1/6^{ATP} almost

resembles that of Pex1/6$^{ATP\gamma S}$. Again, upon hexamerisation, Pex1/Pex6 N-terminal densities emerge apical from the D1 layer, sitting on the top and at the vertices of Pex1/6 complex. Densities for AAA+ domains are oriented towards the symmetry axis, which is accessible from the top of the complex. The Pex6 N-terminal densities arrange in discrete domains establishing contacts to Pex1D2 (yellow asterisk, Figure 3.12). This interaction is also present in the Pex1/6$^{ATP\gamma S}$ complex and might be associated with nucleotide binding to the D2 layer. This notion is consistent with previous publications showing that nucleotide binding of the Pex1 D2 domain is crucial for the interaction with Pex6. However, the diameter of the pore in Pex1/6^{ATP} D1 (26 Å) and D2 (19 Å) domains is still extended compared to Pex1/6 bound to ATPγS.

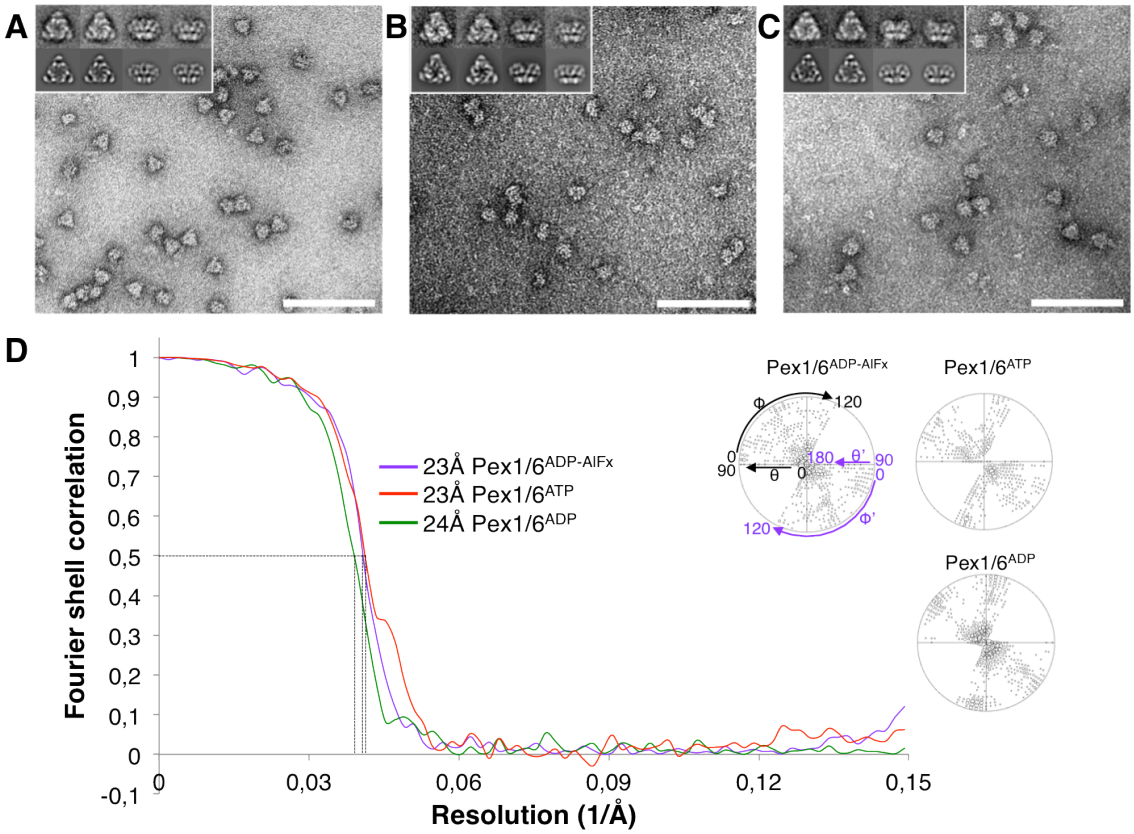

Figure 3.11 Wild type Pex1/6 complexes in the presence of different nucleotides analysed by negative stain. Raw negative stain electron micrographs of purified wild type Pex1/6 complexes (40-50 μg ml^{-1}) treated with (A) ADP-AlFx, (B) ATP and (C) ADP. Microscope was run at 80 keV. Representative class averages derived from MSA show top and side views of Pex1/6 complexes (A-C inset, upper row) and corresponding re-projections of the final 3D reconstruction in the Euler-angle directions assigned to the class averages (A-C inset, lower row). Each class contains an average of five to ten images. Scale bar, 100 nm. (D) FSC curves of final 3D reconstructions with C3 symmetry applied, measured at the 0.5 cut-off criterion (colour code and resolutions are given). The graphs show the FSC plotted against spatial frequency [1/Å]. Inset: Euler plots for Pex1/6 datasets as indicated after final refinement with projection matching. The polar (θ) and azimuthal (Φ) directions are indicated for Pex1/6$^{ADP\text{-}AlFx}$ (directions for mirrored particles, θ' and Φ', are indicated in purple). The C3 symmetry axis is placed in the centre of each Euler plot circle.

In comparison to Pex1/6$^{ATP\gamma S}$, major domain re-arrangements are observed when the complex is reconstituted in the presence of the transition state analogue ADP-AlFx. Domain rotations closes the central pore of the D2 domain simultaneously opening the central channel of the D1 domain to 26 Å. Again, contacts between Pex1D2 and Pex6N are clearly visible, apparently based on nucleotide occupancy in the D2 domain. Unlike Pex1/6 in the presence of ADP or ATP, Pex1/6$^{ADP\text{-}AlFx}$ N-termini shield the entry to the central cavity of the complex.

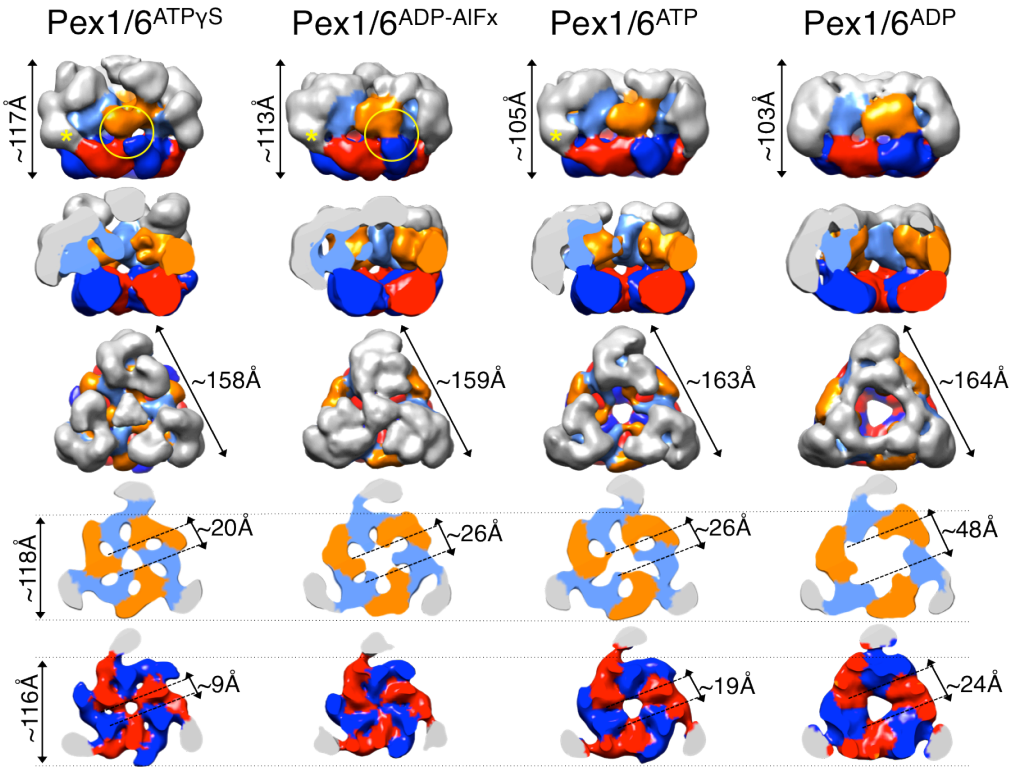

Figure 3.12 Negative stain structures of Pex1/6 complexes treated with different nucleotides. Negative stain EM reconstructions of Pex1/6 complexes in the presence of ATPγS (Pex1/6$^{ATP\gamma S}$), ADP-AlFx (Pex1/6$^{ADP\text{-}AlFx}$), ATP (Pex1/6^{ATP}) and ADP (Pex1/6^{ADP}) seen as side views (upper row), followed by cut-open side views, top views and cross-sections of the D1 and D2 layers (lower rows). Domains are coloured according to Figure 3.9 F.

Obviously, different nucleotides cause domain motions in the Pex1/6 complex that are strikingly different between N domains, D1 or D2 layers. While the pore of the D1 ring never closes, the pore diameter of the D2 ring never exceeds 24 Å and closes in the presence of the transition state analogue ADP-AlFx. The size of the central channel is dynamically adapted through distinctive nucleotide-induced motions of AAA+ domains within the D1 and D2 ring. Furthermore, ATP binding to the D2 ring structures this layer towards tighter domain arrangements. N-terminal domains are apparently altered dependent on the nucleotide present, too, communicating with the D2 domain through direct and/or long-range contacts.

3.3.8 Comparison of Pex1/6$^{ATP\gamma S}$ and Pex1/6$^{ADP\text{-}AlFx}$ EM reconstructions

To further explore whether nucleotide hydrolysis induces domain movements, the 3D reconstructions of Pex1/6 in the presence of ATPγS or ADP-AlFx are compared in more detail.

In the molecular structure of the non-hydrolysable nucleotide analogue ATPγS, a sulfur atom replaces the γ-phosphate, avoiding rapid nucleotide turn over in AAA+ proteins (Chen *et al.*, 2007). Binding of ATPγS to Pex1/6 assembles the complex into a stable, hexameric arrangement with a distinct 6-fold symmetry in the D1 and D2 domains (Figure 3.8) and likely traps the complex in an ATP bound state. For mimicking ATP hydrolysis in the Pex1/6 ATPase domain, the complex is mixed with ADP-AlFx. The transition state analogue forms a trigonal bipyramidal geometry within the nucleotide binding pocket and captures the ATPase between the ATP and ADP bound state (Braig *et al.*, 2000). Notably, ATP hydrolysis causes the D1 domains in Pex1/6$^{ADP\text{-}AlFx}$ to move apart. The domains re-arrange thereby slightly tilting downwards and away from the central cavity. At the same time, the central pore of the D2 ring closes resulting in strong connecting densities between Pex1D1 and Pex6D2 at the outside of the complex that cannot be seen in Pex1/6 complexes bound to ATPγS (yellow circle, Figure 3.12). This diagonal inter-domain communication is only possible because of the displaced arrangement of ATPase domains in D1 and D2 rings (Figure 3.10 B). The N-terminal densities move towards the symmetry axis at the top of the complex, further closing the central opening into the cavity of Pex1/6$^{ADP\text{-}AlFx}$. Closer examination of dynamic re-arrangements in the D2 domain within the 3D reconstructions of both states reveals that ATPase domains flip down towards the exit of the central pore thereby closing the ring (Figure 3.13 A). As judged from the negative stain EM maps, D2 domains undergo a dramatic downward rotation upon ATP hydrolysis. As described above for Pex1/6$^{ATP\gamma S}$, Pex1/Pex6 homology models are docked automatically into the density of the Pex1/6$^{ADP\text{-}AlFx}$ D2 ring using Chimera. The resulting pseudo atomic model fits this layer readily (Figure 3.13 B). Moreover, upon pore closure the ATPase domains are coming closer together in a tight hexameric arrangement. When viewed from the side, the fitted homology models further support the downward directed orientation of the Pex1/Pex6 domains in the D2 layer of Pex1/6$^{ADP\text{-}AlFx}$.

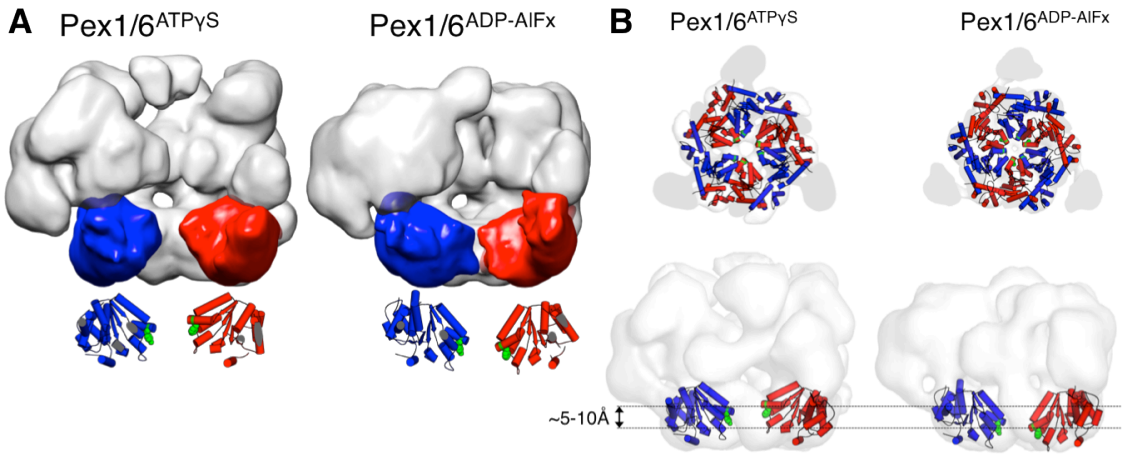

Figure 3.13 Correlation of the Pex1/6^{ATPγS} and Pex1/6$^{ADP-AlFx}$ 3D reconstruction. (A) Side view surface representation of Pex1/6^{ATPγS} and Pex1/6$^{ADP-AlFx}$. One heterodimer is omitted from the 3D reconstructions. Underneath, a cartoon representation based on rigid body fits of homology models into negative stain EM maps is shown. (B) D2 cross-section views (upper row) and side view surface representation (lower row) of EM reconstructions as indicated. Pex1/6 homology models are automatically fitted to the D2 domain and are coloured as in Figure 3.9 F. Conserved aromatic residues Pex1^{F771} and Pex6^{Y805} are shown as green spheres. Movements of pore loops are indicated by black dotted lines.

To verify the underlying processing procedures resulting in these dramatic differences between the ATPγS and ADP-AlFx state, both 3D reconstructions are refined from interchanged starting models. Those refinements result in the original EM density map, proving that the information for domain motions and overall re-arrangements source from intrinsic orientations captured in the respective raw data sets (Figure 3.14).

The domain orientations observed in the 3D reconstructions are considered reliable and the position of conserved aromatic residues in substrate binding loop region 1 of Pex1 or Pex6 (Pex1^{F771}, Pex6^{Y805}) are highlighted in automatically fitted homology models. As depicted in Figure 3.13 B, pore-facing residues Pex1^{F711} and Pex6^{Y805} are oriented towards the central opening of the D2 domain in hexameric homology models. During ATP hydrolysis, they move in plane towards the symmetry axis thereby closing Pex1/6 D2 and also translocate out of plane along the central channel of the Pex1/6 complex (Figure 3.13 B, lower row). It was reported earlier that ATPase subunits of Hsp104 move in a nucleotide dependent manner (Wendler *et al.*, 2009). Observed displacement of residues Pex1^{F771} and Pex6^{Y805}, respectively, induced by ATP hydrolysis points to a similar motion in the Pex1/6 complex.

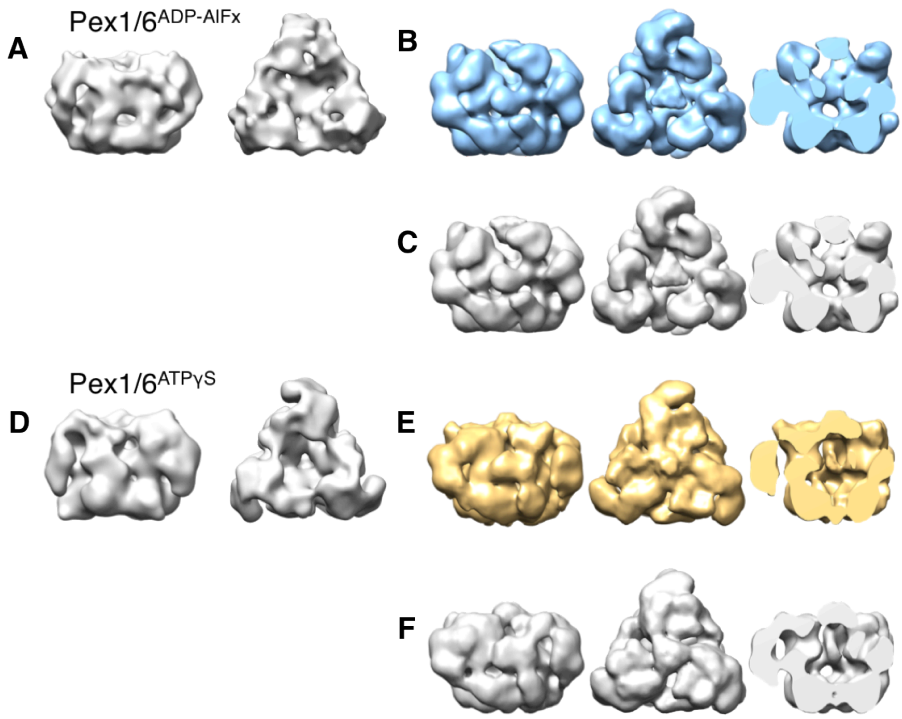

Figure 3.14 Refinement of Pex1/6 $^{ATP\gamma S}$ and Pex1/6$^{ADP\text{-}AlFx}$ from interchanged starting models. (A) Top and side view of initial 3D model derived from angular reconstitution of Pex1/6$^{ADP\text{-}AlFx}$ data set. (B) Final EM reconstruction after projection matching of ATPγS treated single particles to starting model in (A) shown as side, top and side cut open view. (C) Final EM reconstruction after projection matching of ATPγS Pex1/6 data set to starting model in (D) depicted as side, top and side cut open view. (D) Top and side view of initial 3D model derived from angular reconstitution of Pex1/6$^{ATP\gamma S}$ data set. (E) Final EM reconstruction after projection matching of ADP-AlFx treated single particles to starting model in (D), shown as side, top and side cut open view. (F) Final EM reconstruction after projection matching of ADP-AlFx Pex1/6 data set to starting model in (A) depicted as side, top and side cut open view.

3.3.9 Asymmetric reconstructions of Pex1/6 in the presence of ATPγS and ATP

Recent cryo-EM studies of related AAA+ hexamers show a distorted symmetry in AAA+ rings (Matyskiela *et al.*, 2013; Zhao *et al.*, 2015), resulting in an asymmetric arrangement of individual subunits. This domain organization is assumed to be functionally relevant for substrate processing.

It is impossible to define the exact nucleotide state of single active sites within Pex1/6 complexes at the resolution obtained. However, to elucidate the orientations of individual Pex1/6 AAA+ domains, the position of each protomer in the complex is examined. To this end, Pex1/6$^{ATP\gamma S}$ and Pex1/6^{ATP} initial 3D models are refined without imposing symmetry (C1) using projection matching in SPIDER. Final EM density maps of the Pex1/6 complexes preserve a distinct trimeric symmetry in top views and double-layered side views (Figure 3.15 A, B). Although no symmetry was applied during refinement, the D1 and D2 layer of both complexes occupy a distinct 6-fold symmetry. The symmetry-free EM reconstructions show similar dimensions for the central AAA+ core compared to the symmetrized EM density

maps. The resolution of the final C1 Pex1/6 EM maps is somewhat lower (Figure 3.15 C), however, densities for all 12 AAA+ ATPase domains are well resolved and clearly distinguishable. Differences in overall height of Pex1/6$^{ATP\gamma S}$ C1 trace back to movements of N-terminal domains. The overall shape of the complex is almost identical to the symmetrized wild type complex. The densities are homogeneously distributed throughout the 3D reconstruction and dimensions of the central channel of the D1 and the D2 ring differ marginally from the C3 Pex1/6$^{ATP\gamma S}$ EM map. Homology models of Pex1D2 or Pex6D2, respectively, are fitted automatically into each density of individual domains within the D2 ring using Chimera (Figure 3.15 D). Notably, the presence of ATPγS causes a planar domain orientation in the D2 layer, emphasized by the position of the aromatic residues Pex1^{F771} and Pex6^{Y805} located within the substrate binding loops (Figure 3.15 E).

Asymmetric reconstruction has a bigger impact on Pex1/6 complexes in the presence of ATP (Figure 3.15 A). In the Pex1/6^{ATP} C1 complex, the distribution of N domains is similar to the N-terminal arrangement found in the symmetrized Pex1/6^{ADP} EM density map (Figure 3.12). Particularly, N-terminal densities assigned to Pex1 move flexibly on top of the D1 domains. The latter occur stretched in the Pex1/6^{ATP} C1 EM reconstruction, caused by an outward rotation of the D1 domains. Furthermore, one connection between a Pex1D2 and a Pex6N domain is lost, caused by the out of plane movement of the Pex1/6 D2 domain and contraction of the Pex6N domain (yellow asterisk, Figure 3.15 A). This is accompanied by an expansion of the D1 ring, forming a cavity which is 10 Å wider compared to the symmetrized counterpart. Thus, refinement without symmetry constraints reveals domain re-arrangements in the Pex1/6 D1 domain resulting in varying pore sizes in this layer. Domain movements are even more pronounced in the D2 layer of the Pex1/6^{ATP} C1 complex. While the pore size is almost identical to the symmetrized Pex1/6^{ATP} EM reconstruction, automated fits of Pex1/6 homology models reveal an asymmetric arrangement in the D2 ring of Pex1/6^{ATP} C1 (Figure 3.15 E). The arrangement of ATPase subunits in different planes might constitute a dynamic domain organization that is essential for substrate processing along the central pore. Pex1/6 ATPase sites are most likely only partially occupied by ATP in the D2 ring of Pex1/6^{ATP} C1, indicating preferred nucleotide states of AAA+ domains. Highlighted by the orientation of Pex1^{F771} and Pex6^{Y805} in rigid body fits, in Pex1/6^{ATP} C1 AAA+ subunits clearly move out of plane, arranging in a staircase like manner.

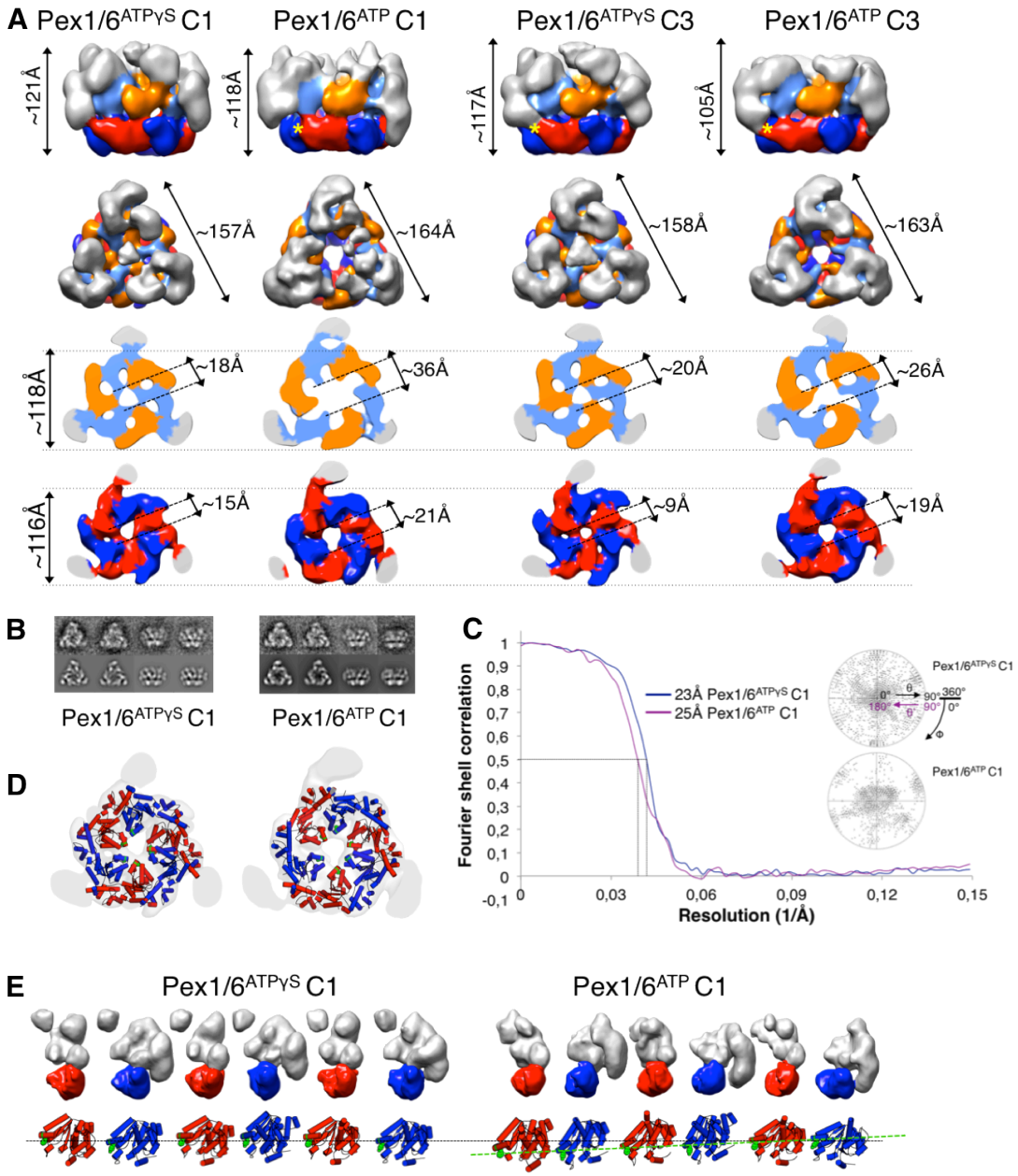

Figure 3.15 Asymmetric 3D reconstruction of Pex1/6ATPγS and Pex1/6ATP. (A) Final Pex1/6^{ATPγS} and Pex1/6^{ATP} C1 or C3 EM reconstructions as side views (upper row), followed by top views and cross-sections of the D1 /D2 layers (lower rows). (B) Representative class averages derived from MSA show characteristic top/side views (upper row) and corresponding re-projections (lower row) of the final Pex1/6^{ATPγS} C1 (left) and Pex1/6^{ATP} C1 (right) EM density maps in the Euler-angle directions assigned to the class averages. (C) FSC curves of final 3D reconstructions without symmetry applied, measured at the 0.5 cut-off criterion (colour code and resolution are given). The graphs show the FSC plotted against spatial frequency [1/Å]. Inset: Euler plots for Pex1/6 datasets after final asymmetric refinement by projection matching. The polar (θ) and azimuthal (Φ) directions are indicated for Pex1/6^{ATPγS} C1 (directions for mirrored particles, θ', are indicated in blue). The central axis is placed in the centre of each Euler plot circle. (D) Pex1/6 homology models fitted to final Pex1/6^{ATPγS} C1 (left) and Pex1/6^{ATP} C1 (right) 3D maps. (E) Surface representation of each protomer of Pex1/6^{ATPγS} C1 and Pex1/6^{ATP} C1 complexes. Underneath, a cartoon representation based on rigid body fits of homology models into negative stain EM maps of each D2 domain is shown. The black dotted line indicates the position of pore facing loops of D2 domains in Pex1/6^{ATPγS} C1 complex and the green dotted line the asymmetric arrangement of D2 domains in the Pex1/6^{ATP} C1 complex.

3.4 Functional analysis of Pex1/6 central pore and arginine finger residues

Functional studies of peroxins in yeast exploit the cell's ability to grow on non-fermentable carbon sources in the absence of glucose (Erdmann *et al.*, 1991; Faber, 1998; Kiel *et al.*, 1999). In this study, comparable complementation assays are performed in order to dissect the effect of so far uncharacterized Pex1 and Pex6 mutants toward yeast cell viability.

As described in 3.3.8, the negative stain EM structures of Pex1/6 complexes demonstrate significant, nucleotide dependent domain re-arrangements, moving pore-facing residues $Pex1^{F771}$ and $Pex6^{Y805}$ along the central symmetry axis, thereby crossing the channel in the D2 domain. Previous studies showed, that mutations within the conserved aromatic-hydrophobic-glycine (F/YVG) sequence do not interfere with ATPase activity but abolish enzyme function (Hinnerwisch *et al.*, 2005; DeLaBarre *et al.*, 2006; Martin *et al.*, 2008). To analyse whether aromatic residues in potential Pex1/6 substrate binding loop regions affect complex function, modified Pex1/6 alleles are tested in oleate growth assays. Target amino acid residues in Pex1 and Pex6 are identified through multiple sequence alignments (Figure 3.5). In addition to the conserved tryptophan of Pex1D2 ($Pex1^{F771}$), Pex1 carries two poorly conserved aromatic residues in the D1 domain ($Pex1^{Y488}$, $Pex1^{H495}$). Similarly, Pex6 harbours a weakly conserved tyrosine in the D1 domain ($Pex6^{Y528}$) and the well-conserved tyrosine in the D2 domain ($Pex6^{Y805}$). It was reported earlier that in crystal structures of related AAA+ proteins the conserved residues of the aromatic-hydrophobic-glycine pattern within substrate binding loops typically line the central pore (Schlieker *et al.*, 2004; Siddiqui *et al.*, 2004; Mueller-Cajar *et al.*, 2011). Consistent with these observations, the conserved aromatic Pex1/Pex6 residues face the axial channel of the Pex1/6 complex when highlighted in homology models, which are automatically fitted to $Pex1/6^{ATP\gamma S}$ (Figure 3.16 A). For subsequent functional characterization, specified aromatic residues are replaced by alanine. Modified Pex1/Pex6 alleles are expressed under the control of their native promotors and expression is induced upon oleate exposure.

When grown on oleic acid-medium cells lacking endogenous Pex1 or Pex6 (*pex1*Δ, *pex6*Δ), show no growth (Figure 3.16 B). In contrast, cells expressing $Pex1^{Y488A}$, $Pex1^{H495A}$ or $Pex6^{Y528A}$ proliferate at comparable levels to cells, which ectopically express the wild type gene. Surprisingly, cells expressing mutants $Pex1^{F771A}$ or $Pex6^{Y805A}$ fail to grow on oleate as the single carbon source. These results emphasize that the biological activity of Pex1/6 complexes depends on functional pore loops in the D2 domains, most likely to preserve interactions with the substrate. The impact of mutations tested in oleate growth assays and the flexibility of substrate binding loops of D2 domains demonstrated in Pex1/6 3D reconstructions proposes a mechanism for substrate translocation through the central pore of the D2 domain.

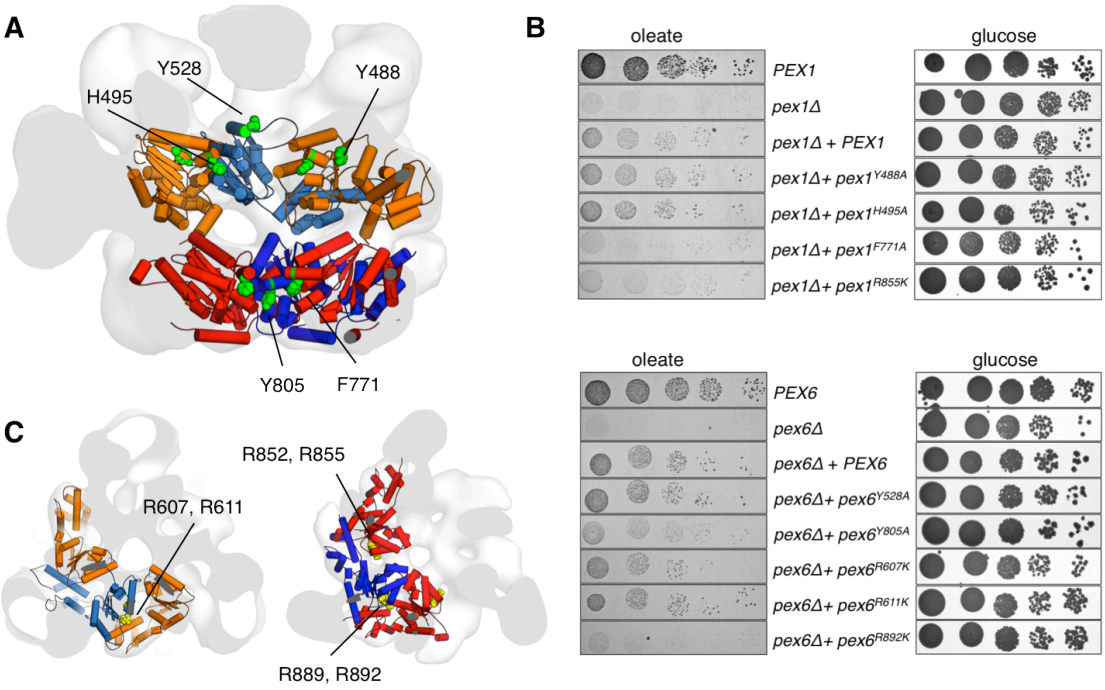

Figure 3.16 Pex1/6 pore loop and arginine finger mutants tested in oleate growth assays. (A) Cut-open side view surface representation of the Pex1/6$^{ATP\gamma S}$ EM reconstruction. Pex1/6 homology models are automatically fitted to the D1 and D2 domain and are coloured as in Figure 3.9 F. Conserved aromatic residues of D1 or D2 domains are highlighted as green spheres. (B) Growth of strains expressing either wild type (*PEX1*, *PEX6)*, no (*pex*1Δ, *pex6Δ)* or mutated *pex1*, *pex6* alleles with modified pore loop (*pex1*^{Y488A}, *pex1*^{H495A}, *pex1*^{F771A}, *pex*6^{Y528A}, *pex6*^{Y805A}*)* or arginine finger residues (*pex1*^{R855K}, *pex6*^{R607K}, *pex6*^{R611K}, *pex6*^{R892K}*)* on either glucose or oleate as single carbon source. (C) D1 and D2 cross-section views of the Pex1/6$^{ATP\gamma S}$ EM reconstructions. Pex1/6 homology models are automatically fitted to the D2 domain and are coloured as in Figure 3.9 F. Yellow spheres highlight Pex1 and Pex6 arginine fingers as indicated.

Besides conserved substrate binding loop regions, Pex1 and Pex6 also contain arginine residues, which match position 1 and 2 arginine fingers of p97 (Figure 3.5). Available crystal structures of oligomeric AAA+ proteins of the classic clade display two conserved arginine fingers at subunit interfaces, of which at least one extends into the ATP binding pocket of the neighbouring protomer (Wendler *et al*. 2012). Together with a multitude of mutational analysis, arginine fingers are found to be essential for ATPase activity of respective complexes and stabilize oligomeric assemblies of AAA+ proteins (Wendler *et al.*, 2012).

As depicted in Figure 3.16 C, potential arginine fingers of Pex1D2 (Pex1$^{R852, R855}$) or Pex6D1 (Pex6$^{R607, R611}$) and Pex6D2 (Pex6$^{R889, R892}$), respectively, are located at the interface between adjacent subunits. To exploit their role in the Pex1/6 complex *in vivo*, target arginine residues are replaced by lysine and examined in oleate growth assays as described above.

On plates containing oleate as the sole carbon source, cells expressing Pex6^{R611K} proliferate compared to cells expressing the wild type gene from an ectopic location, whereas Pex6^{R607K} cells are somewhat sensitive towards oleate exposure (Figure 3.16 B). Notably, expression of

mutants Pex1^{R855K} and Pex6^{R892K} abolishes cell growth on oleate, hinting that functional arginine fingers in Pex1/6 D2 domains are essential for complex function and/or stability *in vivo*. In contrast, arginine residues in Pex6D1 have only a minor effect on peroxisome biogenesis. Although the increased sensitivity of cells expressing Pex6^{R607} in oleate growth assays suggests an intermolecular catalytic mechanism between adjacent Pex6D1 and Pex1D1 domains.

3.5 Capturing the ATPase cycle of Pex1/6: single and double Walker B mutants

The detailed structural comparison of Pex1/6$^{ATP\gamma S}$ and Pex1/6$^{ADP\text{-}AlFx}$ negative stain EM maps revealed striking differences in their overall structure triggered by dynamic domain movements upon ATP binding and hydrolysis (Figure 3.13). Particularly D2 domains undergo major nucleotide dependent re-arrangements. Furthermore, 3D reconstructions without symmetry constraints demonstrated an asymmetric arrangement of single AAA+ domains within the D2 layer of Pex1/6^{ATP} (Figure 3.15) most likely caused by different nucleotide occupancy. Thus, as a heterohexamer the active sites in the Pex1/6 complex might be functionally non-equivalent. Here, Pex1/6 ATPase-deficient variants are analysed to dissect mutually exclusive inter-subunit communication coordinated by ATP hydrolysis. To this end, Pex1 and Pex6 are modified independently and the effects of altered protomers are studied functionally and structurally to further elucidate the mechanism of ATP binding and hydrolysis in Pex1/6 complexes.
Mutagenesis, ATPase activity and parts of oleate growth assays have been performed in collaboration with Prof. Ralf Erdmann's lab (Ruhr-Universität Bochum). Part of the data is kindly provided by I. Grimm (also indicated in figure legends).

3.5.1 Role of single Pex1/Pex6 subunits in ATPase activity and *in vivo* function

For the purpose of analysing the impact of individual nucleotide binding sites of Pex1/6 D2 domains on overall ATPase activity *in vitro*, modified Pex1 or Pex6 proteins, devoid of ATP hydrolysis, are subjected to ATPase activity assays. Multiple sequence alignment shows that both, Pex1 and Pex6 exhibit a highly conserved aspartate and glutamate within the Walker B (WB) consensus sequence of D2 domains (Figure 3.5). Earlier publications of related AAA+ proteins revealed that substitution of Walker B aspartate or glutamate by uncharged equivalents (D/E→N/Q) block ATP hydrolysis but not ATP binding (Weibezahn *et al.*, 2003; Dalal *et al.*, 2004; Schaupp *et al.*, 2007). Therefore, corresponding glutamates of either Pex1D2 or Pex6D2 are mutated to glutamine (Pex1^{E798Q}, Pex6^{E832Q}). Co-purification of mutated gene products from *E. coli* with the wild type of the respective other subunit

(Pex1WB^{ATP}/6, Pex1/6WB^{ATP}) or co-expression of mutated subunits (Pex1/6DWB^{ATP}), results in monodisperse complexes, used for subsequent activity assays (Figure 3.17 A).

As reported previously, the overall ATPase rate of isolated wild type Pex1/6 complexes with a km of ~ 0.17 mM and a Vmax of ~ 0.35 nmol min^{-1} µg^{-1} is comparable to type II AAA+ ATPases p97 or NSF (Saffian *et al.*, 2012). As depicted in Figure 3.17 B, mutations in the Walker B motif of Pex1 reduces the ATPase activity to ~ 80 % of wild type levels. In contrast, Pex1/6WB^{ATP} complexes lost the ability to hydrolyse ATP despite the presence of wild type Pex1. Moreover, ATPase activity of double Walker B complexes is completely compromised. Notably, Walker B mutations in individual subunits result in different *in vitro* ATPase activities of Pex1/6 complexes. Thus, Pex1D2 and Pex6D2 domains contribute differently to the complex' ATPase activity.

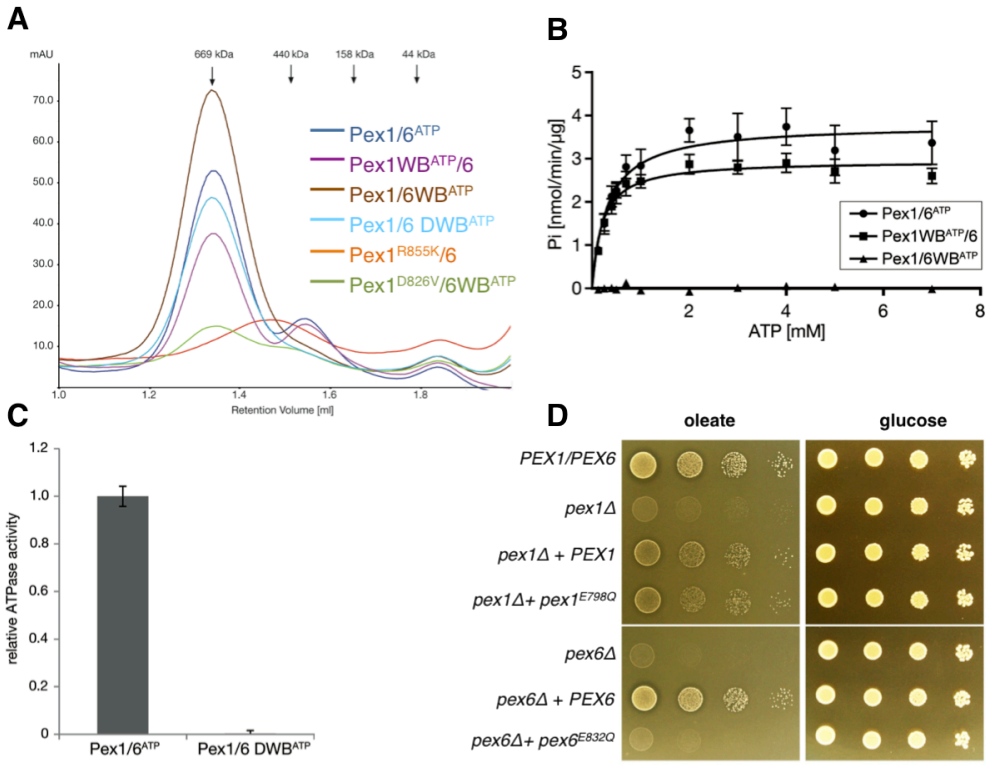

Figure 3.17 Pex1/6 Walker B variants tested in ATPase activity and oleate spotting assays. (A) Size exclusion chromatography A290nm profiles of purified Pex1/6 complexes used for ATPase activity assays. Colour code is given. (B) Michaelis Menten plot of enzyme activity of wild type Pex1/6^{ATP} and single Walker B mutants (Pex1WB^{ATP}/6, Pex1/6WB^{ATP}) at various ATP concentrations. Error bars represent standard deviation of six experiments. (C) ATPase activities of the wild type Pex1/6 complex (Pex1/6^{ATP}) and double Walker B mutants (Pex1/6DWB^{ATP}), as indicated. Assays were performed in the presence of 1mM ATP and 5mM Mg^{2+} at 37°C. Error bars represent standard deviation of five experiments. (D) Growth of strains expressing wild type (*PEX1, PEX6*), no (*pex1Δ, pex6Δ*) or mutated Pex1, Pex6 alleles with modified Walker B motifs (*pex1*^{E798Q}, *pex6*^{E832Q},) on either glucose or oleate as single carbon source. All figures are kindly provided by I. Grimm (in collaboration with the lab of Prof. Ralf Erdmann, Ruhr-Universität Bochum).

Next, to dissect the influence of Pex1/6 D2 active sites on complex function *in vivo* and to compare it to *in vitro* hydrolysis activity, respective ATPase-deficient variants are tested for

genetic complementation. To this end, modified Pex1/Pex6 alleles (*pex1*^{E798Q}, *pex6*^{E832Q}) are expressed under the control of their native promotors and tested towards cell viability upon oleate exposure. In line with the results obtained from ATPase activity assays, Pex1^{E798Q} cells are apparently associated with normal growth comparable to wild type cells (*PEX1*/*PEX6*, Figure 3.17 C). In contrast, cells expressing Pex6^{E832Q} are not viable under oleic acid-conditions.

Hence, Pex1WB^{ATP}/6 complexes retain ~ 80 % of wild type hydrolysis activity and are functionally active *in vivo*. In contrast, mutating the conserved glutamate of the Pex6 D2 domain results in loss of *in vitro* ATPase activity and Pex1/6 complex function *in vivo*. This implies functional differences between Pex1 and Pex6 subunits. While ATP hydrolysis in Pex6D2 is essential for functionally active complexes, hydrolytic activity of Pex1D2 is dispensable for *in vivo* function.

Surprisingly, these findings are in contrast to previous publications that showed that a non-conservative aspartate-to-glutamine mutation in the Walker B motif of Pex1D2 (Pex1^{D797Q}) results in non-functional complexes *in vivo* (Birschmann *et al.*, 2005). To pursue these contradictory results, a more common aspartate-to-asparagine mutation is introduced in the Pex1D2 Walker B motif (Pex1^{D797N}) and tested towards cell viability under oleic-acid conditions. As depicted in Figure 3.18 A, growth of Pex1^{D797N} cells is abolished upon oleate exposure.

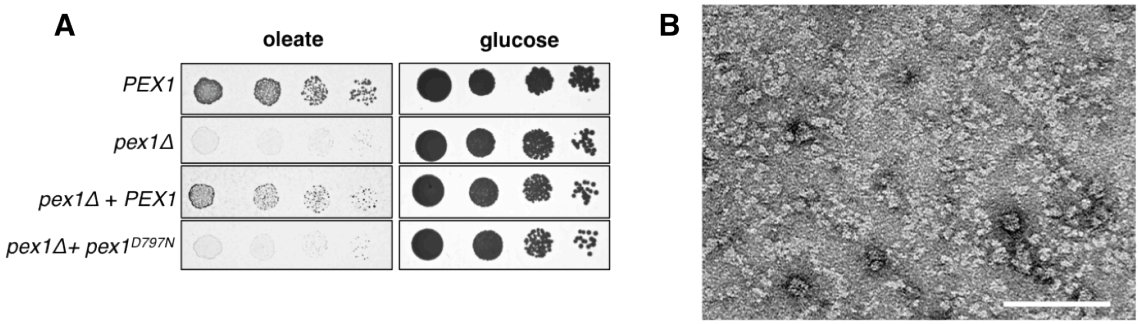

Figure 3.18 Cell viability and negative stain analysis of Pex1 Walker B mutant. (A) Growth of strains expressing either wild type (*PEX1*), no (*pex1Δ*) or mutated Pex1 allele with modified Walker B motif (*pex1*^{D797N}) on either glucose or oleate as single carbon source. (B) Raw negative stain electron micrograph of purified Pex1^{D797N}/Pex6 complexes treated with 4 mM ATP.

Subsequently, Pex1^{D797N} is co-purified with wild type Pex6 followed by size exclusion chromatography in the presence of ATP (performed by I. Grimm, data not shown) and samples of purified Pex1^{D797N}/Pex6^{ATP} complexes are investigated using negative stain EM. To this end, Pex1^{D797N}/Pex6^{ATP} gel filtration fractions corresponding to the molecular weight of hexamers are mixed with ATP, negatively stained and visualized by EM. The raw micrograph shows some single particles resembling the expected size of Pex1/6 complexes, mainly devoid of expected trimeric symmetry, though (Figure 3.18 B). Also, a substantial number of small

particles representing unassembled protein are clearly visible. This result demonstrates a significantly reduced ability of Pex1^{D797N}/Pex6^{ATP} to promote nucleotide-dependent hexamerisation. Accordingly, limited growth of corresponding alleles under oleic acid-conditions could be explained by disturbed complex formation.

Pex1^{D797Q}/Pex6^{ATP} samples could not be further pursued by negative stain EM because protein concentrations after co-purification have been too low, hinting that the Walker B mutation Pex1^{D797Q} also interferes with the complex' capability to form stable hexamers. Thus, diminished complex function upon expression of *Pex1*^{D798Q} *in vivo* most likely correlates with impaired hexamerisation.

3.5.2 Structural architecture of negatively stained Pex1/6 Walker B complexes

To provide a three-dimensional framework of ATPase-deficient Pex1/6 variants in context of wild type hexamers, the negative stain structures of mutant complexes are determined.

To this end, hetero-oligomers mutated either in the Pex1D2 domain (Pex1WB^{ATP}/6), in the Pex6D2 domain (Pex1/6WB^{ATP}) or both domains (Pex1/6DWB^{ATP}) are expressed and isolated from yeast. In the presence of ATP, fractions from glycerol density gradient centrifugation corresponding to the molecular weight of heterohexamers (Figure 3.4 B, C) are negatively stained and subsequently imaged using EM (Figure 3.19 A-C). A negative stain data set is acquired for every Pex1/6 Walker B complex resulting in 2073 (Pex1/6DWB^{ATP}), 2048 (Pex1/6WB^{ATP}) and 2064 (Pex1WB^{ATP}/6) raw particle images. After classification by MSA and MRA, initial 3D models are build in IMAGIC by angular reconstitution and further refined in SPIDER throughout repetitive cycles using projection matching, imposing 3-fold symmetry. Class averages, obtained by MSA after the last round of refinement, are in very good agreement with resultant re-projections of the final 3D reconstructions (Figure 3.19 A-C, inserts). Final Pex1/6 Walker B EM density maps at resolutions of 23 Å (Figure 3.19 D, E) display a trimeric symmetry in top views and double-capped side views (Figure 3.20). The overall dimensions for all reconstituted complexes are similar in height (110 Å-120 Å) and width (161 Å-165 Å). The central AAA+ core of the Walker B complexes shows C6 symmetry and well-resolved densities for ATPase domains. Particularly, the 3D reconstruction of Pex1/6DWB^{ATP} resembles a well-structured domain arrangement in the D1 and D2 layers and is almost identical to Pex1/6$^{ATP\gamma S}$. Apparently, the presence of ATPγS or mutations of the conserved Walker B glutamate in both, Pex1D2 and Pex6D2 locks the active sites in a nucleotide bound state. Hence, ATP binding to the Pex1/6 D2 domains directs the AAA+ domains into an arrangement similar to hexameric crystal structures of p97.

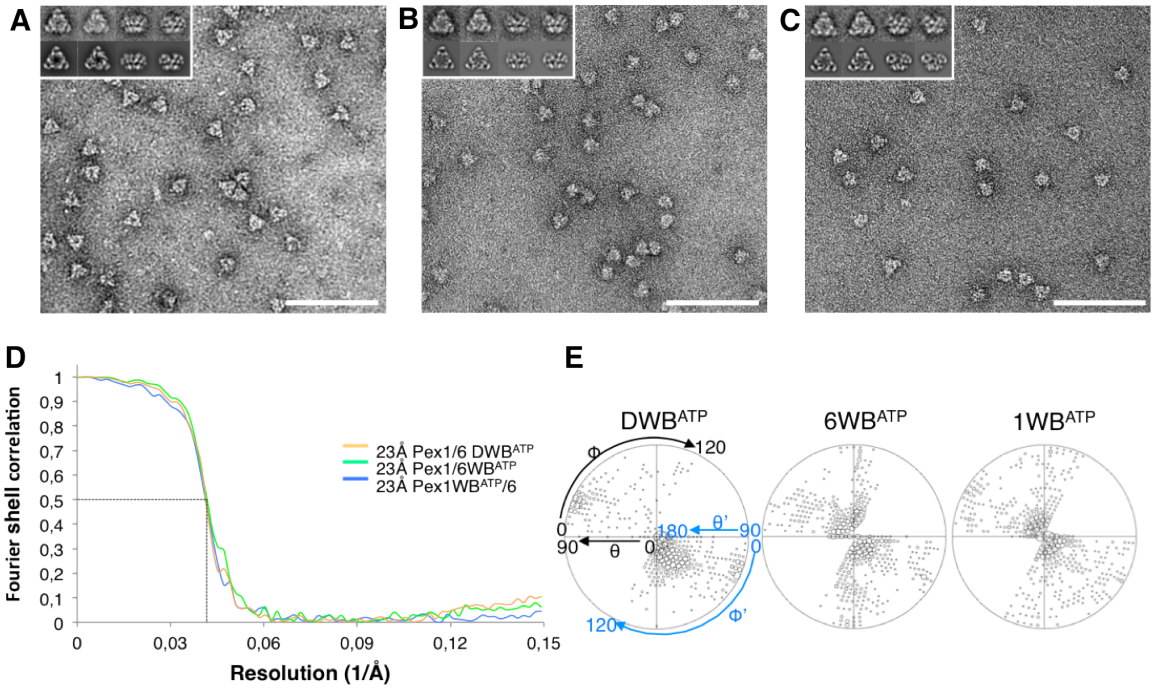

Figure 3.19 Negative stain analysis of Pex1/6 Walker B complexes. Raw electron micrographs of ~ 40-50 μg ml^{-1} Pex1/6DWB^{ATP} (A), Pex1/6WB^{ATP} (B) and Pex1WB^{ATP}/6 (C) mixed with 2 mM ATP. Representative class averages derived from MSA show averaged 2D top and side view projection (A-C inset, upper row) and corresponding re-projections of the final 3D volume in the Euler-angle directions assigned to the projections (A-C inset, lower row). Each class contains on average five to ten images. Scale bar, 100 nm. (D) FSC curves of final 3D volumes, measured at the 0.5 cut-off criterion (colour code and resolutions are given). The graphs show the FSC plotted against spatial frequency [1/Å]. (E) Euler plots for Pex1/6 datasets after final refinement with projection matching. The polar (θ) and azimuthal (Φ) directions are indicated for Pex1/6DWB^{ATP} (directions for mirrored particles, θ' and Φ', are indicated in pink). The C3 symmetry axis is placed in the centre of each Euler plot circle.

The similarity between independently generated 3D reconstructions Pex1/6$^{ATP\gamma S}$ and Pex1/6DWB^{ATP} further verifies the structural integrity of the complexes during negative staining procedures and emphasizes the consistency of the underlying image processing procedures. As observed for wild type Pex1/6 complexes, upon hexamerisation Pex1/Pex6 N-terminal densities emerge apical from the D1 layer, sitting on the top and at the vertices of the Pex1/6DWB^{ATP} complex. The N-termini arrange in discrete domains making contacts between Pex1D2 and Pex6N. Moreover, the Pex1/6DWB^{ATP} complex features a central channel traversing the complex from the D1 to the D2 domain, respectively, its diameter ranging from 14 Å (D2) up to 23 Å (D1). Similar to Pex1/6$^{ATP\gamma S}$, a small N-terminal density appears at the symmetry axis on the apical surface of D1, thereby blocking the central pore.

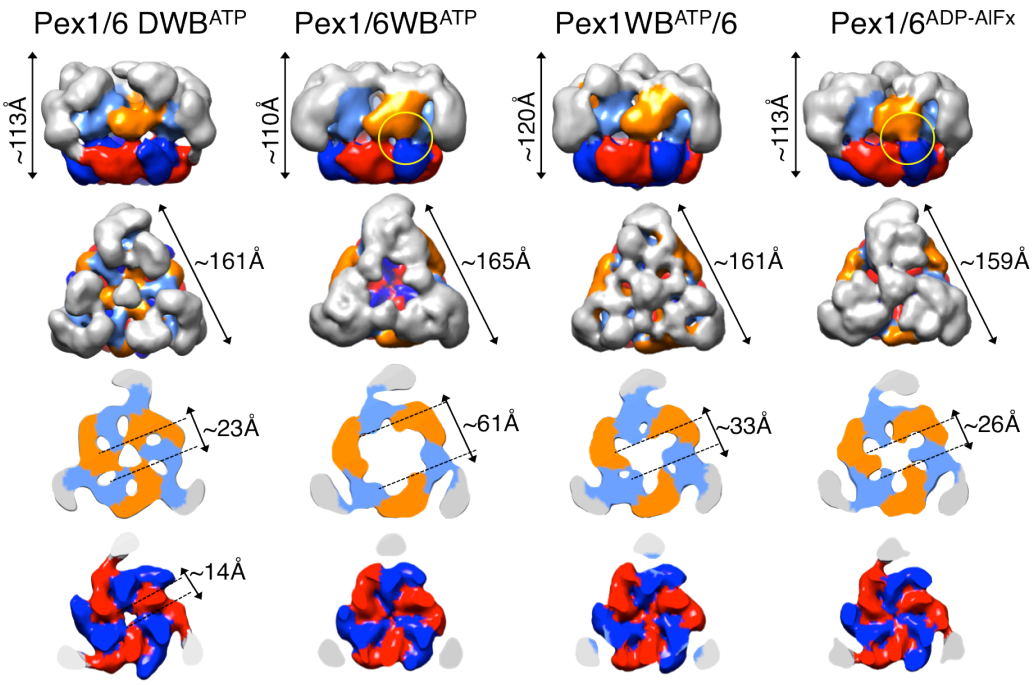

Figure 3.20 Final EM reconstructions of Pex1/6 single and double Walker B complexes. Negative stain EM maps of Pex1/6 complexes harbouring a mutation in the Walker B motif of Pex1D2 and Pex6D2 (Pex1/DWB^{ATP}), Pex6D2 (Pex1/6WB^{ATP}) or Pex1D2 (Pex1WB^{ATP}/6) in the presence of ATP as side views (upper row), followed by top views, and cross-sections of the D1 and D2 layers (lower rows). Pex1/6$^{ADP-AlFx}$ EM reconstruction is shown for comparison. Pex1/6 protomers are coloured corresponding to Figure 3.9 F.

In contrast, flexible N domains of single Walker B complexes protrude towards the central symmetry axis above the D1 domains. While N-termini of Pex1WB^{ATP}/6 still restrict the access to the central channel, Pex1/6WB^{ATP} complexes display an N-terminal entrance into a large cavity. The pore diameter of the Pex1WB^{ATP}/6 D1 domain is significantly extended compared to all other Pex1/6 3D reconstructions described so far in this study. However, intriguingly, the D1 layer of Pex1/6WB^{ATP} expands even more to a large central cavity of 61Å diameter. In line with previous studies of AAA+ protein Hsp104 (Wendler *et al.*, 2007), domains in Pex1/6WB^{ATP} D1 presumably adopt an atypical arrangement in this layer. Hence, in Pex1/6WB^{ATP} individual D1 domains are likely only marginally attached to each other.

As judged from the negative stain EM reconstructions of single Walker B complexes, N-terminal and D1 domains exhibit a significant degree of freedom. Furthermore, permanent binding of ATP in Pex6D2 might trigger inter-domain communications that cause the described outward movement of D1 domains, comparable to the architecture of yeast type II AAA+ protein Hsp104.

However, when compared to the overall shape of Pex1/6$^{ADP-AlFx}$, the orientation of Pex1/6 N-termini and D1 domains of single Walker B complexes are somewhat similar. Accordingly, the D2 domains of Pex1/6$^{ADP-AlF}$, Pex1WB^{ATP}/6 or Pex1/6WB^{ATP} are closed, depicting a tightly packed domain arrangement in this layer. Strong connecting densities between Pex1D1

and Pex6D2 appear at the outside of the Pex1/6WB^{ATP} complex comparable to Pex1/6$^{ADP\text{-}AlFx}$ (Figure 3.20, yellow ring). In analogy to Pex1/6$^{ADP\text{-}AlFx}$, this result indicates that Pex1 protomers might adopt a transition state like orientation when Pex6 is permanently bound to ATP.

3.6 Pex1/6 Walker B complexes: dissecting steps of ATP binding and hydrolysis

ATPase activity assays revealed that Pex1 and Pex6 D2 domains contribute differently to the complex' overall hydrolysis activity. Furthermore, when the conserved glutamate of the Pex1D2 Walker B motif is exchanged to glutamine, the resultant Pex1WB^{ATP}/6 complex is still functional (Figure 3.17). Thus, the Pex1WB^{ATP}/6 EM map shows a hydrolytically active complex. Intriguingly, the overall shape of the hexamer is not significantly altered compared to the inactive Pex1/6WB^{ATP} assembly. In contrast, the appearance of single Walker B complexes is very distinct from Pex1/6DWB^{ATP} assemblies. To further dissect structural differences induced by ATP binding to individual subunits in D2 domains of either Walker B complex, Pex1/6 D2 domain movements are examined in more detail.

In analogy to wild type complexes, Pex1/Pex6 homology models can be readily fitted into the EM densities of the D2 domains of all Pex1/6 Walker B complexes using the automated fitting procedure in Chimera (Figure 3.21 A).

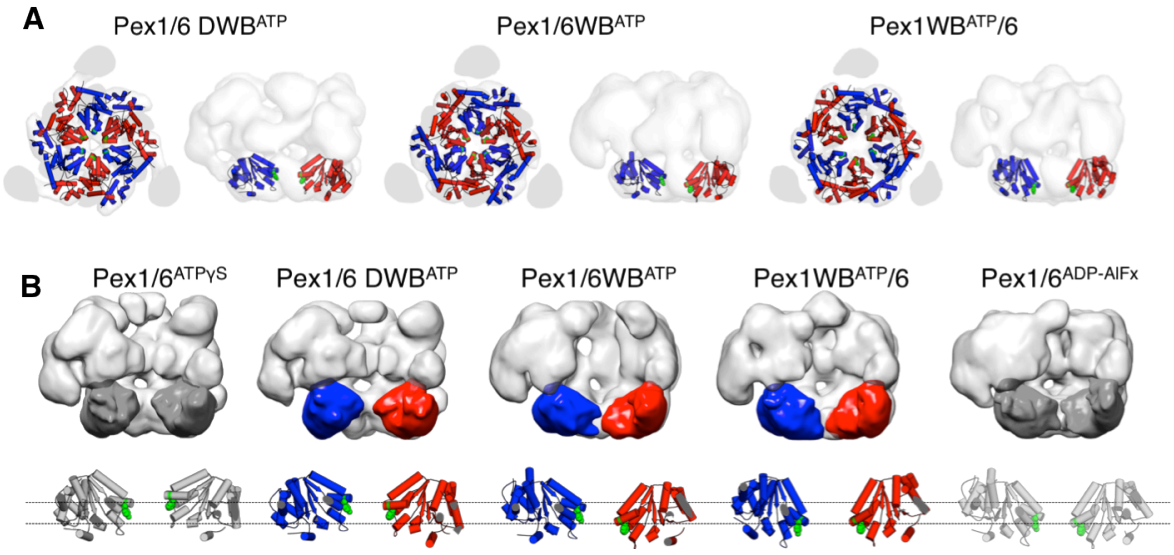

Figure 3.21 Docking of Pex1/6 homology models to the D2 domain of Pex1/6 Walker B EM density maps. (A) D2 cross-section views and side view surface representation of EM reconstructions as indicated. Pex1/6 homology models are automatically fitted to the D2 domain and are coloured as in Figure 3.9 F. (B) Side view surface representation of 3D maps as indicated. One heterodimer is omitted from the 3D reconstructions. Underneath, a cartoon representation based on rigid body fits of homology models into negative stain EM maps is shown. Pex1/6$^{ATP\gamma S}$ and Pex1/6$^{ADP\text{-}AlFx}$ are depicted in grey for comparison. Pore facing aromatic residues Pex1^{F771} and Pex6^{Y805} are shown as green spheres.

The positions of conserved pore-facing residues Pex1^{F771} and Pex6^{Y805} are highlighted in automatically fitted homology models. As depicted in Figure 3.21 A, Pex1^{F711} and Pex6^{Y805} protrude towards the central opening of the D2 domain in the hexameric homology models. Furthermore, fitted homology models emphasize that the ATPase domains of the D2 ring are firmly connected in all Pex1/6 Walker B 3D reconstructions.

Next, domain re-arrangements and resulting localization of Pex1^{F711} and Pex6^{Y805} in reconstructed Walker B complexes are examined in the context of ATP binding and hydrolysis that is structurally described by Pex1/6$^{ATP\gamma S}$ and Pex1/6$^{ADP\text{-}AlFx}$ EM density maps.

As judged from negative stain 3D reconstructions, orientations of Pex1 and Pex6 D2 domains are almost identical in Pex1/6$^{ATP\gamma S}$ or Pex1/6DWB^{ATP} complexes (Figure 3.21 B). ATP binding to Pex1D2 or Pex6D2, respectively, places the D2 domains and concomitantly Pex1^{F711} and Pex6^{Y805} in one plane.

In line with this result, the orientation of Pex6^{Y805} in the Pex1/6WB^{ATP} complex verifies Pex6D2 domains in an ATP locked state. Surprisingly, the position of Pex1^{F771} resembles a transition state like orientation, similar to Pex1/6 complexes captured in the presence of ADP-AlFx. Pex1^{F771} translocates downwards towards the pore exit. Hence, ATP binding to Pex6D2 induces ATP hydrolysis in adjacent Pex1D2 domains.

Intriguingly, in Pex1WB^{ATP}/6 complexes domain movements of Pex1D2 or Pex6D2 hint at ATP hydrolysis in both D2 domains. Aromatic residues Pex1^{F771} and Pex6^{Y805} point toward the channel exit in D2, resulting from a downward movement of those domains.

3.7 ATPase activity of Pex1/6 arginine finger and ISS motif mutants

As judged from rigid body fits to negative stain EM reconstructions of Pex1/6 single Walker B complexes, Pex1 possibly hydrolyses ATP in the D2 domains. Thus, potential intersubunit-signalling pathway between protomers might be responsible for an inhibitory effect on ATP hydrolysis in Pex1.

Previous publications on heterohexameric m-AAA protease Yta10/12 from yeast demonstrated a close signalling network between protomers that involves the arginine finger and residues in the inter-subunit signalling (ISS) motif (Augustin *et al.*, 2009). Corresponding mutations in Pex1 might uncouple an intrinsic hydrolysis activity when tested in ATPase activity assays. Besides a conserved aspartate in the ISS motif consensus sequence of Pex1 (Pex1^{D826}), multiple sequence alignment also reveals arginine residues that match position 1 and 2 arginine fingers of p97 (Figure 3.5, Pex1^{R852}, Pex1^{R855}). For subsequent analysis in activity assays, the aspartate within the ISS motif of Pex1 is modified to valin in Pex1/6WB^{ATP} complexes (*Pex1*^{D826V}/6WB^{ATP}, performed by I. Grimm) whereas the highly conserved position 2 arginine finger of Pex1 is substituted by lysine (Pex1^{R855K}/6, performed by I.

Grimm). If Pex1 ATPase activity is influenced by intersubunit communication, the aspartate-to-valin mutation should uncouple Pex1D2 active sites from ATP bound Pex6 and allow nucleotide cycling in Pex1. The conservative arginine-to-lysine mutation should similarly separate Pex1D2 from adjacent Pex6D2 nucleotide binding pockets. However, negative stain EM of $Pex1^{R855K}/6$ complexes and analytical gel filtration of $Pex1^{D826V}/6WB^{ATP}$ imply that those mutations impair complex formation (Figure 3.17 A, Figure 3.22 B). Thus, when examined in ATPase activity assays, both mutations in Pex1 result in negligible hydrolytic activity (Figure 3.22 A, performed by I. Grimm). The abolished capability to form stable hexamers might also explain the abolished viability of cells expressing $pex1^{R855K}$ arginine finger mutant (Figure 3.16 B).

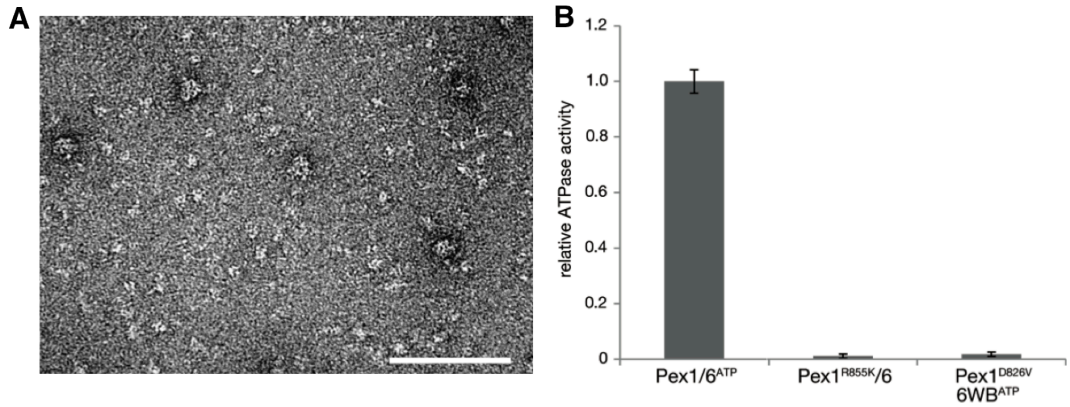

Figure 3.22 ATPase activity and negative stain analysis of arginine finger and ISS motif mutants. (A) Raw negative stain EM micrograph visualizing arginine finger variant $Pex1R^{855K}/6$ in the presence of 4 mM ATP. Scale bar, 100 nm. (B) ATPase activities of the wild type Pex1/6 complex ($Pex1/6^{ATP}$), Pex1 arginine finger ($Pex1^{R855K}/6$) or ISS motif ($Pex1^{D826V}/6WB^{ATP}$) mutants, as indicated. Assays were performed in the presence of 1 mM ATP and 5 mM Mg^{2+} at 37°C. Error bars represent standard deviation of five experiments. Figure is kindly provided by I. Grimm.

In summary, permanent binding of ATP to Pex6D2 domains blocks most of the complex' hydrolytic activity *in vitro* and abolishes complex function *in vivo*. In contrast, ATPase activity of Pex1D2 is non-essential. However, *in vivo* assays show that Pex1 and particularly conserved pore-facing residue $Pex1^{F771}$ are crucial for functional complexes. Furthermore, domain rotations observed in the Pex1/6WBATP EM structure suggests ATP hydrolysis in Pex1D2. Still, Pex6D2 exhibit the main catalytic activity of the complex, whereas Pex1D2 seem to be indispensible for the structural integrity of the complex.

4 Discussion

The AAA+ proteins Pex1/Pex6 are central components of the peroxisomal matrix protein transport system in yeast and humans (Collins *et al.*, 2000; Miyata and Fujiki, 2005). Primary action upon ATP consumption involves release of protein import receptor Pex5 from the peroxisomal membrane to the cytosol (Miyata and Fujiki, 2005; Platta *et al.*, 2005). Single mutations in mammalian Pex1 or Pex6 severely affect normal development in humans (Geisbrecht *et al.*, 1998; Birschmann *et al.*, 2003; Birschmann *et al.*, 2005), highlighting the importance of these peroxins in peroxisome synthesis.

Our study provides a comprehensive structural characterization of the heterohexameric Pex1/6 AAA+ complex using negative stain EM. The role of ATP turnover in individual Pex1/6 active sites is addressed in biochemical assays, revealing that D2 domains are functionally non-redundant. EM analysis of Pex1/6 in the presence of different nucleotides gives valuable mechanistic insights on ATP dependent inter- and intra-domain communications, like diagonal inter-domain contacts between D1 and D2 domains upon ATP hydrolysis in the D2 ring. Furthermore, the Pex1D2 small helical domain interacts with Pex6 N domains in all wild type Pex1/6 complexes incubated with ATP and nucleotide hydrolysis is enabled when two adjacent D2 domains are bound to ATP. Varying pore sizes of D1 or D2 domains likely results from intra-domain communication.

Summarizing the functional and structural data obtained, leads to a model in which the peroxisomal AAA+ complex hydrolyzes ATP in a non-concerted manner to thread its substrate along the central pore.

4.1 Unique architecture of Pex1/6 complexes

Purified Pex1/Pex6 proteins assemble into double-tiered hexamers depicting a unique architecture, yet not observed for other members of the AAA+ family. While the AAA+ domains constitute the central hexameric core of the complex, the N-terminal domains are located lateral and apical of the D1 domains. A comparison of EM structures of wild type Pex1/6 and truncated complexes (Δ188Pex1/Pex6), allocates Pex1 N domains on top of the complex in every second subunit, whereas Pex6 N domains reside at the periphery of the central hexameric fold, resulting in the shape of an equilateral triangle. Accordingly, Pex1/6 hexamers comprise an alternating subunit arrangement, forming a trimer of heterodimers. These results overlap with a recent study (Gardner *et al.*, 2015), which was published while this thesis was in preparation. The authors verify the protomer assignment of Pex1 and Pex6 within the hexamer, using an N-terminal maltose-binding protein (MBP) tag on Pex6.

According to Pex1/6 EM reconstructions in the presence of ATP, ATPγS or double Walker B mutations, Pex1 N-termini arrange as globular densities apical of the D1 domains. On the other hand, in all transition states (ADP-AlFx, Pex1WB^{ATP}/6, Pex1/6WB^{ATP}), Pex1N close or almost close the central channel. Shiozawa *et al*. (2004) proposed that the N-terminal double ψ-barrel fold domain of Pex1 binds adaptors or substrates comparable to its homologs NSF or p97. Hence, flexibility of Pex1N might enable rapid structural adaption required for substrate coordination or adaptor protein interactions. Additionally, in case of a substrate threading mechanism through the central pore of Pex1/6 complexes, dynamic re-arrangements of Pex1 N-terminal domains likely sustain directed substrate translocation.

In contrast, the Pex6 N-termini are thought to locate the ATPase complex to the peroxisomal membrane through binding to Pex15 (Birschmann *et al*., 2003). The static appearance of Pex6N in all nucleotide states suggests a physiological conformation. Thus, placing the complex to the peroxisomal membrane via interactions with Pex15 does not require major conformational re-arrangements in Pex6 N domains.

The unique architecture of Pex1/6 complexes is attributed to the heterohexameric arrangement and differences in the dimensions of the N-terminal domains. In comparison to AAA+ proteins p97 or NSF, N domains of Pex1 or Pex6 are double the size, thus allowing particularly Pex6N to range from the D1 down to the D2 domain at the outside of the hexameric AAA+ core. Accordingly, peripheral Pex6 N-termini might help to maintain the hexameric state of Pex1/6 complexes. Furthermore, extension of Pex6 N domains along the AAA+ rings enables inter-domain contacts with the Pex1D2 small α-helical domain, which are visible in all wild type Pex1/6 EM structures in the presence of ATP. These contacts possibly further stabilize the hexameric arrangement or are required for domain cooperativity.

4.2 The Pex6 D2 domains energize the complex

Hexamer assembly provides a molecular arrangement, which allows efficient ATP hydrolysis in Pex1/6 complexes. Exchanging the glutamate in the conserved Walker B motif in either Pex1D2 (Pex1^{E798Q}) or Pex6D2 (Pex6^{E832Q}) reveals the impact of these individual nucleotide-binding sites on overall ATPase activity *in vitro*. The hydrolytic activity is abolished in complexes mutated in Pex6D2 (Pex1/6WB^{ATP}), whereas ATPase activity of Pex1D2 mutant complexes (Pex1/6WB^{ATP}) results in about ~ 80 % of wild type level. Moreover, mutations in both D2 domains (Pex1/6DWB^{ATP}) entirely compromise ATP hydrolysis. Thus, the hydrolytic behaviour of Pex1/6 D1 and Pex1 D2 domains is negligible and catalytic activity traces back to Pex6D2. Correspondingly, the D1 domains are inactive compared to the D2 domains. Differences in the catalytic activity between AAA+ rings in p97 or other type II AAA+ ATPases suggested a division of labour between D1/D2 domains, divided into an

oligomerisation domain and a hydrolytically active domain (Matveeva *et al.*, 1997; Schlee *et al.*, 2001; Song *et al.*, 2003; Briggs *et al.*, 2008). Hence, the Pex1/6 D1 domain might be needed to stabilize oligomerisation whereas the D2 domain is the main site for ATP hydrolysis.

According to the results from ATP hydrolysis assays, the contribution of Pex1D2 or Pex6D2 to overall hydrolytic activity differs significantly. It is possible that Pex1D2 ATPase activity is compromised in the isolated complex under the conditions assayed. A similar dependency of ATP turnover coupled to experimental conditions was reported for type II AAA+ protein Hsp104. The ATPase activity of Hsp104 varies depending on salt concentrations of the buffers used (Hattendorf and Lindquist, 2002; Schaupp *et al.*, 2007), with Hsp104 starting to dissociate when ionic strength is elevated above 50 mM salt (Schirmer *et al.*, 1998; Schirmer *et al.*, 2001). On the other hand, related type II AAA+ proteins p97, ClpA or NSF generally tolerate salt concentrations up to 300 mM in ATP hydrolysis assays (Rockel *et al.*, 2002; Hinnerwisch *et al.*, 2005; Zhao *et al.*, 2010)

Alternatively, catalytic activity of Pex1 could be elevated in the presence of substrate. The addition of substrates or substrate mimics was shown to stimulate ATPase turnover of HslU (Yoo *et al.*, 1996), Yta10/Yta12 (Augustin *et al.*, 2009) or Hsp104/ClpB (Mogk *et al.*, 2003; Schaupp *et al.*, 2007). Additionally, an ample analysis of AAA+ crystal structures by Zhang and Wigley (2008) propose a signalling network between ATPase subunits and ligand binding sites. The authors state that ATP hydrolysis does not proceed until corresponding complex-ligand interactions are fully established. Thus, hydrolytic activity of Pex1 might be induced once the substrate is bound to the complex. Additionally, the aforementioned inter-domain contact between Pex6N and Pex1D2 small α-helical domain might contribute in the regulation of the ATPase activity in Pex1D2. In contrast, ATP hydrolysis in Pex6D2 has been suggested to coordinate ATP dependent Pex15 anchoring to the peroxisomal membrane (Birschmann *et al*., 2003). Accordingly, the catalytic activity of Pex6 might be less strictly coupled to substrate interactions.

4.3 Possible specialisation of Pex1 and Pex6 D2 domains

To validate the observed *in vitro* hydrolysis activities, growth on oleate as the sole carbon source demonstrates that Pex1WB^{ATP}/6 complexes are functional *in vivo*. In contrast, mutating the conserved glutamate of the Pex6 D2 domain affects viability of cells expressing Pex1/6WB^{ATP} complexes. Those results corroborate major functional differences between Pex1 and Pex6 subunits. While ATP turnover in Pex6D2 is crucial for complex activity, hydrolytic activity of Pex1D2 is dispensable for *in vivo* function.

Surprisingly, these results are in contrast to previous publications that showed that a non-conservative aspartate-to-glutamine mutation in the Walker B motif of Pex1D2 (Pex1^{D797Q})

results in inactive complexes *in vivo* (Birschmann *et al.*, 2005). In our study, a more conserved aspartate-to-asparagine ($Pex1^{D797N}$) mutation also interferes with complex function and stability. We could show that diminished complex function upon expression of $Pex1^{D798N}$ (this study) or $Pex1^{D798Q}$ *in vivo* (Birschmann *et al.*, 2005) results from impaired hexamerisation.

It is possible that exchanging the Pex1 Walker B aspartate to either asparagine or glutamine in the nucleotide binding pocket sterically compromises ATP binding to Pex1D2 and thus, complex formation. This assumption could be verified in future mutational studies, examining the effect of aspartate-to-alanine mutations on complex hexamerisation. Accordingly, correct positioning and coordination of ATP in Pex1D2 active sites might be essential to perpetuate the structural organisation of the Pex1/6 complex *in vivo* and *in vitro*, while hydrolytic activity in Pex6D2 allows the complex to fulfil physiological tasks.

In line with these observations, it was shown that ATP binding to Pex1D2 promotes complex formation (Birschmann *et al*., 2005; Saffian *et al.*, 2012) and functional D2 domains of both, Pex1 and Pex6 are linked to act on substrate Pex5 (Platta *et al.*, 2005). Furthermore, it was suggested that the N-termini of Pex1 bind the substrate (Shiozawa *et al.*, 2004). It is therefore possible that responsibilities of Pex1 and Pex6 D2 domains vary during Pex5 relocation to the cytosol. ATP binding to Pex1D2 may drive hexamerisation and thus, function as structural subunits in Pex1/6 complexes to bridge interactions with Pex5, whereas Pex6 D2 domains supply the dislocation reaction with energy from ATP hydrolysis.

Previous publications on other heterohexameric AAA+ proteins Mcm2-7, the replicative sliding-clamp loader complex, the F1 ATPase or dynein could demonstrate that individual ATPase sites in this complexes adapt distinct roles with only a subset of nucleotide binding sites being catalytically active (Boyer, 1993; Jeruzalmi *et al*., 2001; Kon *et al*., 2004; Bochman *et al*., 2008).

4.4 EM structures suggest that all D2 domains hydrolyse ATP

While biochemical studies have already produced evidence for communication between consecutive subunits in AAA+ rings (Augustin *et al*., 2009, Martin *et al*., 2005, Moreau *et al*., 2007) EM reconstructions of hetero-oligomers, $Pex1WB^{ATP}/6$, $Pex1/6WB^{ATP}$ or $Pex1/6DWB^{ATP}$ are used to structurally dissect the influence of nucleotide binding to distinct binding pockets.

In EM reconstructions of $Pex1/6^{ATP\gamma S}$ or $Pex1/6DWB^{ATP}$ complexes, Pex1 and Pex6 D2 domains show a planar, crystal structure like arrangement. Rigid body fits of Pex1/6 homology models to those EM maps highlight an upward directed position of D2 domains, arranging in one plane. Hence, it can be assumed that the presence of ATPγS or mutations of

the conserved Walker B glutamate in both, Pex1D2 and Pex6D2 locks the active sites in a nucleotide loaded state, thereby placing the domains in an elevated orientation.

The orientation of mutated Pex6 D2 subunits in 3D reconstructions of single Walker B complex Pex1/6WB^{ATP} suggest, that ATP occupies these subunits. Remarkably, the position of the adjacent Pex1 D2 domain adopts a transition state like orientation, comparable to the domain rotation observed for Pex1D2 in the Pex1/6$^{ADP\text{-}AlFx}$ EM map. Hence, nucleotide binding to Pex6D2 may force Pex1D2 in a post-hydrolysis state. Furthermore, this finding implies that ATP hydrolysis is not blocked completely in Pex1 D2 domains. Since Pex6D2 mutant complexes are not hydrolytically active *in vitro*, it is possible that ATP hydrolysis in Pex1D2 occurs only once before these active sites become stalled without releasing nucleotide.

In line with aforementioned results, when Pex1D2 carries a Walker B mutation, adjacent Pex6 D2 subunits are placed in a transition state like orientation as suggested by downward directed motions of this domain in rigid body fits to the Pex1WB^{ATP}/6 EM reconstruction. Intriguingly, the domain arrangement of mutated Pex1D2 subunits in the complex hint at ATP hydrolysis, too. This is somewhat surprising since the Walker B mutation should lock Pex1D2 in an ATP bound state as seen in Pex1/6DWB^{ATP} complexes. However, since Pex1WB^{ATP}/6 complexes actively hydrolyse ATP, the EM map might represent a mixture of conformational states and the interpretation of observed orientations of D2 domains is challenging and less reliable. One explanation for the downward translation of Pex1D2 could be that the down rotation of Pex6D2 causes Pex1D2 to follow.

4.5 Intersubunit signalling

The Walker B mutations in Pex1 and Pex6 have revealed differences between the two proteins in the complex, although nucleotide hydrolysis seems to be dependent on the nucleotide state of neighbouring active sites. Conserved residues that sense the nucleotide occupancy in either binding pocket of Pex1/6 D2 domains likely communicate across subunits thereby regulating ATP hydrolysis. Previous publications on type I m-AAA protease Yta10/Yta12 from yeast demonstrated that the ATPase activity of the heterohexamer is alleviated to 30% of the wild type level when the Walker B motif in Yta10 is mutated, whereas ATPase activity is diminished upon mutation of the Walker B motif in Yta12 (Augustin *et al*., 2009). The authors suggest an intimate communication between protomers that involves the arginine finger and residues of the inter-subunit signalling (ISS) motif that regulates ATP hydrolysis in Yta10 when Yta12 is ATP loaded.

In our study, oleate growth assays established that both Pex1/6 D2 domains posses functional position 2 arginine fingers and corresponding mutation in Pex1 is surveyed in ATPase assays

and negative stain EM (Pex1^{R855K}). Accordingly, arginine finger mutation Pex1^{R855K} interferes with complex hexamerisation and impaired ATP hydrolysis of Pex1^{R855K}/6 complexes results from compromised capability to assemble into hexamers. It is therefore plausible that the position 2 arginine finger is essential for hexamer stability rather than ATP hydrolysis. However, Gardner *et al.* (2015) could show that the mutation of position 1 arginine finger in Pex1 (Pex1^{R852K}) could not release hydrolytic activity in Pex1D2 either. Similarly, exchanging the conserved aspartate of the Pex1D2 ISS motif (Pex1^{D826V}, this study) results in negligible ATPase activity.

4.6 Implications for a substrate threading mechanism in Pex1/6

In the first crystal structure of full-length p97, a zinc ion occludes the D1 domain (DeLaBarre and Brunger, 2003) and following structural studies showed that p97 crystallised predominantly into tightly packed hexamers, independent of the nucleotides present (Huyton et al., 2003; Davies et al., 2008; Tang et al., 2010). Hence, it was assumed that the physiological function of p97 during ERAD does not involve polypeptide translocation through its central pore. In contrast to p97 crystal structures, the diameter of the inner pore of Pex1/6 D1 or D2 domains varies considerably. Furthermore, while D1 and D2 domains are symmetrically stacked on top of each other in p97, the displaced arrangement of D1 and D2 AAA+ rings observed in EM reconstructions of Pex1/6 complexes is structurally closer to the one of ClpA and Hsp104 (Guo *et al.*, 2002; Wendler *et al.*, 2007; Effantin *et al.*, 2010).

AAA+ members from the Clp/Hsp100 protein family are thought to process substrates via translocation through their central pore, involving conserved pore loops (Weibezahn *et al.*, 2004; Hinnerwisch *et al.*, 2005; Martin *et al.*, 2008; Kress *et al.*, 2009). Our EM structures show that Pex1 and Pex6 assemble into double-ring hexamers, featuring a central channel, which extends from the D1 to the D2 domain in most nucleotide states. In rigid body fits of Pex1/6 homology models to EM reconstructions of wild type or mutated Pex1/6 complexes, conserved substrate binding residues surround the pore of the D2 ring. Those residues correspond structurally and sequentially to pore 1 loops of related AAA+ proteins (Hinnerwisch *et al.*, 2005; DeLaBarre *et al.*, 2006; Martin *et al.*, 2008), shown to be essential for substrate processing. In Pex1 or Pex6, mutations of those pore-protruding residues severely affect complex function *in vivo*, suggesting physiological substrate interaction with both, Pex1 and Pex6, respectively, during the ATPase cycle of Pex1/6 complexes.

The positions of those substrate interacting residues in rigid body fits to the Pex1/6$^{ATP\gamma S}$ or Pex1/6DWB^{ATP} EM reconstructions show that D2 domains rotate into the pore, moving pore 1 loops upward into similar axial planes and closer together (Figure 4.1, full ATP). ATPγS is

generally thought to prolong the ATP bound state of AAA+ proteins and has been shown to stimulate substrate binding (Bolon *et al.*, 2004). Thus, positioning of the substrate binding loops in the upmost position of the D2 ring compares to grabbing of the substrate. ATP hydrolysis in D2 domains, structurally presented by the Pex1/6$^{ADP\text{-}AlFx}$ complex, induces domain translocation downwards along the central channel, placing substrate binding loops at the C-terminal exit of the D2 layer, concomitantly closing the ring. The latter movement possibly prevent the substrate from slipping or translocating back. Accordingly, large-scale domain translocation upon ATP hydrolysis creates a power stroke, which would pull the substrate towards the pore exit (Figure 4.1, post-hydrolysis). A comparable out of plane rotation of entire AAA+ domains upon ATP hydrolysis has been observed for p97 D2 domains, highlighted by structural comparison of ADP and AMPPNP bound p97 crystal structures (DeLaBarre *et al.*, 2006). In our study, Pex1/6 D2 domains are translocated by ~10Å when ATP is hydrolysed. This step size agrees to data obtained in single molecule studies for ClpX during substrate threading (Aubin-Tam *et al.*, 2011; Maillard *et al.*, 2011).

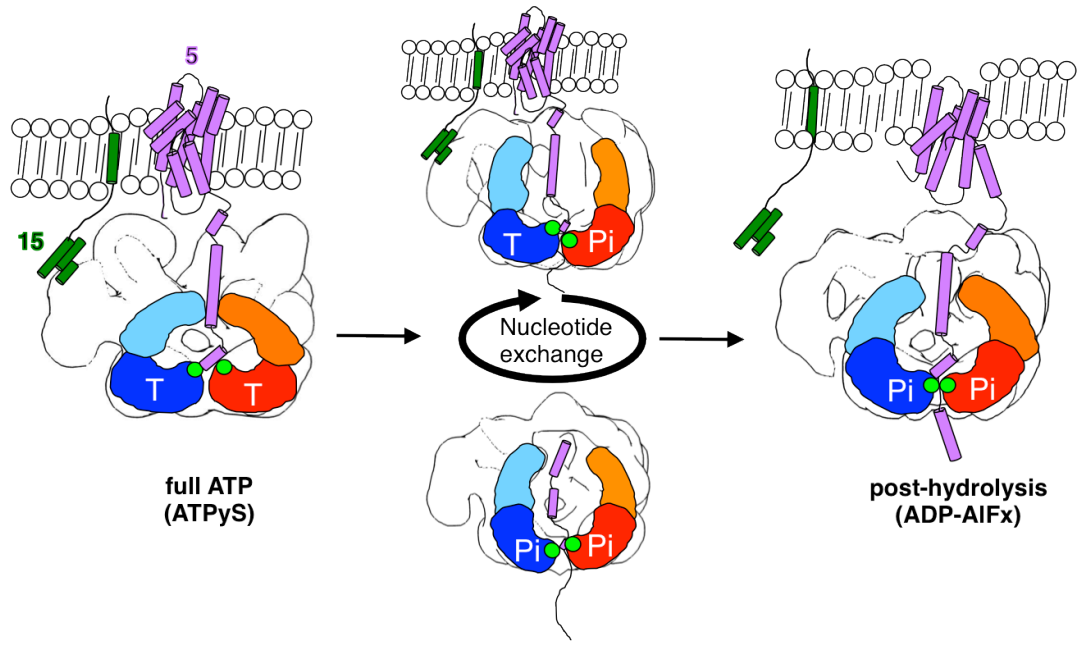

Figure 4.1 Model for Pex1/6 movements during ATP binding and hydrolysis. The Pex1/6 complex anchors to the peroxisomal membrane via binding of Pex6 N domains to Pex15. Pex1 N domains establish interactions with substrate Pex5. ATP binding to Pex1D2 and Pex6D2 (full ATP, ATPγS) elevates substrate-binding loops in D2, ready to establish interactions with Pex5. ATP hydrolysis induces a power stroke that rotates the D2 domains downwards and pulls bound substrate along the pore (post-hydrolysis, ADP-AlFx). ATP consumption in Pex6D2 (Pex1/6WBATP, Pex1WBATP/6) energizes substrate threading along the central pore. One Pex1 and Pex6 protomer are denoted as simple cartoon representation. Pex1/6 are coloured as in Figure 3.9 F. Conserved aromatic residues of substrate-binding loops are shown as green dots. Representative tertiary structures of substrate protein Pex5 (purple) and membrane anchor Pex15 (green) are depicted as cartoon representations. Nucleotide occupancy of each D2 domain is indicated by T for ATP or Pi for the transition state.

Thus, continuous re-arrangements of entire ATPase domains between ATPγS and ADP-AlFx bound states might constitute the driving force behind substrate threading in Pex1/6 complexes. Furthermore, our EM structures suggest that ATP hydrolysis in D2 domains requires two adjacent subunits to be bound to ATP. This is further corroborated by orientations of D2 domains in Pex1/6 complexes harbouring a single Walker B mutation. ATP binding to one D2 subunit forces the right hand neighbour in a transition state like orientation. In Pex1/6WB^{ATP} complexes, substrate binding loops arrange in a staggered fashion with Pex6D2 occupied by ATP, as suggested by upward directed pore loops in rigid body fits, thus ready to engage with the substrate (Figure 4.1, Pex1/6WB^{ATP}). Upon ATP hydrolysis in Pex6D2 (Figure 4.1, Pex1WB^{ATP}/Pex6), those domains translocate downwards along the central channel. Hence, repeated cycles of ATP hydrolysis in Pex6D2 could create a downward pull in Pex1/6 D2 domains, forcing the bound substrate along the pore.

In contrast to the more active Pex1/6 D2 domains, D1 domains lack hydrolytic activity and well-conserved substrate binding residues. The here presented EM structures suggest that D1 domains function as a structural hub. Therefore it is possible that D1 domains transmit conformational changes during ATP hydrolysis in D2 domains into larger N-terminal motion. In the presence of the transition state analogue ADP-AlFx or single Walker B mutations D1 domains stretch, concomitantly closing the central pore via the N-terminal domains. Accordingly, closure of D2 domains induces a significant expansion of the D1 ring. Particularly, in complexes harbouring a Walker B mutation in Pex6D2, the D1 domains adopt an atypical arrangement in this layer and neighbouring AAA+ domains cannot be tightly connected to each other, in line with flexible domain motions observed in cryo-EM reconstructions of Hsp104 (Wendler *et al*., 2007). In contrast, binding of ATPγS results in expansion of D2 domains, while D1 domains narrow the central cavity, possibly pushing bound substrate towards the substrate binding loops in the D2 ring. Furthermore, flexible conformational dynamics of D1 domains imply that Pex1/6 accommodate larger structural elements of substrate intermediates while cycling through different nucleotide states.

4.7 Non-uniform ATP occupancy in Pex1/Pex6 D2 domains

Efficient translocation of the substrate can only occur when not all subunits let go at the same time. Symmetry free EM maps and rigid body fits thereof imply that Pex1/6 D2 domains hydrolyse and exchange nucleotide in an asymmetric manner in the presence of ATP. Substrate binding loops arrange in different axial planes, indicating a preferred order of nucleotide states. Obviously, Pex1 and Pex6 D2 domains do not hydrolyse ATP simultaneously, suggesting a sequential or rotary sequence for the ATPase cycle. Domain arrangements imply that the hydrolytic capacity in individual AAA+ subunits levers entire

AAA+ domains along the central pore. Accordingly, non-uniform nucleotide occupancy results in individual ATPase site and pore loop orientations, which likely enable a substrate translocation mechanism upon ATP hydrolysis. The asymmetric Pex1/6^{ATP} complex deviates from an inter-locked domain arrangement observed in crystal structures of p97 (Zhang *et al.*, 2000; Huyton *et al.*, 2003; Davies *et al.*, 2008), corroborating remarkable conformational dynamics in Pex1/6 while cycling through different nucleotide states. Furthermore, EM densities of N-terminal domains in symmetry free Pex1/6^{ATP} complexes display an asymmetrical arrangement, which differs among individual subunits. Hence, Pex1/6 N domains are likely coupled to the nucleotide states in D2 domains.

In contrast, symmetry free EM reconstructions in the presence of ATPγS reveal a high level of symmetry with an almost planar arrangement in the D1 and D2 domains. Thus, active sites might be almost equally occupied by nucleotide. Hence, symmetry breaks in the D2 ring might occur after ATP hydrolysis or when substrate is bound.

4.8 Outlook

In this thesis we provide 8 different EM structures of hexameric Pex1/6 complexes in the presence of different nucleotides. The Pex1/6 structures adopt a unique triangular overall shape, mainly attributed to an asymmetric arrangement of Pex1/6 N-termini being a special feature of the complex. However, lacking structural information, homology modelling of those domains fails. Thus, in order to further clarify the function of the N domains, high-resolution structural analysis would be very beneficial. Nevertheless, our negative stain reconstructions already established a structural theme for Pex1/6 N-termini and observed positions of the corresponding densities seem to be biological relevant. However, future work will have to focus on the interactions of Pex1/6 with its substrate Pex5. Thus far, ATP and ubiquitin dependent extraction of the PTS1 receptor from the peroxisomal membrane has been established, possibly sustained by adaptor proteins like Ubp15. Biochemical evidence for direct binding of Pex5 by Pex1/6 is missing, though. Cross-linking experiments with full-length Pex5 or substrate mimics could capture dynamic interactions of this protein with the AAA+ complex, further corroborating a substrate translocation mechanism as proposed in our study. Furthermore, characterising the potential influence of Pex5 on the hydrolytic activity of Pex1/6 could unravel the physiological role of ATPase activity in Pex1D2. Notably, the impact of Pex15 on the hydrolytic behaviour of Pex1/6 complexes was published recently (Gardner *et al*., 2015). The authors show that Pex15 decreases ATP hydrolysis of Pex1/6 complexes to ~13 % of wild type level. Gardner *et al*. claim that Pex15 allosterically influences catalytic activity of Pex1D2. When compared to our results, reduction of overall

ATPase activity would rather trace back to impaired ATP turnover in Pex6D2, which could be a rate-limiting step for substrate engagement at the peroxisomal membrane. Thus, future experiments will be required to elucidate cooperativity between Pex1/6 complexes and Pex15 at the peroxisomal membrane.

The function and mechanism of the Pex1/6 complex strictly depends on ATP consumption. Here, we provide first structural evidence for an asymmetric nucleotide loading of D2 domains, which was already observed for related AAA+ proteins, likely representing a conserved feature in AAA+ proteins. Nevertheless, high resolution cryo EM structures of Pex1/6 complexes bound to different nucleotides have to be obtained, which enable us to identify the nucleotide state in each binding pocket of the AAA+ domains.

Our structural and functional work might provide a starting point to improve the understanding of non-functional Pex1/6 proteins and molecular consequences in the human system. Patients devoid of functional peroxisomes suffer from genetic diseases of the Zellweger spectrum. The here presented structures might not only allow to literally visualize the importance of both peroxins in complex function and stability, but could also provide a spatial framework for substrate and adaptor binding sites, amenable to future drug testing. Thus, our findings, obtained in collaboration with work from Ralf Erdmann's lab, might add up to existing data and initialize future experiments to broaden our knowledge in the field of peroxisome biogenesis and further explore common functions and mechanism of AAA+ proteins.

5 References

Adams, B.G. (1972). Induction of galactokinase in Saccharomyces cerevisiae: kinetics of induction and glucose effects. J. Bacteriol. *111*, 308-315.

Agrawal, G., Joshi, S., and Subramani, S. (2011). Cell-free sorting of peroxisomal membrane proteins from the endoplasmic reticulum. Proc. Natl. Acad. Sci. USA *108*, 9113-9118.

Ammelburg, M., Frickey, T., and Lupas, A.N. (2006). Classification of AAA+ proteins. J. Struct. Biol. *156*, 2-11.

Angermuller, S., and Fahimi, H.D. (1986). Ultrastructural cytochemical localization of uricase in peroxisomes of rat liver. The journal of histochemistry and cytochemistry : official journal of the Histochemistry Society *34*, 159-165.

Aubin-Tam, M.E., Olivares, A.O., Sauer, R.T., Baker, T.A., and Lang, M.J. (2011). Single-molecule protein unfolding and translocation by an ATP-fueled proteolytic machine. Cell *145*, 257-267.

Augustin, S., Gerdes, F., Lee, S., Tsai, F.T., Langer, T., and Tatsuta, T. (2009). An intersubunit signaling network coordinates ATP hydrolysis by m-AAA proteases. Mol. Cell *35*, 574-585.

Babst, M., Wendland, B., Estepa, E.J., and Emr, S.D. (1998). The Vps4p AAA ATPase regulates membrane association of a Vps protein complex required for normal endosome function. EMBO J. *17*, 2982-2993.

Baker, A., Graham, I.A., Holdsworth, M., Smith, S.M., and Theodoulou, F.L. (2006). Chewing the fat: β-oxidation in signalling and development. Trends Plant Sci. *11*, 124-132.

Bar-Nun, S., and Glickman, M.H. (2012). Proteasomal AAA-ATPases: Structure and function. Biochim. Biophys. Acta *1823*, 67-82.

Barthelme, D., Chen, J.Z., Grabenstatter, J., Baker, T.A., and Sauer, R.T. (2014). Architecture and assembly of the archaeal Cdc48*20S proteasome. Proc. Natl. Acad. Sci. USA *111*, E1687-1694.

Berger, J., and Gärtner, J. (2006). X-linked adrenoleukodystrophy: Clinical, biochemical and pathogenetic aspects. Biochim. Biophys. Acta *1763*, 1721-1732.

Bernhardt, K., Wilkinson, S., Weber, A.P., and Linka, N. (2012). A peroxisomal carrier delivers NAD(+) and contributes to optimal fatty acid degradation during storage oil mobilization. Plant J. *69*, 1-13.

Beyer, A. (1997). Sequence analysis of the AAA protein family. Protein Sci. *6*, 2043-2058.

Birschmann, I., Rosenkranz, K., Erdmann, R., and Kunau, W.H. (2005). Structural and functional analysis of the interaction of the AAA-peroxins Pex1p and Pex6p. FEBS J. *272*, 47-58.

Birschmann, I., Stroobants, A.K., van den Berg, M., Schafer, A., Rosenkranz, K., Kunau, W.H., and Tabak, H.F. (2003). Pex15p of Saccharomyces cerevisiae provides a molecular basis for recruitment of the AAA peroxin Pex6p to peroxisomal membranes. Mol Biol Cell *14*, 2226-2236.

Black, P.N., and DiRusso, C.C. (2007). Yeast acyl-CoA synthetases at the crossroads of fatty acid metabolism and regulation. Biochim. Biophys. Acta *1771*, 286-298.

Bochman, M.L., Bell, S.P., and Schwacha, A. (2008). Subunit organization of Mcm2-7 and the unequal role of active sites in ATP hydrolysis and viability. Mol. Cell. Biol. *28*, 5865-5873.

Bochtler, M., Hartmann, C., Song, H.K., Bourenkov, G.P., Bartunik, H.D., and Huber, R. (2000). The structures of HsIU and the ATP-dependent protease HsIU-HsIV. Nature *403*, 800-805.

Bolon, D.N., Grant, R.A., Baker, T.A., and Sauer, R.T. (2004). Nucleotide-dependent substrate handoff from the SspB adaptor to the AAA+ ClpXP protease. Mol. Cell *16*, 343-350.

Boyer, P.D. (1993). The binding change mechanism for ATP synthase--some probabilities and

possibilities. Biochim. Biophys. Acta *1140*, 215-250.

Braig, K., Menz, R.I., Montgomery, M.G., Leslie, A.G., and Walker, J.E. (2000). Structure of bovine mitochondrial F(1)-ATPase inhibited by Mg(2+) ADP and aluminium fluoride. Structure *8*, 567-573.

Braverman, N., Chen, L., Lin, P., Obie, C., Steel, G., Douglas, P., Chakraborty, P.K., Clarke, J.T., Boneh, A., Moser, A.*, et al.* (2002). Mutation analysis of PEX7 in 60 probands with rhizomelic chondrodysplasia punctata and functional correlations of genotype with phenotype. Hum. Mutat. *20*, 284-297.

Breidenbach, R.W., and Beevers, H. (1967). Association of the glyoxylate cycle enzymes in a novel subcellular particle from castor bean endosperm. Biochem. Biophys. Res. Commun. *27*, 462-469.

Brenner, S., and Horne, R.W. (1959). A negative staining method for high resolution electron microscopy of viruses. Biochim. Biophys. Acta *34*, 103-110.

Briggs, L.C., Baldwin, G.S., Miyata, N., Kondo, H., Zhang, X., and Freemont, P.S. (2008). Analysis of nucleotide binding to P97 reveals the properties of a tandem AAA hexameric ATPase. J. Biol. Chem. *283*, 13745-13752.

Brocard, C., and Hartig, A. (2006). Peroxisome targeting signal 1: Is it really a simple tripeptide? Biochim. Biophys. Acta *1763*, 1565-1573.

Brosche, T., and Platt, D. (1998). The biological significance of plasmalogens in defense against oxidative damage. Experimental gerontology *33*, 363-369.

Bush, M., and Dixon, R. (2012). The role of bacterial enhancer binding proteins as specialized activators of sigma54-dependent transcription. Microbiol. Mol. Biol. Rev. *76*, 497-529.

Chang, L.F., Chen, S., Liu, C.C., Pan, X., Jiang, J., Bai, X.C., Xie, X., Wang, H.W., and Sui, S.F. (2012). Structural characterization of full-length NSF and 20S particles. Nat. Struct. Mol. Biol. *19*, 268-275.

Chen, B., Doucleff, M., Wemmer, D.E., De Carlo, S., Huang, H.H., Nogales, E., Hoover, T.R., Kondrashkina, E., Guo, L., and Nixon, B.T. (2007). ATP ground- and transition states of bacterial enhancer binding AAA+ ATPases support complex formation with their target protein, sigma54. Structure *15*, 429-440.

Chistol, G., Liu, S., Hetherington, C.L., Moffitt, J.R., Grimes, S., Jardine, P.J., and Bustamante, C. (2012). High degree of coordination and division of labor among subunits in a homomeric ring ATPase. Cell *151*, 1017-1028.

Collins, C.S., and Gould, S.J. (1999). Identification of a common PEX1 mutation in Zellweger syndrome. Hum. Mutat. *14*, 45-53.

Collins, C.S., Kalish, J.E., Morrell, J.C., McCaffery, J.M., and Gould, S.J. (2000). The peroxisome biogenesis factors pex4p, pex22p, pex1p, and pex6p act in the terminal steps of peroxisomal matrix protein import. Mol. Cell. Biol. *20*, 7516-7526.

Crowther, R.A., Henderson, R., and Smith, J.M. (1996). MRC image processing programs. J. Struct. Biol. *116*, 9-16.

Dalal, S., Rosser, M.F., Cyr, D.M., and Hanson, P.I. (2004). Distinct roles for the AAA ATPases NSF and p97 in the secretory pathway. Mol Biol Cell *15*, 637-648.

Davies, J.M., Brunger, A.T., and Weis, W.I. (2008). Improved structures of full-length p97, an AAA ATPase: implications for mechanisms of nucleotide-dependent conformational change. Structure *16*, 715-726.

Davies, J.M., Tsuruta, H., May, A.P., and Weis, W.I. (2005). Conformational changes of p97 during nucleotide hydrolysis determined by small-angle X-Ray scattering. Structure *13*, 183-195.

De Duve, C., and Baudhuin, P. (1966). Peroxisomes (microbodies and related particles). Physiol. Rev. *46*, 323-357.

Debelyy, M.O., Platta, H.W., Saffian, D., Hensel, A., Thoms, S., Meyer, H.E., Warscheid, B., Girzalsky, W., and Erdmann, R. (2011). Ubp15p, a ubiquitin hydrolase associated with the peroxisomal export machinery. J. Biol. Chem. *286*, 28223-28234.

DeLaBarre, B., and Brunger, A.T. (2003). Complete structure of p97/valosin-containing protein reveals communication between nucleotide domains. Nat. Struct. Biol. *10*, 856-863.

DeLaBarre, B., and Brunger, A.T. (2005). Nucleotide dependent motion and mechanism of action of p97/VCP. J. Mol. Biol. *347*, 437-452.

DeLaBarre, B., Christianson, J.C., Kopito, R.R., and Brunger, A.T. (2006). Central pore residues mediate the p97/VCP activity required for ERAD. Mol. Cell *22*, 451-462.

Dirusso, C.C., Connell, E.J., Faergeman, N.J., Knudsen, J., Hansen, J.K., and Black, P.N. (2000). Murine FATP alleviates growth and biochemical deficiencies of yeast fat1Delta strains. Eur. J. Biochem. *267*, 4422-4433.

Distel, B., Erdmann, R., Gould, S.J., Blobel, G., Crane, D.I., Cregg, J.M., Dodt, G., Fujiki, Y., Goodman, J.M., Just, W.W*., et al.* (1996). A unified nomenclature for peroxisome biogenesis factors. J. Cell Biol. *135*, 1-3.

Dodt, G., and Gould, S.J. (1996). Multiple PEX genes are required for proper subcellular distribution and stability of Pex5p, the PTS1 receptor: evidence that PTS1 protein import is mediated by a cycling receptor. J. Cell Biol. *135*, 1763-1774.

Dreveny, I., Kondo, H., Uchiyama, K., Shaw, A., Zhang, X., and Freemont, P.S. (2004). Structural basis of the interaction between the AAA ATPase p97/VCP and its adaptor protein p47. EMBO J. *23*, 1030-1039.

Dubochet, J., Ducommun, M., Zollinger, M., and Kellenberger, E. (1971). A new preparation method for dark-field electron microscopy of biomacromolecules. Journal of ultrastructure research *35*, 147-167.

Ebberink, M.S., Kofster, J., Wanders, R.J., and Waterham, H.R. (2010). Spectrum of PEX6 mutations in Zellweger syndrome spectrum patients. Hum. Mutat. *31*, E1058-1070.

Ebberink, M.S., Mooijer, P.A., Gootjes, J., Koster, J., Wanders, R.J., and Waterham, H.R. (2011). Genetic classification and mutational spectrum of more than 600 patients with a Zellweger syndrome spectrum disorder. Hum. Mutat. *32*, 59-69.

Effantin, G., Ishikawa, T., De Donatis, G.M., Maurizi, M.R., and Steven, A.C. (2010). Local and global mobility in the ClpA AAA+ chaperone detected by cryo-electron microscopy: functional connotations. Structure *18*, 553-562.

Einerhand, A.W., Kos, W.T., Distel, B., and Tabak, H.F. (1993). Characterization of a transcriptional control element involved in proliferation of peroxisomes in yeast in response to oleate. Eur. J. Biochem. *214*, 323-331.

El Magraoui, F., Baumer, B.E., Platta, H.W., Baumann, J.S., Girzalsky, W., and Erdmann, R. (2012). The RING-type ubiquitin ligases Pex2p, Pex10p and Pex12p form a heteromeric complex that displays enhanced activity in an ubiquitin conjugating enzyme-selective manner. FEBS J. *279*, 2060-2070.

Elgersma, Y., Kwast, L., Berg, M.v.d., B.Snyder, W., Distel, B., Subramani, S., and F.Tabak, H. (1997). Overexpression of Pex15p, a phosphorylated peroxisomal integral membrane protein required for peroxisome assembly in S.cerevisiae, causes proliferation of the endoplasmic reticulum membrane. The EMBO Journal
16, 7326-7341.

Enemark, E.J., and Joshua-Tor, L. (2006). Mechanism of DNA translocation in a replicative hexameric helicase. Nature *442*, 270-275.

Erdmann, R., and Kunau, W.H. (1992). A genetic approach to the biogenesis of peroxisomes in the yeast Saccharomyces cerevisiae. Cell Biochem. Funct. *10*, 167-174.

Erdmann, R., and Schliebs, W. (2005). Peroxisomal matrix protein import: the transient pore model. Nat. Rev. Mol. Cell Biol. *6*, 738-742.

Erdmann, R., Wiebel, F.F., Flessau, A., Rytka, J., Beyer, A., Frohlich, K.U., and Kunau, W.H. (1991). PAS1, a yeast gene required for peroxisome biogenesis, encodes a member of a novel family of putative ATPases. Cell *64*, 499-510.

Erzberger, J.P., and Berger, J.M. (2006). Evolutionary relationships and structural mechanisms of AAA+ proteins. Annu. Rev. Biophys. Biomol. Struct. *35*, 93-114.

Faber, K.N.H., J.A and Subramani ,S. (1998). Two AAA Family Peroxins, PpPex1p and PpPex6p, Interact with Each Other in an ATP-Dependent Manner and Are Associated with Different Subcellular Membranous Structures Distinct from Peroxisomes. Mol. Cell. Biol. *18*, 936-963.

Fahimi, H.D., Reinicke, A., Sujatta, M., Yokota, S., Ozel, M., Hartig, F., and Stegmeier, K.

(1982). The short- and long-term effects of bezafibrate in the rat. Ann. N. Y. Acad. Sci. *386*, 111-135.

Fakieh, M.H., Drake, P.J., Lacey, J., Munck, J.M., Motley, A.M., and Hettema, E.H. (2013). Intra-ER sorting of the peroxisomal membrane protein Pex3 relies on its luminal domain. Biology open *2*, 829-837.

Fang, Y., Morrell, J.C., Jones, J.M., and Gould, S.J. (2004). PEX3 functions as a PEX19 docking factor in the import of class I peroxisomal membrane proteins. J. Cell Biol. *164*, 863-875.

Ferdinandusse, S., and Houten, S.M. (2006). Peroxisomes and bile acid biosynthesis. Biochim. Biophys. Acta *1763*, 1427-1440.

Frank, J., Radermacher, M., Penczek, P., Zhu, J., Li, Y., Ladjadj, M., and Leith, A. (1996). SPIDER and WEB: processing and visualization of images in 3D electron microscopy and related fields. J. Struct. Biol. *116*, 190-199.

Fujiki, Y., Okumoto, K., Kinoshita, N., and Ghaedi, K. (2006). Lessons from peroxisome-deficient Chinese hamster ovary (CHO) cell mutants. Biochim. Biophys. Acta *1763*, 1374-1381.

Fujiki, Y., Okumoto, K., Mukai, S., Honsho, M., and Tamura, S. (2014). Peroxisome biogenesis in mammalian cells. Frontiers in physiology *5*, 307.

Gai, D., Zhao, R., Li, D., Finkielstein, C.V., and Chen, X.S. (2004). Mechanisms of conformational change for a replicative hexameric helicase of SV40 large tumor antigen. Cell *119*, 47-60.

Gardner, B.M., Chowdhury, S., Lander, G.C., and Martin, A. (2015). The Pex1/Pex6 Complex Is a Heterohexameric AAA+ Motor with Alternating and Highly Coordinated Subunits. J. Mol. Biol. *427*, 1375-1388.

Gartner, J. (2000). Disorders related to peroxisomal membranes. J Inherit Metab Dis *23*, 264-272.

Geisbrecht, B.V., Collins, C.S., Reuber, B.E., and Gould, S.J. (1998). Disruption of a PEX1–PEX6 interaction is the most common cause of the neurologic disorders Zellweger syndrome, neonatal adrenoleukodystrophy, and infantile Refsum disease. Proc. Natl. Acad. Sci. USA *95*, 8630-8635.

Girzalsky, W., Saffian, D., and Erdmann, R. (2010). Peroxisomal protein translocation. Biochim. Biophys. Acta *1803*, 724-731.

Glynn, S.E., Martin, A., Nager, A.R., Baker, T.A., and Sauer, R.T. (2009). Structures of asymmetric ClpX hexamers reveal nucleotide-dependent motions in a AAA+ protein-unfolding machine. Cell *139*, 744-756.

Goto, S., Mano, S., Nakamori, C., and Nishimura, M. (2011). Arabidopsis ABERRANT PEROXISOME MORPHOLOGY9 is a peroxin that recruits the PEX1-PEX6 complex to peroxisomes. Plant Cell *23*, 1573-1587.

Goujon, M., McWilliam, H., Li, W., Valentin, F., Squizzato, S., Paern, J., and Lopez, R. (2010). A new bioinformatics analysis tools framework at EMBL-EBI. Nucleic Acids Res. *38*, W695-699.

Gould, S.J., and Valle, D. (2000). Peroxisome biogenesis disorders: genetics and cell biology. Trends Genet. *16*, 340-345.

Gouveia, A.M., Guimaraes, C.P., Oliveira, M.E., Reguenga, C., Sa-Miranda, C., and Azevedo, J.E. (2003). Characterization of the peroxisomal cycling receptor, Pex5p, using a cell-free in vitro import system. J. Biol. Chem. *278*, 226-232.

Greenleaf, W.B., Shen, J., Gai, D., and Chen, X.S. (2008). Systematic study of the functions for the residues around the nucleotide pocket in simian virus 40 AAA+ hexameric helicase. J. Virol. *82*, 6017-6023.

Grimm, I., Saffian, D., Platta, H.W., and Erdmann, R. (2012). The AAA-type ATPases Pex1p and Pex6p and their role in peroxisomal matrix protein import in Saccharomyces cerevisiae. Biochim. Biophys. Acta *1823*, 150-158.

Groll, M., Bajorek, M., Kohler, A., Moroder, L., Rubin, D.M., Huber, R., Glickman, M.H., and Finley, D. (2000). A gated channel into the proteasome core particle. Nat. Struct. Biol. *7*, 1062-1067.

Guenther, B., Onrust, R., Sali, A., O'Donnell, M., and Kuriyan, J. (1997). Crystal structure of the delta' subunit of the clamp-loader complex of E. coli DNA polymerase III. Cell *91*, 335-345.

Guo, F., Maurizi, M.R., Esser, L., and Xia, D. (2002). Crystal structure of ClpA, an Hsp100 chaperone and regulator of ClpAP protease. J. Biol. Chem. *277*, 46743-46752.

Hanson, P.I., and Whiteheart, S.W. (2005). AAA+ proteins: have engine, will work. Nat. Rev. Mol. Cell Biol. *6*, 519-529.

Hattendorf, D.A., and Lindquist, S. (2002). Cooperative kinetics of both Hsp104 ATPase domains and interdomain communication revealed by AAA sensor-1 mutants. The EMBO Journal *21*, 12-21.

Heinemeyer, W., Trondle, N., Albrecht, G., and Wolf, D.H. (1994). PRE5 and PRE6, the last missing genes encoding 20S proteasome subunits from yeast? Indication for a set of 14 different subunits in the eukaryotic proteasome core. Biochemistry *33*, 12229-12237.

Hensel, A., Beck, S., El Magraoui, F., Platta, H.W., Girzalsky, W., and Erdmann, R. (2011). Cysteine-dependent ubiquitination of Pex18p is linked to cargo translocation across the peroxisomal membrane. J. Biol. Chem. *286*, 43495-43505.

Hettema, E.H., Erdmann, R., van der Klei, I., and Veenhuis, M. (2014). Evolving models for peroxisome biogenesis. Curr. Opin. Cell Biol. *29C*, 25-30.

Hettema, E.H., van Roermund, C.W., Distel, B., van den Berg, M., Vilela, C., Rodrigues-Pousada, C., Wanders, R.J., and Tabak, H.F. (1996). The ABC transporter proteins Pat1 and Pat2 are required for import of long-chain fatty acids into peroxisomes of Saccharomyces cerevisiae. EMBO J. *15*, 3813-3822.

Heupel, R., and Heldt, H.W. (1994). Protein organization in the matrix of leaf peroxisomes. A multi-enzyme complex involved in photorespiratory metabolism. Eur. J. Biochem. *220*, 165-172.

Hicke, L., Schubert, H.L., and Hill, C.P. (2005). Ubiquitin-binding domains. Nat. Rev. Mol. Cell Biol. *6*, 610-621.

Hiltunen, J.K., Mursula, A.M., Rottensteiner, H., Wierenga, R.K., Kastaniotis, A.J., and Gurvitz, A. (2003). The biochemistry of peroxisomal beta-oxidation in the yeast Saccharomyces cerevisiae. FEMS Microbiol. Rev. *27*, 35-64.

Hinnerwisch, J., Fenton, W.A., Furtak, K.J., Farr, G.W., and Horwich, A.L. (2005). Loops in the central channel of ClpA chaperone mediate protein binding, unfolding, and translocation. Cell *121*, 1029-1041.

Hoefler, G., Hoefler, S., Watkins, P.A., Chen, W.W., Moser, A., Baldwin, V., McGillivary, B., Charrow, J., Friedman, J.M., Rutledge, L.*, et al.* (1988). Biochemical abnormalities in rhizomelic chondrodysplasia punctata. The Journal of pediatrics *112*, 726-733.

Hoskins, J.R., Pak, M., Maurizi, M.R., and Wickner, S. (1998). The role of the ClpA chaperone in proteolysis by ClpAP. Proc. Natl. Acad. Sci. USA *95*, 12135-12140.

Hruban, Z., Vigil, E.L., Slesers, A., and Hopkins, E. (1972). Microbodies: constituent organelles of animal cells. Lab. Invest. *27*, 184-191.

Huyton, T., Pye, V.E., Briggs, L.C., Flynn, T.C., Beuron, F., Kondo, H., Ma, J., Zhang, X., and Freemont, P.S. (2003). The crystal structure of murine p97/VCP at 3.6A. J. Struct. Biol. *144*, 337-348.

Imamura, A., Shimozawa, N., Suzuki, Y., Zhang, Z., Tsukamoto, T., Fujiki, Y., Orii, T., Osumi, T., Wanders, R.J., and Kondo, N. (2000). Temperature-sensitive mutation of PEX6 in peroxisome biogenesis disorders in complementation group C (CG-C): comparative study of PEX6 and PEX1. Pediatr Res *48*, 541-545.

Imamura, A., Tamura, S., Shimozawa, N., Suzuki, Y., Zhang, Z., Tsukamoto, T., Orii, T., Kondo, N., Osumi, T., and Fujiki, Y. (1998). Temperature-sensitive mutation in PEX1 moderates the phenotypes of peroxisome deficiency disorders. Hum. Mol. Genet. *7*, 2089-2094.

Ishikawa, T., Beuron, F., Kessel, M., Wickner, S., Maurizi, M.R., and Steven, A.C. (2001). Translocation pathway of protein substrates in ClpAP protease. Proc. Natl. Acad. Sci. USA *98*, 4328-4333.

Islinger, M., Grille, S., Fahimi, H.D., and Schrader, M. (2012). The peroxisome: an update on

mysteries. Histochemistry and cell biology *137*, 547-574.
Iyer, L.M., Leipe, D.D., Koonin, E.V., and Aravind, L. (2004). Evolutionary history and higher order classification of AAA+ ATPases. J. Struct. Biol. *146*, 11-31.
Jansen, G.A., and Wanders, R.J.A. (2006). Alpha-Oxidation. Biochim. Biophys. Acta *1763*, 1403-1412.
Jentsch, S., and Rumpf, S. (2007). Cdc48 (p97): a "molecular gearbox" in the ubiquitin pathway? Trends Biochem. Sci. *32*, 6-11.
Jeruzalmi, D., Yurieva, O., Zhao, Y., Young, M., Stewart, J., Hingorani, M., O'Donnell, M., and Kuriyan, J. (2001). Mechanism of processivity clamp opening by the delta subunit wrench of the clamp loader complex of E. coli DNA polymerase III. Cell *106*, 417-428.
Johnson, D.W., ten Brink, H.J., Schuit, R.C., and Jakobs, C. (2001). Rapid and quantitative analysis of unconjugated C(27) bile acids in plasma and blood samples by tandem mass spectrometry. J. Lipid Res. *42*, 9-16.
Johnston, M., and Davis, R.W. (1984). Sequences that regulate the divergent GAL1-GAL10 promoter in Saccharomyces cerevisiae. Mol. Cell. Biol. *4*, 1440-1448.
Jones, J.M., Morrell, J.C., and Gould, S.J. (2004). PEX19 is a predominantly cytosolic chaperone and import receptor for class 1 peroxisomal membrane proteins. J. Cell Biol. *164*, 57-67.
Joo, H.J., Kim, K.Y., Yim, Y.H., Jin, Y.X., Kim, H., Kim, M.Y., and Paik, Y.K. (2010). Contribution of the peroxisomal acox gene to the dynamic balance of daumone production in Caenorhabditis elegans. J. Biol. Chem. *285*, 29319-29325.
Joshi, S.A., Baker, T.A., and Sauer, R.T. (2003). C-terminal domain mutations in ClpX uncouple substrate binding from an engagement step required for unfolding. Mol. Microbiol. *48*, 67-76.
Karata, K., Inagawa, T., Wilkinson, A.J., Tatsuta, T., and Ogura, T. (1999). Dissecting the role of a conserved motif (the second region of homology) in the AAA family of ATPases. Site-directed mutagenesis of the ATP-dependent protease FtsH. J. Biol. Chem. *274*, 26225-26232.
Kiel, J.A., Emmrich, K., Meyer, H.E., and Kunau, W.H. (2005a). Ubiquitination of the peroxisomal targeting signal type 1 receptor, Pex5p, suggests the presence of a quality control mechanism during peroxisomal matrix protein import. J. Biol. Chem. *280*, 1921-1930.
Kiel, J.A., Hilbrands, R.E., van der Klei, I.J., Rasmussen, S.W., Salomons, F.A., van der Heide, M., Faber, K.N., Cregg, J.M., and Veenhuis, M. (1999). Hansenula polymorpha Pex1p and Pex6p are peroxisome-associated AAA proteins that functionally and physically interact. Yeast *15*, 1059-1078.
Kiel, J.A., van der Klei, I.J., van den Berg, M.A., Bovenberg, R.A., and Veenhuis, M. (2005b). Overproduction of a single protein, Pc-Pex11p, results in 2-fold enhanced penicillin production by Penicillium chrysogenum. Fungal Genet. Biol. *42*, 154-164.
Kienow, L., Schneider, K., Bartsch, M., Stuible, H.-P., Weng, H., Miersch, O., Wasternack, C., and Kombrink, E. (2008). Jasmonates meet fatty acids: functional analysis of a new acyl-coenzyme A synthetase family from Arabidopsis thaliana. J. Exp. Bot. *59*, 403-419.
Kon, T., Nishiura, M., Ohkura, R., Toyoshima, Y.Y., and Sutoh, K. (2004). Distinct functions of nucleotide-binding/hydrolysis sites in the four AAA modules of cytoplasmic dynein. Biochemistry *43*, 11266-11274.
Kragt, A., Voorn-Brouwer, T., van den Berg, M., and Distel, B. (2005). The Saccharomyces cerevisiae peroxisomal import receptor Pex5p is monoubiquitinated in wild type cells. J. Biol. Chem. *280*, 7867-7874.
Kress, W., Mutschler, H., and Weber-Ban, E. (2009). Both ATPase domains of ClpA are critical for processing of stable protein structures. J. Biol. Chem. *284*, 31441-31452.
Krzewska, J., Konopa, G., and Liberek, K. (2001). Importance of two ATP-binding sites for oligomerization, ATPase activity and chaperone function of mitochondrial Hsp78 protein. J. Mol. Biol. *314*, 901-910.
Kunau, W.H., Beyer, A., Franken, T., Gotte, K., Marzioch, M., Saidowsky, J., Skaletz-Rorowski, A., and Wiebel, F.F. (1993). Two complementary approaches to study

peroxisome biogenesis in Saccharomyces cerevisiae: forward and reversed genetics. Biochimie *75*, 209-224.

Laemmli, U.K. (1970). Cleavage of structural proteins during the assembly of the head of bacteriophage T4. Nature *227*, 680-685.

Lakomek, K., Stoehr, G., Tosi, A., Schmailzl, M., and Hopfner, K.P. (2015). Structural Basis for Dodecameric Assembly States and Conformational Plasticity of the Full-Length AAA+ ATPases Rvb1.Rvb2. Structure.

Lam, S.K., Yoda, N., and Schekman, R. (2010). A vesicle carrier that mediates peroxisome protein traffic from the endoplasmic reticulum. Proc. Natl. Acad. Sci. USA *107*, 21523-21528.

Lander, G.C., Estrin, E., Matyskiela, M.E., Bashore, C., Nogales, E., and Martin, A. (2012). Complete subunit architecture of the proteasome regulatory particle. Nature *482*, 186-191.

Larkin, M.A., Blackshields, G., Brown, N.P., Chenna, R., McGettigan, P.A., McWilliam, H., Valentin, F., Wallace, I.M., Wilm, A., Lopez, R.*, et al.* (2007). ClustalW and ClustalX version 2. Bioinformatics *23*, 2947-2948.

Lazarow, P.B. (2006). The import receptor Pex7p and the PTS2 targeting sequence. Biochim. Biophys. Acta *1763*, 1599-1604.

Lazarow, P.B., and De Duve, C. (1976). A fatty acyl-CoA oxidizing system in rat liver peroxisomes; enhancement by clofibrate, a hypolipidemic drug. Proc. Natl. Acad. Sci. USA *73*, 2043-2046.

Lazarow, P.B., and Fujiki, Y. (1985). Biogenesis of peroxisomes. Annual review of cell biology *1*, 489-530.

Lee, S., Augustin, S., Tatsuta, T., Gerdes, F., Langer, T., and Tsai, F.T. (2011). Electron cryomicroscopy structure of a membrane-anchored mitochondrial AAA protease. J. Biol. Chem. *286*, 4404-4411.

Lee, S., Sowa, M.E., Watanabe, Y.H., Sigler, P.B., Chiu, W., Yoshida, M., and Tsai, F.T. (2003a). The structure of ClpB: a molecular chaperone that rescues proteins from an aggregated state. Cell *115*, 229-240.

Lee, S.Y., De La Torre, A., Yan, D., Kustu, S., Nixon, B.T., and Wemmer, D.E. (2003b). Regulation of the transcriptional activator NtrC1: structural studies of the regulatory and AAA+ ATPase domains. Genes Dev. *17*, 2552-2563.

Lenzen, C.U., Steinmann, D., Whiteheart, S.W., and Weis, W.I. (1998). Crystal structure of the hexamerization domain of N-ethylmaleimide-sensitive fusion protein. Cell *94*, 525-536.

Liu, F., Lu, Y., Pieuchot, L., Dhavale, T., and Jedd, G. (2011). Import oligomers induce positive feedback to promote peroxisome differentiation and control organelle abundance. Dev. Cell *21*, 457-468.

Lizard, G., Rouaud, O., Demarquoy, J., Cherkaoui-Malki, M., and Iuliano, L. (2012). Potential roles of peroxisomes in Alzheimer's disease and in dementia of the Alzheimer's type. Journal of Alzheimer's disease : JAD *29*, 241-254.

Lum, R., Tkach, J.M., Vierling, E., and Glover, J.R. (2004). Evidence for an unfolding/threading mechanism for protein disaggregation by Saccharomyces cerevisiae Hsp104. J. Biol. Chem. *279*, 29139-29146.

Lupas, A.N., and Martin, J. (2002). AAA proteins. Curr. Opin. Struct. Biol. *12*, 746-753.

Lyubimov, A.Y., Strycharska, M., and Berger, J.M. (2011). The nuts and bolts of ring-translocase structure and mechanism. Curr. Opin. Struct. Biol. *21*, 240-248.

Maillard, R.A., Chistol, G., Sen, M., Righini, M., Tan, J., Kaiser, C.M., Hodges, C., Martin, A., and Bustamante, C. (2011). ClpX(P) generates mechanical force to unfold and translocate its protein substrates. Cell *145*, 459-469.

Majewski, J., Wang, Z., Lopez, I., Al Humaid, S., Ren, H., Racine, J., Bazinet, A., Mitchel, G., Braverman, N., and Koenekoop, R.K. (2011). A new ocular phenotype associated with an unexpected but known systemic disorder and mutation: novel use of genomic diagnostics and exome sequencing. J. Med. Genet. *48*, 593-596.

Martin, A., Baker, T.A., and Sauer, R.T. (2005). Rebuilt AAA + motors reveal operating

principles for ATP-fuelled machines. Nature *437*, 1115-1120.
Martin, A., Baker, T.A., and Sauer, R.T. (2008). Pore loops of the AAA+ ClpX machine grip substrates to drive translocation and unfolding. Nat. Struct. Mol. Biol. *15*, 1147-1151.
Matsuzono, Y., and Fujiki, Y. (2006). In vitro transport of membrane proteins to peroxisomes by shuttling receptor Pex19p. J. Biol. Chem. *281*, 36-42.
Matveeva, E.A., He, P., and Whiteheart, S.W. (1997). N-Ethylmaleimide-sensitive fusion protein contains high and low affinity ATP-binding sites that are functionally distinct. J. Biol. Chem. *272*, 26413-26418.
Matyskiela, M.E., Lander, G.C., and Martin, A. (2013). Conformational switching of the 26S proteasome enables substrate degradation. Nat. Struct. Mol. Biol. *20*, 781-788.
McCollum, D., Monosov, E., and Subramani, S. (1993). The pas8 mutant of Pichia pastoris exhibits the peroxisomal protein import deficiencies of Zellweger syndrome cells--the PAS8 protein binds to the COOH-terminal tripeptide peroxisomal targeting signal, and is a member of the TPR protein family. The Journal of Cell Biology *121*, 761-774.
McNew, J.A., and Goodman, J.M. (1996). The targeting and assembly of peroxisomal proteins: some old rules do not apply. Trends Biochem. Sci. *21*, 54-58.
Meyer, H., Bug, M., and Bremer, S. (2012). Emerging functions of the VCP/p97 AAA-ATPase in the ubiquitin system. Nat. Cell Biol. *14*, 117-123.
Meyer, H., and Weihl, C.C. (2014). The VCP/p97 system at a glance: connecting cellular function to disease pathogenesis. J. Cell Sci.
Mindell, J.A., and Grigorieff, N. (2003). Accurate determination of local defocus and specimen tilt in electron microscopy. J. Struct. Biol. *142*, 334-347.
Miyata, N., and Fujiki, Y. (2005). Shuttling mechanism of peroxisome targeting signal type 1 receptor Pex5: ATP-independent import and ATP-dependent export. Mol. Cell. Biol. *25*, 10822-10832.
Moffitt, J.R., Chemla, Y.R., Aathavan, K., Grimes, S., Jardine, P.J., Anderson, D.L., and Bustamante, C. (2009). Intersubunit coordination in a homomeric ring ATPase. Nature *457*, 446-450.
Mogk, A., Schlieker, C., Strub, C., Rist, W., Weibezahn, J., and Bukau, B. (2003). Roles of individual domains and conserved motifs of the AAA+ chaperone ClpB in oligomerization, ATP hydrolysis, and chaperone activity. J. Biol. Chem. *278*, 17615-17624.
Mosser, J., Douar, A.M., Sarde, C.O., Kioschis, P., Feil, R., Moser, H., Poustka, A.M., Mandel, J.L., and Aubourg, P. (1993). Putative X-linked adrenoleukodystrophy gene shares unexpected homology with ABC transporters. Nature *361*, 726-730.
Motley, A.M., Brites, P., Gerez, L., Hogenhout, E., Haasjes, J., Benne, R., Tabak, H.F., Wanders, R.J., and Waterham, H.R. (2002). Mutational spectrum in the PEX7 gene and functional analysis of mutant alleles in 78 patients with rhizomelic chondrodysplasia punctata type 1. Am. J. Hum. Genet. *70*, 612-624.
Mueller-Cajar, O., Stotz, M., Wendler, P., Hartl, F.U., Bracher, A., and Hayer-Hartl, M. (2011). Structure and function of the AAA+ protein CbbX, a red-type Rubisco activase. Nature *479*, 194-199.
Muller, C.W., and Schulz, G.E. (1992). Structure of the complex between adenylate kinase from Escherichia coli and the inhibitor Ap5A refined at 1.9 A resolution. A model for a catalytic transition state. J. Mol. Biol. *224*, 159-177.
Nagan, N., and Zoeller, R.A. (2001). Plasmalogens: biosynthesis and functions. Progress in lipid research *40*, 199-229.
Neuwald, A.F., Aravind, L., Spouge, J.L., and Koonin, E.V. (1999). AAA+: A class of chaperone-like ATPases associated with the assembly, operation, and disassembly of protein complexes. Genome Res. *9*, 27-43.
Nishikori, S., Esaki, M., Yamanaka, K., Sugimoto, S., and Ogura, T. (2011). Positive cooperativity of the p97 AAA ATPase is critical for essential functions. J. Biol. Chem. *286*, 15815-15820.
Nyquist, K., and Martin, A. (2014). Marching to the beat of the ring: polypeptide translocation by AAA+ proteases. Trends Biochem. Sci. *39*, 53-60.

Ogura, T., Whiteheart, S.W., and Wilkinson, A.J. (2004). Conserved arginine residues implicated in ATP hydrolysis, nucleotide-sensing, and inter-subunit interactions in AAA and AAA+ ATPases. J. Struct. Biol. *146*, 106-112.

Ogura, T., and Wilkinson, A.J. (2001). AAA+ superfamily ATPases: common structure--diverse function. Genes Cells *6*, 575-597.

Opperdoes, F.R., Borst, P., and Spits, H. (1977). Particle-bound enzymes in the bloodstream form of Trypanosoma brucei. Eur. J. Biochem. *76*, 21-28.

Ortega, J., Singh, S.K., Ishikawa, T., Maurizi, M.R., and Steven, A.C. (2000). Visualization of substrate binding and translocation by the ATP-dependent protease, ClpXP. Mol. Cell *6*, 1515-1521.

Palmieri, L., Rottensteiner, H., Girzalsky, W., Scarcia, P., Palmieri, F., and Erdmann, R. (2001). Identification and functional reconstitution of the yeast peroxisomal adenine nucleotide transporter. EMBO J. *20*, 5049-5059.

Park, E., Rho, Y.M., Koh, O.J., Ahn, S.W., Seong, I.S., Song, J.J., Bang, O., Seol, J.H., Wang, J., Eom, S.H.*, et al.* (2005). Role of the GYVG pore motif of HslU ATPase in protein unfolding and translocation for degradation by HslV peptidase. J. Biol. Chem. *280*, 22892-22898.

Patel, S., and Latterich, M. (1998). The AAA team: related ATPases with diverse functions. Trends Cell Biol. *8*, 65-71.

Pettersen, E.F., Goddard, T.D., Huang, C.C., Couch, G.S., Greenblatt, D.M., Meng, E.C., and Ferrin, T.E. (2004). UCSF Chimera--a visualization system for exploratory research and analysis. Journal of computational chemistry *25*, 1605-1612.

Platta, H.W., El Magraoui, F., Schlee, D., Grunau, S., Girzalsky, W., and Erdmann, R. (2007). Ubiquitination of the peroxisomal import receptor Pex5p is required for its recycling. J. Cell Biol. *177*, 197-204.

Platta, H.W., and Erdmann, R. (2007). Peroxisomal dynamics. Trends Cell Biol. *17*, 474-484.

Platta, H.W., Girzalsky, W., and Erdmann, R. (2004). Ubiquitination of the peroxisomal import receptor Pex5p. Biochem. J. *384*, 37-45.

Platta, H.W., Grunau, S., Rosenkranz, K., Girzalsky, W., and Erdmann, R. (2005). Functional role of the AAA peroxins in dislocation of the cycling PTS1 receptor back to the cytosol. Nat. Cell Biol. *7*, 817-822.

Platta, H.W., Hagen, S., Reidick, C., and Erdmann, R. (2014). The peroxisomal receptor dislocation pathway: to the exportomer and beyond. Biochimie *98*, 16-28.

Poirier, Y., Antonenkov, V.D., Glumoff, T., and Hiltunen, J.K. (2006). Peroxisomal β-oxidation−A metabolic pathway with multiple functions. Biochim. Biophys. Acta *1763*, 1413-1426.

Poll-The, B.T., Gootjes, J., Duran, M., De Klerk, J.B., Wenniger-Prick, L.J., Admiraal, R.J., Waterham, H.R., Wanders, R.J., and Barth, P.G. (2004). Peroxisome biogenesis disorders with prolonged survival: phenotypic expression in a cohort of 31 patients. Am. J. Med. Genet. A *126A*, 333-338.

Puig, O., Caspary, F., Rigaut, G., Rutz, B., Bouveret, E., Bragado-Nilsson, E., Wilm, M., and Seraphin, B. (2001). The tandem affinity purification (TAP) method: a general procedure of protein complex purification. Methods *24*, 218-229.

Püschel, A.W., O'Connor, V., and Betz, H. (1994). The N-ethylmaleimide-sensitive fusion protein (NSF) is preferentially expressed in the nervous system. FEBS Lett. *347*, 55-58.

Pye, V.E., Dreveny, I., Briggs, L.C., Sands, C., Beuron, F., Zhang, X., and Freemont, P.S. (2006). Going through the motions: the ATPase cycle of p97. J. Struct. Biol. *156*, 12-28.

Quarmby, L. (2000). Cellular Samurai: katanin and the severing of microtubules. J. Cell Sci. *113 (Pt 16)*, 2821-2827.

Reddy, J.K., Warren, J.R., Reddy, M.K., and Lalwani, N.D. (1982). Hepatic and renal effects of peroxisome proliferators: biological implications. Ann. N. Y. Acad. Sci. *386*, 81-110.

Rehling, P., Skaletz-Rorowski, A., Girzalsky, W., Voorn-Brouwer, T., Franse, M.M., Distel, B., Veenhuis, M., Kunau, W.H., and Erdmann, R. (2000). Pex8p, an intraperoxisomal peroxin of Saccharomyces cerevisiae required for protein transport into peroxisomes binds the PTS1 receptor pex5p. J. Biol. Chem. *275*, 3593-3602.

Reuber, B.E., Germain-Lee, E., Collins, C.S., Morrell, J.C., Ameritunga, R., Moser, H.W., Valle, D., and Gould, S.J. (1997). Mutations in PEX1 are the most common cause of peroxisome biogenesis disorders. Nat. Genet. *17*, 445-448.

Rhodin, J. (1954). Correlation of ultrastructural organization and function in normal and experimentally changed proximal convoluted tubule cells of the mouse kidney. Stockholm, Aktiebolaget Godvil.

Rockel, B., Jakana, J., Chiu, W., and Baumeister, W. (2002). Electron cryo-microscopy of VAT, the archaeal p97/CDC48 homologue from Thermoplasma acidophilum. J. Mol. Biol. *317*, 673-681.

Roseman, A.M. (2004). FindEM--a fast, efficient program for automatic selection of particles from electron micrographs. J. Struct. Biol. *145*, 91-99.

Rosenkranz, K., Birschmann, I., Grunau, S., Girzalsky, W., Kunau, W.H., and Erdmann, R. (2006). Functional association of the AAA complex and the peroxisomal importomer. FEBS J. *273*, 3804-3815.

Rottensteiner, H., Kramer, A., Lorenzen, S., Stein, K., Landgraf, C., Volkmer-Engert, R., and Erdmann, R. (2004). Peroxisomal membrane proteins contain common Pex19p-binding sites that are an integral part of their targeting signals. Mol Biol Cell *15*, 3406-3417.

Rottensteiner, H., and Theodoulou, F.L. (2006). The ins and outs of peroxisomes: Co-ordination of membrane transport and peroxisomal metabolism. Biochim. Biophys. Acta *1763*, 1527-1540.

Rouiller, I., DeLaBarre, B., May, A.P., Weis, W.I., Brunger, A.T., Milligan, R.A., and Wilson-Kubalek, E.M. (2002). Conformational changes of the multifunction p97 AAA ATPase during its ATPase cycle. Nat. Struct. Biol. *9*, 950-957.

Rucktäschel, R., Girzalsky, W., and Erdmann, R. (2011). Protein import machineries of peroxisomes. Biochim. Biophys. Acta *1808*, 892-900.

Rucktäschel, R., Thoms, S., Sidorovitch, V., Halbach, A., Pechlivanis, M., Volkmer, R., Alexandrov, K., Kuhlmann, J., Rottensteiner, H., and Erdmann, R. (2009). Farnesylation of pex19p is required for its structural integrity and function in peroxisome biogenesis. J. Biol. Chem. *284*, 20885-20896.

Russell, D.W. (2003). The enzymes, regulation, and genetics of bile acid synthesis. Annu. Rev. Biochem. *72*, 137-174.

Saffian, D., Grimm, I., Girzalsky, W., and Erdmann, R. (2012). ATP-dependent assembly of the heteromeric Pex1p-Pex6p-complex of the peroxisomal matrix protein import machinery. J. Struct. Biol. *179*, 126-132.

Sali, A., and Blundell, T.L. (1993). Comparative protein modelling by satisfaction of spatial restraints. J. Mol. Biol. *234*, 779-815.

Sambrook, J., Fritsch, E.F., and Maniatis, T. (1989). Molecular Cloning, a laboratory Manual. Cold Spring Harbor Laboratory Press, New York.

Sanchez, Y., and Lindquist, S.L. (1990). HSP104 required for induced thermotolerance. Science *248*, 1112-1115.

Sanders, C.M., Kovalevskiy, O.V., Sizov, D., Lebedev, A.A., Isupov, M.N., and Antson, A.A. (2007). Papillomavirus E1 helicase assembly maintains an asymmetric state in the absence of DNA and nucleotide cofactors. Nucleic Acids Res. *35*, 6451-6457.

Schaupp, A., Marcinowski, M., Grimminger, V., Bosl, B., and Walter, S. (2007). Processing of proteins by the molecular chaperone Hsp104. J. Mol. Biol. *370*, 674-686.

Schirmer, E.C., Queitsch, C., Kowal, A.S., Parsell, D.A., and Lindquist, S. (1998). The ATPase activity of Hsp104, effects of environmental conditions and mutations. J. Biol. Chem. *273*, 15546-15552.

Schirmer, E.C., Ware, D.M., Queitsch, C., Kowal, A.S., and Lindquist, S.L. (2001). Subunit interactions influence the biochemical and biological properties of Hsp104. Proc. Natl. Acad. Sci. USA *98*, 914-919.

Schlee, S., Groemping, Y., Herde, P., Seidel, R., and Reinstein, J. (2001). The chaperone function of ClpB from Thermus thermophilus depends on allosteric interactions of its two ATP-binding sites. J. Mol. Biol. *306*, 889-899.

Schliebs, W., Girzalsky, W., and Erdmann, R. (2010). Peroxisomal protein import and ERAD:

variations on a common theme. Nat. Rev. Mol. Cell Biol. *11*, 885-890.
Schliebs, W., and Kunau, W.-H. (2006). PTS2 Co-receptors: Diverse proteins with common features. Biochim. Biophys. Acta *1763*, 1605-1612.
Schlieker, C., Weibezahn, J., Patzelt, H., Tessarz, P., Strub, C., Zeth, K., Erbse, A., Schneider-Mergener, J., Chin, J.W., Schultz, P.G.*, et al.* (2004). Substrate recognition by the AAA+ chaperone ClpB. Nat. Struct. Mol. Biol. *11*, 607-615.
Schluter, A., Real-Chicharro, A., Gabaldon, T., Sanchez-Jimenez, F., and Pujol, A. (2010). PeroxisomeDB 2.0: an integrative view of the global peroxisomal metabolome. Nucleic Acids Res. *38*, D800-805.
Schrader, M., and Fahimi, H.D. (2008). The peroxisome: still a mysterious organelle. Histochemistry and cell biology *129*, 421-440.
Schuldiner, M., Metz, J., Schmid, V., Denic, V., Rakwalska, M., Schmitt, H.D., Schwappach, B., and Weissman, J.S. (2008). The GET complex mediates insertion of tail-anchored proteins into the ER membrane. Cell *134*, 634-645.
Shaikh, T.R., Gao, H., Baxter, W.T., Asturias, F.J., Boisset, N., Leith, A., and Frank, J. (2008). SPIDER image processing for single-particle reconstruction of biological macromolecules from electron micrographs. Nat. Protoc. *3*, 1941-1974.
Shiozawa, K., Maita, N., Tomii, K., Seto, A., Goda, N., Akiyama, Y., Shimizu, T., Shirakawa, M., and Hiroaki, H. (2004). Structure of the N-terminal domain of PEX1 AAA-ATPase. Characterization of a putative adaptor-binding domain. J. Biol. Chem. *279*, 50060-50068.
Siddiqui, S.M., Sauer, R.T., and Baker, T.A. (2004). Role of the processing pore of the ClpX AAA+ ATPase in the recognition and engagement of specific protein substrates. Genes Dev. *18*, 369-374.
Simonetta, K.R., Kazmirski, S.L., Goedken, E.R., Cantor, A.J., Kelch, B.A., McNally, R., Seyedin, S.N., Makino, D.L., O'Donnell, M., and Kuriyan, J. (2009). The mechanism of ATP-dependent primer-template recognition by a clamp loader complex. Cell *137*, 659-671.
Singh, S.K., Grimaud, R., Hoskins, J.R., Wickner, S., and Maurizi, M.R. (2000). Unfolding and internalization of proteins by the ATP-dependent proteases ClpXP and ClpAP. Proc. Natl. Acad. Sci. USA *97*, 8898-8903.
Singh, S.K., and Maurizi, M.R. (1994). Mutational analysis demonstrates different functional roles for the two ATP-binding sites in ClpAP protease from Escherichia coli. J. Biol. Chem. *269*, 29537-29545.
Singleton, M.R., Sawaya, M.R., Ellenberger, T., and Wigley, D.B. (2000). Crystal structure of T7 gene 4 ring helicase indicates a mechanism for sequential hydrolysis of nucleotides. Cell *101*, 589-600.
Smith, J.J., and Aitchison, J.D. (2009). Regulation of peroxisome dynamics. Curr. Opin. Cell Biol. *21*, 119-126.
Snyder, W.B., Koller, A., Choy, A.J., and Subramani, S. (2000). The peroxin Pex19p interacts with multiple, integral membrane proteins at the peroxisomal membrane. J. Cell Biol. *149*, 1171-1178.
Soding, J., Biegert, A., and Lupas, A.N. (2005). The HHpred interactive server for protein homology detection and structure prediction. Nucleic Acids Res. *33*, W244-248.
Song, C., Wang, Q., and Li, C.C. (2003). ATPase activity of p97-valosin-containing protein (VCP). D2 mediates the major enzyme activity, and D1 contributes to the heat-induced activity. J. Biol. Chem. *278*, 3648-3655.
Spiegel, C.N., Batista-Pereira, L.G., Bretas, J.A., Eiras, A.E., Hooper, A.M., Peixoto, A.A., and Soares, M.J. (2011). Pheromone gland development and pheromone production in lutzomyia longipalpis (Diptera: Psychodidae: Phlebotominae). J. Med. Entomol. *48*, 489-495.
Steinberg, S., Chen, L., Wei, L., Moser, A., Moser, H., Cutting, G., and Braverman, N. (2004). The PEX Gene Screen: molecular diagnosis of peroxisome biogenesis disorders in the Zellweger syndrome spectrum. Mol. Genet. Metab. *83*, 252-263.
Steinberg, S.J., Dodt, G., Raymond, G.V., Braverman, N.E., Moser, A.B., and Moser, H.W. (2006). Peroxisome biogenesis disorders. Biochim. Biophys. Acta *1763*, 1733-1748.

Stinson, B.M., Nager, A.R., Glynn, S.E., Schmitz, K.R., Baker, T.A., and Sauer, R.T. (2013). Nucleotide binding and conformational switching in the hexameric ring of a AAA+ machine. Cell *153*, 628-639.

Suno, R., Niwa, H., Tsuchiya, D., Zhang, X., Yoshida, M., and Morikawa, K. (2006). Structure of the whole cytosolic region of ATP-dependent protease FtsH. Mol. Cell *22*, 575-585.

Szilard, R.K., Titorenko, V.I., Veenhuis, M., and Rachubinski, R.A. (1995). Pay32p of the yeast Yarrowia lipolytica is an intraperoxisomal component of the matrix protein translocation machinery. The Journal of Cell Biology *131*, 1453-1469.

Tamura, S., Okumoto, K., Toyama, R., Shimozawa, N., Tsukamoto, T., Suzuki, Y., Osumi, T., Kondo, N., and Fujiki, Y. (1998). Human PEX1 cloned by functional complementation on a CHO cell mutant is responsible for peroxisome-deficient Zellweger syndrome of complementation group I. Proc. Natl. Acad. Sci. USA *95*, 4350-4355.

Tamura, S., Yasutake, S., Matsumoto, N., and Fujiki, Y. (2006). Dynamic and functional assembly of the AAA peroxins, Pex1p and Pex6p, and their membrane receptor Pex26p. J. Biol. Chem. *281*, 27693-27704.

Tamura, S.S., N.; Suzuki, Y.; Tsukamoto, T.; Osumi, T. and Fujiki, Y. (1998). A Cytoplasmic AAA Family Peroxin, Pex1p, Interacts with Pex6p. Biochem. Biophys. Res. Commun. *245*, 883-886.

Tang, W.K., Li, D., Li, C.C., Esser, L., Dai, R., Guo, L., and Xia, D. (2010). A novel ATP-dependent conformation in p97 N-D1 fragment revealed by crystal structures of disease-related mutants. EMBO J. *29*, 2217-2229.

Tehlivets, O., Scheuringer, K., and Kohlwein, S.D. (2007). Fatty acid synthesis and elongation in yeast. Biochim. Biophys. Acta *1771*, 255-270.

Tessarz, P., Mogk, A., and Bukau, B. (2008). Substrate threading through the central pore of the Hsp104 chaperone as a common mechanism for protein disaggregation and prion propagation. Mol. Microbiol. *68*, 87-97.

Thoms, S., and Erdmann, R. (2006). Peroxisomal matrix protein receptor ubiquitination and recycling. Biochim. Biophys. Acta *1763*, 1620-1628.

Thoms, S., Harms, I., Kalies, K.U., and Gartner, J. (2012). Peroxisome formation requires the endoplasmic reticulum channel protein Sec61. Traffic *13*, 599-609.

Titorenko, V.I., and Terlecky, S.R. (2011). Peroxisome metabolism and cellular aging. Traffic *12*, 252-259.

Tolbert, N.E. (1981). Metabolic pathways in peroxisomes and glyoxysomes. Annu. Rev. Biochem. *50*, 133-157.

Towbin, H., Staehelin, T., and Gordon, J. (1979). Electrophoretic transfer of proteins from polyacrylamide gels to nitrocellulose sheets: procedure and some applications. Proc. Natl. Acad. Sci. USA *76*, 4350-4354.

Tower, R.J., Fagarasanu, A., Aitchison, J.D., and Rachubinski, R.A. (2011). The peroxin Pex34p functions with the Pex11 family of peroxisomal divisional proteins to regulate the peroxisome population in yeast. Mol Biol Cell *22*, 1727-1738.

Tsukamoto, T., Miura, S., Nakai, T., Yokota, S., Shimozawa, N., Suzuki, Y., Orii, T., Fujiki, Y., Sakai, F., Bogaki, A*., et al.* (1995). Peroxisome assembly factor-2, a putative ATPase cloned by functional complementation on a peroxisome-deficient mammalian cell mutant. Nat. Genet. *11*, 395-401.

Tucker, P.A., and Sallai, L. (2007). The AAA+ superfamily--a myriad of motions. Curr. Opin. Struct. Biol. *17*, 641-652.

van den Brink, D.M., and Wanders, R.J. (2006). Phytanic acid: production from phytol, its breakdown and role in human disease. Cell. Mol. Life Sci. *63*, 1752-1765.

van der Klei, I.J., Hilbrands, R.E., Swaving, G.J., Waterham, H.R., Vrieling, E.G., Titorenko, V.I., Cregg, J.M., Harder, W., and Veenhuis, M. (1995). The Hansenula polymorpha PER3 gene is essential for the import of PTS1 proteins into the peroxisomal matrix. J. Biol. Chem. *270*, 17229-17236.

Van der Leij, I., Franse, M.M., Elgersma, Y., Distel, B., and Tabak, H.F. (1993). PAS10 is a tetratricopeptide-repeat protein that is essential for the import of most matrix proteins into

peroxisomes of Saccharomyces cerevisiae. Proceedings of the National Academy of Sciences *90*, 11782-11786.

van der Zand, A., Braakman, I., and Tabak, H.F. (2010). Peroxisomal membrane proteins insert into the endoplasmic reticulum. Mol Biol Cell *21*, 2057-2065.

van Heel, M., Harauz, G., Orlova, E.V., Schmidt, R., and Schatz, M. (1996). A new generation of the IMAGIC image processing system. J. Struct. Biol. *116*, 17-24.

van Roermund, C.W., Ijlst, L., Majczak, W., Waterham, H.R., Folkerts, H., Wanders, R.J., and Hellingwerf, K.J. (2012). Peroxisomal fatty acid uptake mechanism in Saccharomyces cerevisiae. J. Biol. Chem. *287*, 20144-20153.

Voorn-Brouwer, T., van der Leij, I., Hemrika, W., Distel, B., and Tabak, H.F. (1993). Sequence of the PAS8 gene, the product of which is essential for biogenesis of peroxisomes in Saccharomyces cerevisiae. Biochim. Biophys. Acta *1216*, 325-328.

Walker, J.E., Saraste, M., Runswick, M.J., and Gay, N.J. (1982). Distantly related sequences in the a- and f-subunits of ATP synthase, myosin,kinases and otherATP-requiring enzymes and a common nucleotide binding fold. The EMBO Journal *1*, 945-951.

Walton, P.A., Hill, P.E., and Subramani, S. (1995). Import of stably folded proteins into peroxisomes. Mol Biol Cell *6*, 675-683.

Wanders, R.J. (2000). Peroxisomes, lipid metabolism, and human disease. Cell biochemistry and biophysics *32 Spring*, 89-106.

Wanders, R.J. (2004). Metabolic and molecular basis of peroxisomal disorders: a review. Am. J. Med. Genet. A *126A*, 355-375.

Wanders, R.J., and Waterham, H.R. (2006a). Biochemistry of mammalian peroxisomes revisited. Annu. Rev. Biochem. *75*, 295-332.

Wanders, R.J.A., and Waterham, H.R. (2006b). Peroxisomal disorders: The single peroxisomal enzyme deficiencies. Biochim. Biophys. Acta *1763*, 1707-1720.

Wang, J., Song, J.J., Franklin, M.C., Kamtekar, S., Im, Y.J., Rho, S.H., Seong, I.S., Lee, C.S., Chung, C.H., and Eom, S.H. (2001). Crystal structures of the HslVU peptidase-ATPase complex reveal an ATP-dependent proteolysis mechanism. Structure *9*, 177-184.

Wang, Q., Song, C., and Li, C.C. (2003). Hexamerization of p97-VCP is promoted by ATP binding to the D1 domain and required for ATPase and biological activities. Biochem. Biophys. Res. Commun. *300*, 253-260.

Wardinsky, T.D., Pagon, R.A., Powell, B.R., McGillivray, B., Stephan, M., Zonana, J., and Moser, A. (1990). Rhizomelic chondrodysplasia punctata and survival beyond one year: a review of the literature and five case reports. Clin. Genet. *38*, 84-93.

Waterham, H.R., and Ebberink, M.S. (2012). Genetics and molecular basis of human peroxisome biogenesis disorders. Biochim. Biophys. Acta *1822*, 1430-1441.

Waterhouse, A.M., Procter, J.B., Martin, D.M., Clamp, M., and Barton, G.J. (2009). Jalview Version 2--a multiple sequence alignment editor and analysis workbench. Bioinformatics *25*, 1189-1191.

Weibezahn, J., Schlieker, C., Bukau, B., and Mogk, A. (2003). Characterization of a trap mutant of the AAA+ chaperone ClpB. J. Biol. Chem. *278*, 32608-32617.

Weibezahn, J., Tessarz, P., Schlieker, C., Zahn, R., Maglica, Z., Lee, S., Zentgraf, H., Weber-Ban, E.U., Dougan, D.A., Tsai, F.T.*, et al.* (2004). Thermotolerance requires refolding of aggregated proteins by substrate translocation through the central pore of ClpB. Cell *119*, 653-665.

Wendler, P., Ciniawsky, S., Kock, M., and Kube, S. (2012). Structure and function of the AAA+ nucleotide binding pocket. Biochim. Biophys. Acta *1823*, 2-14.

Wendler, P., Shorter, J., Plisson, C., Cashikar, A.G., Lindquist, S., and Saibil, H.R. (2007). Atypical AAA+ subunit packing creates an expanded cavity for disaggregation by the protein-remodeling factor Hsp104. Cell *131*, 1366-1377.

Wendler, P., Shorter, J., Snead, D., Plisson, C., Clare, D.K., Lindquist, S., and Saibil, H.R. (2009). Motor mechanism for protein threading through Hsp104. Mol. Cell *34*, 81-92.

White, S.R., and Lauring, B. (2007). AAA+ ATPases: achieving diversity of function with conserved machinery. Traffic *8*, 1657-1667.

Whiteheart, S.W., Rossnagel, K., Buhrow, S.A., Brunner, M., Jaenicke, R., and Rothman, J.E.

(1994). N-ethylmaleimide-sensitive fusion protein: a trimeric ATPase whose hydrolysis of ATP is required for membrane fusion. J. Cell Biol. *126*, 945-954.

Williams, C., van den Berg, M., Panjikar, S., Stanley, W.A., Distel, B., and Wilmanns, M. (2012). Insights into ubiquitin-conjugating enzyme/ co-activator interactions from the structure of the Pex4p:Pex22p complex. EMBO J. *31*, 391-402.

Williams, C., van den Berg, M., Sprenger, R.R., and Distel, B. (2007). A conserved cysteine is essential for Pex4p-dependent ubiquitination of the peroxisomal import receptor Pex5p. J. Biol. Chem. *282*, 22534-22543.

Wilson, D.W., Wilcox, C.A., Flynn, G.C., Chen, E., Kuang, W.J., Henzel, W.J., Block, M.R., Ullrich, A., and Rothman, J.E. (1989). A fusion protein required for vesicle-mediated transport in both mammalian cells and yeast. Nature *339*, 355-359.

Yamada-Inagawa, T., Okuno, T., Karata, K., Yamanaka, K., and Ogura, T. (2003). Conserved pore residues in the AAA protease FtsH are important for proteolysis and its coupling to ATP hydrolysis. J. Biol. Chem. *278*, 50182-50187.

Ye, J., Osborne, A.R., Groll, M., and Rapoport, T.A. (2004). RecA-like motor ATPases--lessons from structures. Biochim. Biophys. Acta *1659*, 1-18.

Yeung, H.O., Forster, A., Bebeacua, C., Niwa, H., Ewens, C., McKeown, C., Zhang, X., and Freemont, P.S. (2014). Inter-ring rotations of AAA ATPase p97 revealed by electron cryomicroscopy. Open biology *4*, 130142.

Yoo, S.J., Seol, J.H., Shin, D.H., Rohrwild, M., Kang, M.S., Tanaka, K., Goldberg, A.L., and Chung, C.H. (1996). Purification and characterization of the heat shock proteins HslV and HslU that form a new ATP-dependent protease in Escherichia coli. J. Biol. Chem. *271*, 14035-14040.

Yu, R.C., Jahn, R., and Brunger, A.T. (1999). NSF N-terminal domain crystal structure: models of NSF function. Mol. Cell *4*, 97-107.

Zhang, X., Shaw, A., Bates, P.A., Newman, R.H., Gowen, B., Orlova, E., Gorman, M.A., Kondo, H., Dokurno, P., Lally, J.*, et al.* (2000). Structure of the AAA ATPase p97. Mol. Cell *6*, 1473-1484.

Zhang, X., and Wigley, D.B. (2008). The 'glutamate switch' provides a link between ATPase activity and ligand binding in AAA+ proteins. Nat. Struct. Mol. Biol. *15*, 1223-1227.

Zhao, C., Matveeva, E.A., Ren, Q., and Whiteheart, S.W. (2010). Dissecting the N-ethylmaleimide-sensitive factor: required elements of the N and D1 domains. J. Biol. Chem. *285*, 761-772.

Zhao, C., Smith, E.C., and Whiteheart, S.W. (2012). Requirements for the catalytic cycle of the N-ethylmaleimide-Sensitive Factor (NSF). Biochim. Biophys. Acta *1823*, 159-171.

Zhao, M., Wu, S., Zhou, Q., Vivona, S., Cipriano, D.J., Cheng, Y., and Brunger, A.T. (2015). Mechanistic insights into the recycling machine of the SNARE complex. Nature.

6 List of abbreviations

3D	three-dimensional
µ	micro
Å	Ångström
AAA+	ATPases associated with various cellular activities
ADP	adenosin-5'-diphosphate
Amp	ampicillin
ATP	adenosine-5'-triphosphate
ATPγS	adenosin-5'-O-(3-thio)-triphosphate
APS	ammonium peroxydisulfate
bp	base pair
CCD	charged-coupled device
C-terminal	carboxy-terminal
CTF	contrast transfer function
dNTP	deoxynucleoside triphosphate
DTT	dithiothreitol
e^-	electron
ECL	enhanced chemiluminescence
EDTA	ethylenediaminetetraacetic acid
EM	electron microscopy
FSC	Fourier shell correlation
g	gram
h	hour
HA	human influenza hemagglutinin
HAc	acetic acid
His	histidin
HRP	horseradish peroxidase
IgG	Immunoglobulin protein G
kb	kilo base pairs
kDa	kilo Dalton
l	liter
LB	lysogeny broth
MCS	multiple cloning site
m	milli
M	molar
MAT	mating type
min	minutes
MSA	multivariate statistical analysis
MRA	multi reference alignment
MW	molecular weight
n	nano
N-terminal	amino-terminal
NaDoc	sodium deoxycholate
OD	optical density
ORF	open reading frame

PAGE	polyacrylamide gel electrophoresis
PBDs	Peroxisomal biogenesis disorders
PCR	polymerase chain reaction
Pex	peroxin
PMSF	phenylmethylsulfonyl fluoride
ProA	protein A
PTS1	peroxisomal targeting signal 1
PTS2	Peroxisomal targeting signal 2
rpm	revolutions per minute
RT	room temperature
s	second
SDS	sodium dodecyl sulfate
TBE	tris, boric acid, EDTA
TCA	trichloroacetic acid
TEV	tobacco etch virus
Tris	tris(hydroxymethyl)aminomethane
TST	tris buffered saline, tween-20
U	unit
UA	uranyl acetate
Ub	ubiquitin
V	volt
v/v	volume per volume
w/v	weight per volume
YP	yeast bactopeptone